Applications of Metal Oxides in the Contact Systems of Organic Electronic Devices

Edward Charles Lofts

Department of Physics

Imperial College London

Submitted for the degree of Doctor of Philosophy

August 2015

I declare that all the work included this thesis is my own or has been referenced to the original owner.

The copyright of this thesis rests with the author and is made available under a Creative Commons Attribution Non-Commercial No Derivatives licence. Researchers are free to copy, distribute or transmit the thesis on the condition that they attribute it, that they do not use it for commercial purposes and that they do not alter, transform or build upon it. For any reuse or redistribution, researchers must make clear to others the licence terms of this work

This work was performed with support by the EPSRC.

Particular thanks go to Prof. Donal D. C. Bradley and Dr Xuhua Wang for all the help they have given me.

Abstract

Metal oxides are a group of materials that have shown great promise in improving the efficiency of devices based on organic materials through inclusion in the contact structures of such devices. In this work, the deposition technique of spray pyrolysis is developed for use for the deposition of doped zinc oxide films and molybdenum oxide films. Spray pyrolysis is of great interest as a technique for use in the organic electronics field due to its cost, scalability and compatibility with other solution processing techniques. This makes the technique particularly interesting for use in devices intended for large scale applications such as lighting

The study of doped zinc oxide focuses on its application as an alternative transparent conducting layer to the standard indium tin oxide layer. The zinc oxide layer was doped with aluminium to increase its conductivity, and the effect of lithium doping was investigated with the intent of improving the conductivity of the layers further. Annealing of the layers in a nitrogen environment was found to produce layers of a similar conductivity to that of indium tin oxide and the lithium doping was found to result in higher conductivities in annealed layers.

The study of molybdenum oxide focuses on its application as a hole injection layer included in the anode contact of organic light emitting diodes. The deposition temperature was found to have a large effect on the resulting device efficiencies. This effect was determined to be due to variation of the work function and ion ratios present in the molybdenum oxide layer with deposition temperature. This work resulted in the fabrication of devices with efficiencies double that of the standard solution processed hole injection layer.

Contents

List of abbreviations

PPV: P-Phenylene Vinylene
HOMO: Highest Occupied Molecular Orbital
LUMO: Lowest Unoccupied Molecular Orbital
OLED: Organic Light Emitting Diode
HTL: Hole Transport Layer
ETL: Electron Transport Layer
ITO: Indium Tin Oxide
PEDOT:PSS: Poly(3,4-ethylenedioxythiophene):Poly(styrene sulfonic acid)
ZnO: Zinc Oxide
MoO_3/MoO_x: Molybdenum oxide
WO_3 : Tungsten Oxide
V_2O_5: Vanadium Oxide
TiO_2: Titanium Oxide
ZrO_2: Zirconium Oxide
PET: Polyethylene Terephthalate
TGA: Thermogrametric Analysis
AFM: Atomic Force Microscopy
UPS: Ultraviolet Photoelectron Spectroscopy
XPS: X-Ray Photoelectron Spectroscopy
SCL: Space Charge Limited
AmMo: Ammonium Molybdate Tetrahydrate
$Mo(Acac)_2$: Bis(acetylacetonato)dioxomolybdenum(VI)
AZO: Aluminium Zinc Oxide
PLD: Pulsed Laser Deposition
NiO: Nickel Oxide
α-NPD: *N,N*'-Di(1-naphthyl)-*N,N*'-diphenyl-(1,1'-biphenyl)-4,4'-diamine
PFO: Polyfluorene
F8BT: Poly(9,9-dioctylfluorene-alt-benzothiadiazole)
PLED: Polymer Light Emitting Diode
PFB: Poly(9,9- dioctylfluorene-co-bis-N,N-(4-butylphenyl)-bis- N,N-phenyl-1,4-phenylenediamine)
TFMO: poly(9,9- dioctylfluorene-co-N-(4-methoxyphenyl)diphenylamine)
TFB: poly(9,9-dioctylfluorene-co- N-(4-butylphenyl) diphenylamine)
$(PPy)_2Ir(acac)$: Bis(2-phenylpyridine)(acetylacetonate)iridium(III)
26DCzPPy: 2,6-Bis(3-(9H-carbazol-9-yl)phenyl)pyri- dine
TCTA: 4,4',4''-tris(N -carbazolyl) triphenylamine

List of figures and tables

1 Introduction

The development of inorganic semiconductors and the devices that are constructed from such materials is an extremely important technological development of the last century. It is difficult to over-exaggerate the effect of such technologies on the development of human society, and developments in transistor, light emitting diode and solar cell technology, as shown in Figure 1, as well as whole host of other technology areas, continue to improve these devices.

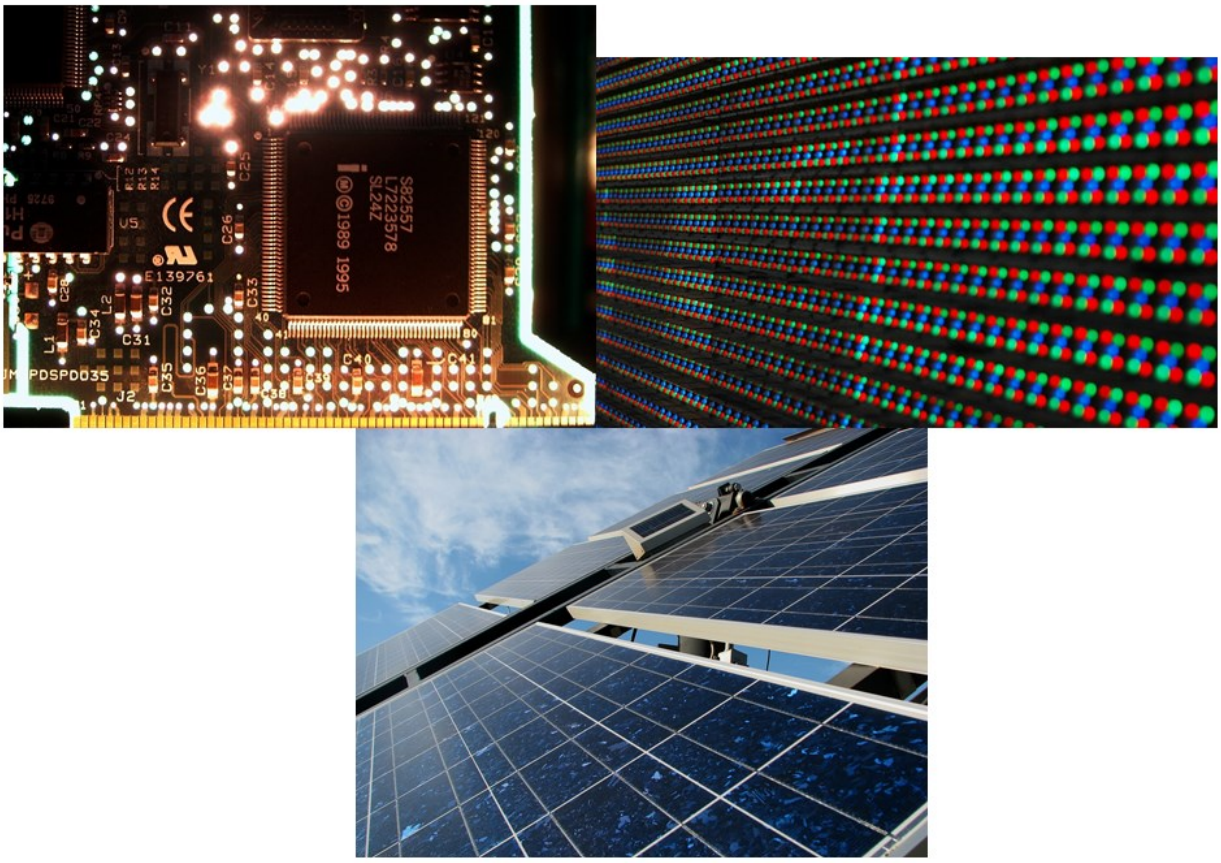

Figure 1: Some examples of devices based on semiconducting materials. From the top left these are transistors assembled into computer chips, light emitting diodes and solar cells.[1]

However, inorganic semiconductors suffer from a number of fundamental limitations which, despite the progress made in their development over the last 50 years, may make them undesirable for future use. In particular, the fabrication of inorganic devices typically requires extremely pure materials as well as high temperature and high vacuum processing. These requirements lead to the need for a certain style

of manufacturing that prevent reductions of cost of devices and also requires a large financial commitment to build a production line suitable for device manufacture.

It is these factors which have resulted in the large interest in the possibility of organic semiconductors, first discovered in the 1960s.[2]The possibility of using organic materials to produce electronic devices, along with the associated changes in manufacturing technique, have driven research in the area of plastic electronics in the last fifty years. Some examples of organic electronic devices include high definition televisions and mobile phones made by companies such as Panasonic and Samsung.

Organic semiconductors

The major differences in the manufacturing requirements of inorganic and organic semiconductors arise from the physical differences between the materials that give them their properties. Fundamentally the properties of inorganic semiconductors are due to their atom based crystalline structure and the periodic lattice that this provides.

In contrast to this, the properties of organic semiconductors are due to the molecular structure of the material. The crystalline or amorphous nature of the organic material also has a large effect on the physical properties of the material, but is not responsible for the fundamental semiconducting properties.

This leads to the two distinct advantages. As the properties of the material are not necessarily dependant on the presence of a crystalline structure, features of the fabrication process of inorganic semiconductors normally required to produce this, such as extremely high purity materials as well as high temperature and vacuum processing, can be discarded.

The dependence of material properties on molecular rather than crystalline arrangement also greatly increases the opportunities for the discovery of new materials. The effectively infinite combinations of different functional groups and structures available offer a large scope for producing materials with desirable or unusual properties. This is in contrast to the inorganic field where influence on the material properties has traditionally been limited to doping of the crystal lattice with other elements, although the more recent developments in the field of nanotechnology have shown that these limitations can be overcome by reducing the length scales of the materials. Quantum confinement then provides a new parameter to influence the behaviour of the material, the most publicised example of this technique being that of quantum dots.[3]

However, there are currently various limitations of organic semiconductors that prevent their widespread adoption as the material of choice in modern electronic devices.

The focus of this project is on the specific problem of the electrode systems for organic electronic devices, that is the materials responsible for bringing carriers to or from the active layers of the device. Two major problems exist with development of contact layers for organic devices when compared to previous work on inorganic materials.

The first of these is the nature of the band structure of the materials involved. When inorganic materials are used to fabricate semiconducting devices, p or n type doping can be used to manipulate the energy levels of the material to achieve the desired properties, for example in a p-n junction. As the physical behaviour of organic semiconductors is molecular in origin, doping processes occur in a different manner, and cannot be used to manipulate the electronic structure of a device in the same way, although doping can be used as a strategy to increase the conductivity of carrier transport layers.[4] Organic semiconductors often have deep energy levels that places a stringent requirement on the contact materials used in the device.[5]

The second issue is related to typical deposition methods of semiconductor materials. As has been mentioned, one of the major advantages of organic semiconducting materials is the lower energy non-vacuum processes that can be used to deposit them. This advantage is diminished, however, if other layers used to fabricate the device still require higher energy vacuum techniques to deposit. One of the final goals of the applications of organic semiconductors is to fabricate devices using only low energy deposition techniques, which requires every layer in the device to have been deposited using such techniques.

The aim of this project is to investigate one of these lower energy deposition methods, that of spray pyrolysis, and apply it to the deposition of some of the layers required for the operation of organic semiconducting devices. In particular, the project concerns the spray pyrolysis of the metal oxides zinc oxide and molybdenum oxide in those devices. Spray pyrolysis is a particularly interesting technique in its potential for large area high speed deposition of material, and although its application as a deposition technique has long been a topic of study, the specific application of the technique to the field of organic electronics is relatively unknown. This project hopes to explore the deposition technique with application to the field organic electronics. The experimental focus of the project was specifically on fabricating organic light emitting diodes, but as the work performed is on contact materials the results

obtained are applicable to the organic electronic field in general, as the layers can be incorporated in various types of semiconducting devices.

2 Background Theory

2.1 Introduction

This section aims to give the reader the necessary context for the experimental work performed in this project. This section is thus divided into three sections which represent the main background of the project.

The first section details with the basic theoretical background associated with organic semiconductors and physics associated with contacts formed of semiconducting materials. A brief introduction to the two categories of organic semiconductors will be given, and some of the differences between the physics of inorganic and organic semiconductors will be described. This will be followed by a discussion of the basic physics of interfaces between materials. The effect of the physical properties of materials on the interface that forms at a contact between those materials will be discussed.

The second section deals with the common device structures used when fabricating an organic semiconducting device. This section aims to give the reader a background in the common layers and overall structure used to fabricate an organic device. The section will then deal with some of the general considerations for layers that are going to be incorporated into a device stack, such as roughness and transparency.

The third and final section then describes some of the currently used layers in organic semiconducting devices. This section aims to give the reader context as to the current state of the art for contact layers in organic semiconducting devices. Current research and development on various types of layers will be discussed, along with the typical layers used for comparison to new developments. This will allow the reader to compare the experimental results obtained in the body of the work to the current state of the art.

2.2 Organic semiconductors

Small molecule and polymer organic semiconductors

Immediately, it is useful to draw a distinction between the two main branches of organic semiconductor research. All organic semiconductors are defined by the presence of π-delocalised electron systems in their structures. The overlapping of these delocalised systems produces the semiconducting behaviour of the material.

However, organic materials can then be divided into two distinct groups, those of small molecule structure and those of polymer structure.

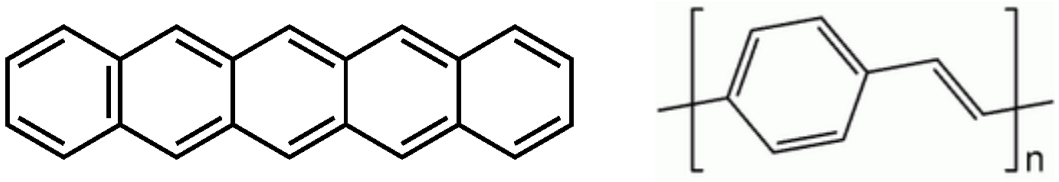

Figure 2: Pentacene, (Left) and Poly(p-phenylene vinylene), or PPV. (Right) Pentacene is an example of a small molecule organic semiconductor that can be used to produce organic transistors. PPV is an example of a polymer organic semiconductor that can be used as an emitting layer in light emitting devices

Pentacene is an example of a small molecule organic semiconductor, and is shown in Figure 2. Small molecule organics are usually processed using physical deposition methods such as evaporation due to their insolubility. Physical deposition techniques produce films with relatively high luminescent efficiencies, and as a result most commercial applications in displays of organic semiconductors have been based on small molecule materials.

The other class of organic semiconducting materials are polymers. Poly(*p*-phenylene vinylene), or PPV, as shown in Figure 2,was the first conjugated polymer to be successfully incorporated in a light emitting diode.[6] Polymer semiconducting materials are deposited using solution processing. Although solution processing does have various advantages over physical deposition methods, the luminescent efficiencies of polymer semiconducting materials has traditionally been lower than small molecule materials.[7] In contrast to this, in the photovoltaic device area conjugated polymer and fullerene blends have achieved higher efficiencies, as the solution processing techniques available lend themselves to forming a bulk hetrojunction structure.[8]

The distinction between these two classes of material is important due to the differences in the way they are fabricated. Although they may have better properties, small molecules are typically deposited using methods similar to that of inorganic semiconductors, although research is being performed into overcoming this barrier.[9,10] In contrast to this, polymer materials are deposited using solution processing that has advantages such as higher possible throughputs and reduced limitation on substrate size.

The HOMO and LUMO level

The energy levels of semiconducting materials are an important property when understanding their behaviour in devices. In organic materials, the analogous features to the valance and conduction band of an inorganic material are the highest occupied molecular orbital and lowest unoccupied molecular orbital, or HOMO and LUMO respectively.

The origin of these energy levels is the hybridised energy levels of the carbon atom. The presence of SP^2 hybridisation or 'double bonds' in a molecule leads to the presence of an electron state orientated perpendicular to the bond between carbon atoms. This π-delocalised system can either be in phase or out of phase with neighbouring systems, in what is known as the bonding and anti-bonding states respectively. If two interacting atoms are considered, this results in the splitting of the single atomic energy level into a lower energy π state and a higher energy π* state. The two electrons available in the π delocalised system then occupy and fill the π state leaving the π* state empty.

The Hückel approximation, which describes a 1-D π-delocalised system as a linear sum of atomic orbitals, can then be used to describe a π-delocalised system containing 2N atoms. The additional orbitals cause the splitting of the molecular energy levels into 2N states, the bottom half of which are filled by the available 2N electrons, leading to N filled states with N empty states lying above them. It would be expected that such a system would show metallic behaviour. However, the materials instead show semiconducting behaviour. This deviation is explained in terms of Peierl's distortion, which considers that the polymer chain does not form a chain of equally spaced atoms, instead forming a dimerised chain. This effective doubling of the lattice period opens a band gap between the highest π state and the lowest π* state of the delocalised system, resulting in semiconducting electronic behaviour.

The energy required to remove an electron to vacuum from the HOMO of an organic polymer is termed the ionisation potential. The energy required to place an electron into the LUMO is termed the

electronic affinity. The values of these quantities for some common organic materials are shown in Figure 3.

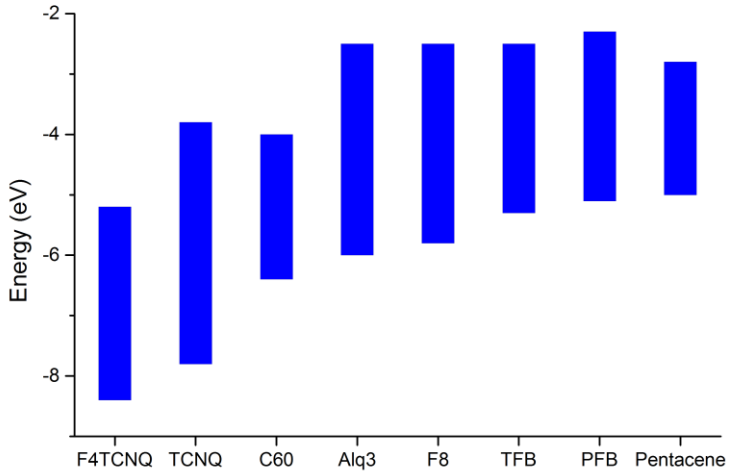

Figure 3: The HOMO and LUMO levels of some common small molecule and polymer organic semiconductors.[5] The columns indicate the band gap of the materials, with the HOMO and LUMO levels being present at the bottom and top of the column respectively.

Carrier types

Another important consideration when working with organic semiconductors is the nature of carriers responsible for charge transport. In inorganic semiconductors, charge transport is usually dominated by free electrons and holes moving in the conduction and valance bands. In organics, charge transport is due to polarons.

In an inorganic semiconductor, electrons in allowed Bloch wavestates are considered to be delocalised across the crystal and free to move through the crystal lattice. However, this long range order does not necessarily exist in an organic structure. Transport is considered to instead take place via 'hopping' of electrons between the ionic centres of the chain, both along the polymer backbone and also between distinct polymer chains. This hopping process is governed by the overlap of the electronic wave functions of the two states. However, the presence of the electron on the atom causes a change in the surrounding molecular arrangement. This 'lattice relaxation' of the molecule associated with the electron and hole causes a shift in the energy levels of the states away from the HOMO and LUMO

levels, and the combined electron or hole and associated lattice relaxation is termed an electron polaron and hole polaron.

Another important species in organic behaviour is the exciton. When an electron is excited to the conduction band, leaving a hole in the valance band, it is possible for the pair to become bound together by the coulomb interaction between the oppositely charged carriers. If the carriers become bound in this way, they can diffuse through the crystal structure as a single neutral particle which is termed an exciton. The potential gained though the coulomb attraction between the two charges is termed the exciton binding energy, and results in the electronic transition associated with excitions being at a slightly lower energy than the band gap of a material.[11]

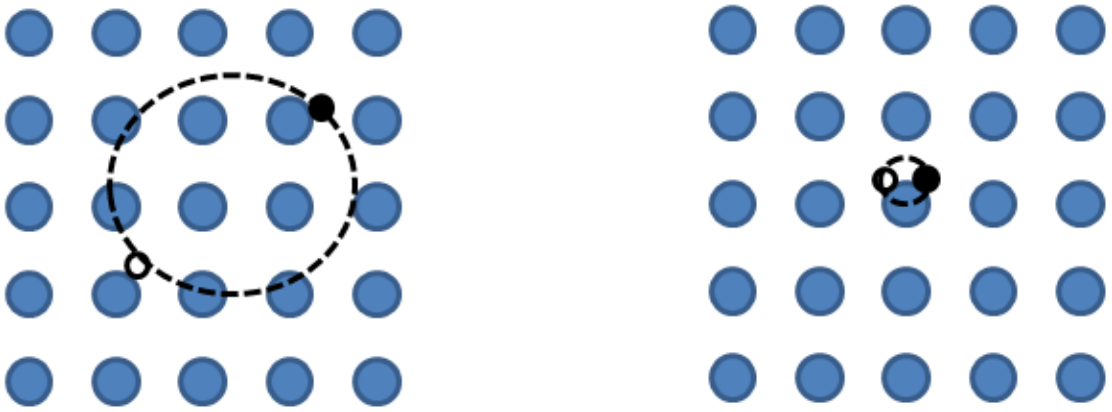

Figure 4: A schematic diagram of the two categories of exciton. The left image shows a delocalised Mott-Wannier excition of low binding energy, typical in inorganic semiconductors. The right image shows a localised Frenkel exciton with a relatively high binding energy, typical in organic semiconductors.

In inorganic semiconductors, the relatively large dielectric constant of the material usually results in screening of the coulomb interaction between the carrier pair, resulting in small exciton binding energies (<20meV) which are usually not stable at room temperature, resulting in the device properties being dominated by free carriers. Excitons of this type are termed Mott-Wannier excitons, whose low binding energy results in a hole-electron pair that is delocalised across multiple lattice spacings and can be easily dissociated.

In organic semiconductors, however, the dielectric constant of the material is usually lower, resulting in exciton binding energies of the order of 0.5eV. These Frenkel excitons are tightly bound, and the hole-

electron pair is thus localised on a single molecule. The exciton binding energy in this case is significantly higher than the room temperature energy k_BT, where k_B is Boltzmann's constant (0.025eV). Figure 4 shows examples of each type of exciton.

Excitonic properties have significant effects on organic semiconductor behaviour. One of the most important of these is that the nature of the interaction between the spin state of the electron and hole wavefunction leads to four possible excitonic states. One of these states has spin quantum number 0, and is referred to as the singlet state. The other three degenerate states have spin quantum number 1, and are collectively referred to as the triplet state.

These states are important as in organic molecules only the singlet exciton has an associated radiative decay process, known as fluorescence. As statistically it would be expected that only 25% of excitons produced would be in the singlet state, this greatly lowers the efficiency of emission from the material, as all triplet excitons decay non-radiatively. This is because radiative decay of a triplet state would require the change in spin of one of the species forming the exciton.[12] This problem can be overcome by the introduction of a dye in which radiative triplet decay, or phosphorescence, can occur. [13]This can theoretically allow 100% of generated excitons to emit a photon from the material, as the presence of the heavy metal allows intersystem crossing and the triplet to emit radiatively.[12]

2.3 Device Structure

The previous section dealt with some of the basic theory describing the interfaces in organic semiconducting materials. This next section will discuss the considerations when several different materials are selected and assembled into layers to form a working device.

Common device structure

The structure of the layers within the device is also an important consideration for optimal device performance. Fundamentally, at least three components must be present. These are the cathode and anode for electron and hole injection and an active layer for the emission of light. This basic structure in the case of an organic light emitting diode (OLED) is shown in the left image of Figure 5.

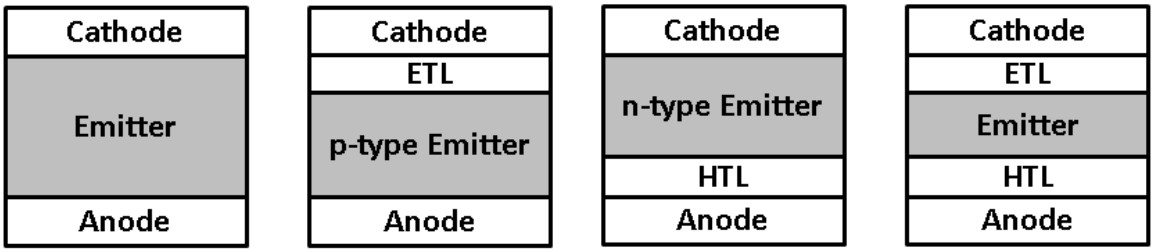

Figure 5: Common OLED architectures showing the most basic device structure in the far left image, utilising an electron transport layer in the left image, a hole transport layer in the right image, and a combination of both in the far right.[14]

For any device that requires the emission of photons either the cathode or the anode material must be at least semi-transparent. The efficiency of the device is then heavily dependent on the degree of transparency of the layer.

A schematic diagram of the energy levels and emission process in a device with basic structure is shown in Figure 6.

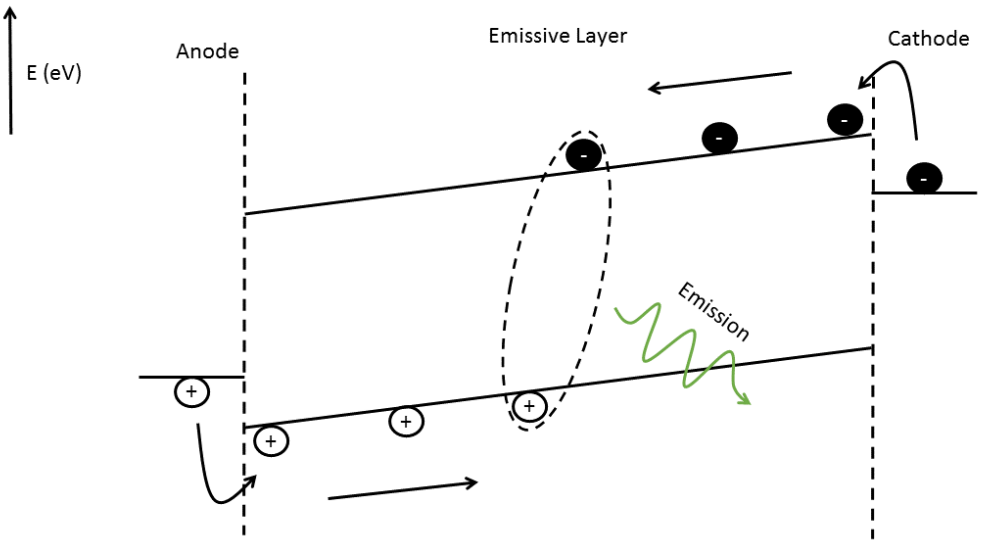

Figure 6: A schematic diagram of the emission process in a basic OLED. The black circles represent electrodes and the black circles represent holes. Holes are injected into the emissive layer from the anode. The holes must overcome an injection barrier to do so, which is the difference between the work function of the anode and the HOMO level of the emissive material. A similar process occurs for electrons at the cathode. The holes and electrons then move to an emissive zone in the device where they bind in an exciton and decay radiatively to emit light.

In a simple single layer device the structure places a large number of constraints on the organic material being used as an emitting material. High electroluminescent quantum yields are desirable for efficient photon production. The HOMO and LUMO levels of the material should be at the correct levels to facilitate maximum and balanced carrier injection from the cathode and anodes. This means in practice that the work function of the anode should be as deep as possible and the work function of the cathode should be a shallow as possible. This reduces the hole and electron injection barriers that are apparent in Figure 6 to as low a value as possible, which increases injection efficiency and therefore device efficiency.[15] The band gap of the material should be of the correct size to produce desirable spectral emission.[14]

In addition to this, high and balanced mobility of both electrons and holes within the material is another desirable property of the emission layer. This good carrier transport is useful as mismatched carrier mobility in a single layer device leads to relaxation and emission occurring close to either of the injection contacts of the device, a situation that reduces the overall efficiency of the device due to surface plasmon resonance with the injection contact material.[16] These various considerations give rise to an equation for OLED efficiency:

$$\Phi_{EL} = \Phi_{PL} \times \eta \times \Gamma_{S-T} \qquad \textit{Equation 1}$$

Where Φ_{EL} is the electroluminescence quantum efficiency of the device, Φ_{PL} is the photoluminescence quantum efficiency of the material, η is a charge balance factor and Γ_{S-T} is the singlet to triplet ratio. It should be clear that it would be very unlikely that any single material could exist that is ideal for all of these requirements. In particular, most fluorescent organic materials have either n-type or p-type transport characteristics with most of the relevant organic materials being p-type,[14] resulting in hole mobilities orders of magnitude higher than electron mobilities.

To produce devices of higher efficiency it is thus necessary to combine multiple layers which are optimised to perform one or more of the various requirements for a device. An emission layer can be chosen to provide the desired spectral output with as high a luminescent efficiency as possible. Carrier transport layers can be selected to reduce the injection barrier for the relevant carrier, as well as to block transport of the opposite carrier

If the example of an organic device using a p-type organic emission layer with an electron transport layer is used, with reference to Figure 6 it can be seen that a transport layer with a correctly selected conduction band or LUMO level will facilitate electron injection into the device by reducing the potential barrier for injection from the cathode. An extra layer would provide this function by having a shallower valance band than the cathode, leading to a reduced electron injection barrier. A correctly positioned valance band or HOMO level, on the other hand, produces a large potential barrier which prevents holes from reaching the cathode and recombining non-radiatively. A hole transport layer could also be added to this device if the correct material was selected to provide the opposite action at the anode. However, adding more layers to a device complicates the fabrication process, especially so when solution deposition is used.

Conductivity of contact layers

In the above treatment the injecting contact is considered to be an infinite reservoir of carriers, which is capable of injecting (or extracting) as many carriers as is required into the device. In addition to this, the injecting contacts must be capable of 'spreading' current equally across the entire surface area of the device to produce uniform emission in an OLED. This effect is shown in Figure 7.

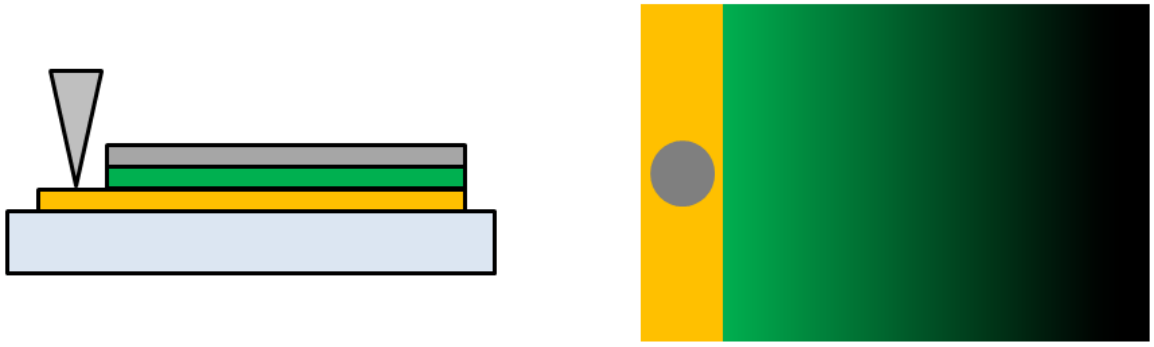

Figure 7: A schematic representation of the effect of a low conductivity material used as the contact in an emissive device. The left image shows the layout of the pixel, with the yellow layer representing a conducting layer and the green a emissive layer. When a voltage is applied at the connecting pin, the drop in potential across the conductive layer leads to a variation of light emission as shown in the right image of the pixel when viewed from below.

Silver is the material with the highest known conductivity of $6.3\times10^{5}Scm^{-1}$.[17] This value is characteristic of metals commonly used for semiconductor devices, such as aluminium. When dealing with a two-dimensional contact, the typical figure of merit is the sheet resistance of the contact, defined by:

$$R_{\square} = \frac{\rho}{d} = \frac{1}{\sigma d} \qquad \textit{Equation 2}$$

Where ρ is the resistivity of the material making up the contact, σ is the conductivity and d is the thickness of the contact. It is clear that to minimize the sheet resistance the conductivity and thickness of the contact should be maximised.

Although ideally the conductivity of a contact layer will be as high as possible, other requirements may conflict with this. In particular, one of the conductive layers in an optical device is required to be transparent. This is a major issue since the transparency and the conductivity of a material are correlated properties, as they are both dependant on the distribution of electronic states in the material.

Three metal oxides, those of indium, tin and zinc, can exhibit the property of remaining reasonably transparent while retaining a modest level of conductivity.[18] Tin doped indium oxide, or ITO, has been established as the most common commercial choice when choosing a transparent conduction layer for a device.[19] This is fundamentally because of the superior conductivity of ITO when compared to any other transparent conducting material.

Transparency of contact layers

The optical behaviour of any material can be described by the complex refractive index:

$$\tilde{n} = n + ik \qquad \textit{Equation 3}$$

The imaginary part of the refractive index, characterised by the extinction coefficient *k* is then related to the loss of intensity of light passing through the material by the absorption coefficient *α* and the Beer-Lambert law:

$$I = I_0 e^{-\alpha x} \qquad \textit{Equation 4} \qquad \textit{where } \alpha = \frac{4\pi k}{\lambda}$$

Where *x* is the thickness of the material and *λ* is the wavelength of the incident light. To achieve minimal absorption transparent contacts have been based on wide band gap metal oxides that have a low extinction coefficient at energies corresponding to visible light.[18] The thickness of the contact should also be minimised, but this must be balanced with the overall sheet resistance of the contact which will increase with decreased thickness.

Refractive index coupling

In addition to the absorption of a material, the behaviour of light at interfaces within the device is also a factor that must be considered. The reflection of light from an interface is determined by the Fresnel equations and at normal incidence is independent of polarisation:

$$R_p = R_s = \left(\frac{n_0 - n_1}{n_0 + n_1}\right)^2 \qquad \textit{Equation 5}$$

Where n_0 and n_1 are the refractive indices of the two materials that make up the interface. The Fresnel equations show that a material with a large refractive index will have a large reflection coefficient at an interface with air. This will result in light extraction from the device being difficult, and is a particular problem with inorganic semiconductors due to their relatively larger permittivity $\tilde{\varepsilon}$, and thus refractive index, which are related by:

$$\tilde{n} = \sqrt{\tilde{\varepsilon}} \qquad \textit{Equation 6}$$

Extraction is usually not as large a problem when working with organic materials due to their relatively lower permittivity than inorganics, but the inclusion of index coupling layers for increased extraction is an option available for improving efficiency.[20]

In contrast to this, it is usually desirable for the other contact to be as reflective as possible to maximize the output of light thorough the transparent contact of the device. This is usually easily achieved through the use of a metallic contact, but becomes a consideration if the geometry of the device does not allow for this. If the device is intended to be used in high ambient light conditions, however, the reflectivity of the back contact may need to be reduced to prevent the reflection of ambient light back out of the display.

2.4 Current contact layers

The previous two sections have discussed some of the basic theory and requirements of contact layers in semiconductor devices. This final section of the background theory deals with some of the materials commonly used in the contact structure, to give the reader a background for comparison with the work then performed later in the thesis.

The work in this project has focused on the anode contact structure, the section of the device responsible for hole injection into the device. This section will thus deal with the typical hole injection structure of an organic semiconducting device.

High work function metals

The ideal metal for use as an anode material is gold, with a work function value of 5.1eV[21] when clean. If injection into even lower lying HOMO levels is required, then platinum, with a work function value of 6.3eV[22], can be used. Gold is also a desirable contact material due to its chemically inert behaviour and thus chemical stability in air once deposited in a device as a contact material.

However, for devices requiring the emission or absorption of photons to operate, one of the contacts of the device is required to be transparent. Due to the convenience of the semiconductor industries past development of ITO as a transparent conductor, along with the lack of suitable transparent conducting materials to act as a cathode contact, the standard device structure requires a transparent anode contact. However, research into the so called inverted device structure, where the cathode is transparent, is ongoing.[23]

An approach to allow gold as the anode contact material in the standard device is to attempt to reduce the absorption of the gold layer. Examples of this include fabricating a layer as thin as possible to reduce absorption[24], where layers a thin as 7nm are used. Nano-structuring of the metal layer is another approach[25], where a percolating network of gold nanowires, for example, maintains conductivity levels while reducing the absorption of the films.

However, any attempt at reducing the thickness of the layer has a corresponding effect on the conductivity of the layer, and achieving properties comparable to ITO can be problematic. In addition to

this, most methods require extra processing steps to prepare the layer compared to contacts consisting of the bulk material.

Tin doped indium oxide

Indium tin oxide is the material of choice when considering a transparent contact in a device. Commercially available ITO has a resistivity value of $1\times10^{-4}\Omega$cm, which corresponds to a sheet resistance of $10\Omega_{\square}$ for a typical layer thickness of 100nm.[26] Commercial ITO layers are typically deposited via magnetron sputtering from an ITO target which is typically composed of 90% In_2O_3 and 10% SnO_2. ITO's work function is measured to be 4.45eV[27], although this value varies with contamination.[28]

Fundamentally, it is this conductivity that has made ITO the material of choice for use as a transparent conductor in most devices, as this is the property that allows devices to work at high efficiencies. However, ITO does have a number of disadvantages that have led to a large research effort in an attempt to replace it with other materials.

The first of these is the problem of the scarcity of indium as a raw material for use in devices. Supplies of the metal are considered under threat, and as the majority of indium production takes place in China, there is great interest in an alternative transparent conducting material to reduce the reliance of modern technology on indium.[29]

In addition to this, another issue with ITO with respect to plastic electronics is its lack of flexibility. While having good properties when deposited on glass substrates, ITO is not suitable for use in plastic electronics on plastic substrates.[30] This is due to the fact that flexing of the layer causes fractures in the crystalline structure, with a corresponding reduction in the conductivity of the material.

Another problem with the use of ITO is the temperature required to deposit a layer of good properties. To obtain a layer with high levels of conductivity, transparency and other properties that have an effect on device performance such as surface roughness, sputter coating at temperatures that are not plastic compatible is required.[31] Moderate properties can be obtained by sputter coating at room temperature, however.[32] The requirement for sputter deposition also can place limits on the physical size of the substrate due to limitations in the size of the sputter chamber, although the technique may be performed in a roll-to-roll process.

The research effort to improve the transparent conductors available has followed two main themes. The first of these is the attempt to find a replacement material with some of the desirable properties of ITO, while the second has focused on improving the properties of deposition techniques used both for ITO and for other materials.[9]

Solution processed materials

The materials discussed so far in this section are typically deposited using evaporation or sputtering processes. These techniques will be discussed in more detail in the next section. However, as has been discussed earlier, one of the main advantages of polymer semiconducting material is their compatibility with solution processing techniques. There was thus a need to develop contact materials that are also compatible with these fabrication methods.

Poly(3,4-ethylenedioxythiophene):Poly(styrene sulfonic acid) (PEDOT:PSS)

PEDOT is an electrically conductive polymer which is insoluble. The addition of PSS during polymerisation results in a water soluble transparent material that can easily be spin coated to form conductive layers.[33] The structure of PEDOT:PSS is shown in Figure 8.

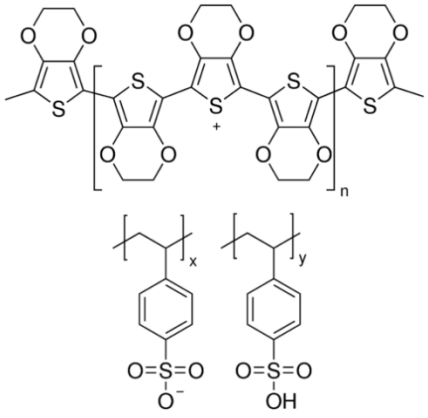

Figure 8: The chemical structure of Poly(3,4-ethylenedioxythiophene):Poly(styrene sulfonic acid) (PEDOT:PSS) a material commonly used in the contact structure of organic electronic devices. The top image shows the PEDOT component of the material, and the bottom the PSS component in its ionic (left) and acid (right) forms

PEDOT:PSS is incorporated into the anode contact structure for several reasons. The first of these is to reduce the surface roughness of the stack. ITO typically has a surface roughness of 3nm, depending on the surface treatments used.[34] PEDOT:PSS films can have surface roughness of lower than 1nm.[35] This reduced surface roughness is favourable for device performance. In addition to this, it has been found

that the ITO layer may act as source of oxygen leading to oxidation of the active layer, formation of quenching sites and thus degradation of the device.[36] The incorporation of a PEDOT:PSS layer blocks this degradation while still allowing charge transport.

In addition to this, PEDOT:PSS has a higher work function than ITO, measured as 5.1eV.[37] This means the inclusion of a layer can reduce the hole injection barrier present at the anode, leading to better charge injection into the device.

The conducting properties of PEDOT:PSS have led to interest in the possibility of therefore utilising the material as the sole contact for the device,[38] removing the need for the presence of ITO in the device and the limitations that come with this. Conductivities of over 1000Scm^{-1} have been achieved using various methods.[39] Various approaches are being applied to increase the conductivity of PEDOT:PSS, such as chemical modification of PEDOT as it is synthesised[40] or by doping the layer with additives to affect the morphology.[41]

These successes in improving the properties of PEDOT: have led to the ITO/PEDOT combined contact becoming the standard design used for the anode contact in polymer semiconducting devices.

Metal oxides

The inclusion of metal oxides into semiconductor devices began when ITO became the standard material to be used as a transparent contact. However, in recent years metal oxides as a general group of materials has been shown to increase the efficiency of organic semiconducting devices when incorporated into the contact structure.[42]

Examples of this include the incorporation of molybdenum oxide (MoO_3)[43], tungsten oxide (WO_3) [43] ,and vanadium oxide (V_2O_5)[44] in the anode contact, or the use of titanium oxide (TiO_2) [45] and zirconium oxide (ZrO_2)[23] in the cathode contact. The properties of metal oxides show a wide variation which is determined by the positions of the 4d bands of the metals and how these bands are filled.

The incorporation of metal oxides into organic devices to form so called hybrid devices has several advantages. The varied conduction and valance bands of the different metal oxides provides the opportunity for metal oxides to perform a number of different functions in the device, the main point of interest being the possibility of being incorporated into the anode or the cathode of a device.

In addition to this, metal oxides have been found to reduce the degradation of hybrid devices that they are incorporated into. This is due to the fact that in both the anode and cathode the metal oxide will usually be replacing a material such as PEDOT:PSS in the anode or calcium in the cathode. The strong bonding in the metal oxide lattice in most cases results in an increased resistance to degradation.

Many metal oxides have the additional advantage of a wide band gap, being around 3eV for several of the examples already mentioned. This results in the materials being non absorbing of visible light, allowing their inclusion in devices based on the absorption or emission of light without any increase in unwanted absorption and therefore decrease in device efficiency.

Zinc oxide

Zinc oxide is a material that has come under attracted considerable interest for a number of reasons. The first of these is that is has a wide band gap of 3.37eV.[46] This band gap has led to interest in the use of ZnO in optoelectronic devices for the blue and UV regions of the spectrum. In addition to this, ZnO also has a excitonic binding energy of 60meV[47], a large value for an inorganic material, and larger than k_BT at room temperature. This means ZnO is of interest for application in materials based on excitonic effects.

In addition to this, ZnO has shown the possibility for use in thin film transistors due to the relatively high mobility that can be achieved when deposited as a thin semiconducting layer in addition to advantages in ease of fabrication compared to other alternatives.[48,49]

There is also great interest in the use of doped ZnO as an alternative transparent conducting layer to ITO.[50] Zinc oxide's wide band gap as discussed above is the fundamental property that results in its transparency. The interest in zinc oxide in particular is due to the scarcity of indium as a raw material. Replacing indium with the much more common materials zinc and aluminium, in the case of aluminium doped zinc oxide, would be useful in the reducing dependence of the display and solar industries on a single material.

Finally, ZnO is also of interest for piezoelectric devices[51] and for its luminescent properties[52], as well as other niche applications.

Source of conductivity in Zinc Oxide

Zinc oxide forms crystals of the wurtzite lattice structure. Its work function is measured to be 5.3eV, although this is reduced to 4.5eV when doped with aluminium.[53] Zinc oxide films have in general been found to be n-type, although the cause of this property is under significant current debate.[54] The conduction and valance bands of ZnO have been calculated to be at 4.1eV and 7.5eV respectively.[55]

ZnO has been shown to have intrinsic n-type conductivity even when no intentional dopants have been introduced. This conductivity is assumed to be due to the presence of oxygen vacancies and zinc interstitials in the lattice.[56,57] However, there is current debate as to whether this is indeed the case, and impurities such as copper, as well as the possibility of hydrogen interstitials acting as shallow donors in the material have also been considered.[54] Nonetheless, the exact source of the n-type behaviour remains under discussion.

There are plausible dopants available to attempt to produce both n and p type zinc oxide. Possible donor materials include boron, aluminium, gallium and indium as substituents for zinc in the crystal lattice, as well as fluorine as a substituent for oxygen.[54] The possibility of hydrogen interstitials has also been discussed. In practice, by far the most common option considered is aluminium, and aluminium doped zinc oxide or AZO films will be discussed in more detail in the next section.

Theoretically, there are also several acceptor materials available to produce p-type zinc oxide, a material that would be very useful in allowing the fabrication of ZnO diodes and other optoelectronic devices. Lithium, sodium and potassium are possible candidates as substituents for zinc in the lattice, and nitrogen, phosphorus, arsenic and antimony are potential substituents for oxygen.[54]

There have been various attempts to use these acceptor possibilities to produce p-type ZnO films and devices based on such layers.[58–60] However, either there is no demonstration of a working device based on the layer, or there has been difficulty in reproducing the performance of such devices. So it can be seen that the p-doping of ZnO remains a controversial but interesting area of research.

Deposition of Zinc Oxide

The properties of an aluminium doped zinc oxide layer depend significantly on the method and conditions of the deposition of the layer. The standard method of deposition of an AZO film is sputter deposition.[18,61] However, there are a number of disadvantages to deposition of the layer through this method. In addition to the problems with sputter deposition described in the section dealing with ITO, depositing a uniform resistivity film through sputter coating has been shown to be difficult.[62]

There is thus an interest in an alternative method of depositing the zinc oxide layer, and two approaches that have been gaining in popularity are spray pyrolysis and pulsed laser deposition. Pulsed laser deposition, or PLD, is a process that is in some respects similar to sputter coating, except a high power pulsed laser beam is used to ablate the target instead of a ion beam.[63] PLD has been used to successfully deposit various transparent conducting materials, including ITO and AZO, with impressive levels of conductivity.[18]

Spray Pyrolysis of Zinc Oxide

As discussed in the previous section, zinc oxide has received significant attention for use as a transparent conducting material due to possible scarcity and price issues of relying on indium as a component material in indium tin oxide. The general advantages of spray pyrolysis have also been discussed in the experimental methods section, the main advantage being its scalability when compared to sputter deposition based techniques. This makes the technique particularly desirable when considering transparent conductors, which have significant use in many modern devices.

It can thus be seen that use of the spray pyrolysis technique to deposit zinc oxide as a transparent conducting layer would lead to significant reductions in the cost of fabricating electronic devices. Spray pyrolysis is particularly suited for the deposition as zinc oxide often requires doping to produce acceptable levels of conductivity in the material. Spray pyrolysis is particularly suited to the doping of materials due to the ease by which dopants can be incorporated into the layer by inclusion of a doping precursor in the initial spray solution.

There have been previous attempts to deposit doped zinc oxide as a conductive layer via spray pyrolysis. These methods use various different dopants[64] and spray precursors[65,66], but all the methods suffer from either an unacceptably high resistivity when compared to that of indium-tin oxide, or require a post deposition annealing step to achieve similar levels of conductivity.

In this work, the effect of adding additional dopants to the spray process is considered. Previous work has shown that the addition of small quantities of lithium to zinc oxide films prepared by spray pyrolysis can increase the mobility of the film when incorporated into thin film transistors.[67] It was postulated in that work that the increase in mobility seen was due to the lithium acting as a sintering aid and increasing the grain size of the deposited film.

Applying the same principle to the deposition of a conductive film may also lead to higher conductivities when deposited at a similar temperature to previous methods, or an equivalent conductivity achieved at a lower deposition temperature. Previous doping of zinc oxide with lithium has been attempted with the view of achieving p-type behaviour in zinc oxide,[58,68,69] and thus other possibilities with lithium doping have not been much investigated.

Molybdenum Oxide

Molybdenum oxide (MoO_x) has generated interest for use in anode structures in devices. A thin (<30nm) layer of MoO_x deposited between the ITO anode and the active layer of a device has been shown to produce a significant increase in the electroluminescent performance of the device.[43] The metal oxide layer is typically sputter deposited or evaporated onto the layer of ITO in the device.

However, the source of this improvement in device performance is under considerable debate. Part of the confusion arises from the fact that there are substantial variations in the literature as to where the fundamental energy levels of MoO_x are reported to lie.

In earlier studies, MoO_x is stated to have a work function of 5.4eV,[43] and the conduction and valance bands are reported to lie at 2.3eV and 5.4eV respectively.[70,71] It should be noted that these figures are quoted as recently as 2007. These values led to an explanation of the improvement in device performance consistent with these figures. It was explained that the low conduction band energy of MoO_x relative to vacuum, when compared to the LUMO levels of organic materials, for example 3.3eV in the case of F8BT, acted as an electron blocking layer. Correspondingly, the valance band at 5.4eV when compared to the work function of ITO at 4.5eV, was considered to improve hole injection into the deep lying HOMO levels of the organic semiconductor in the device by reducing the injection barrier. MoO_x was thus considered to be acting as an electron blocking-hole transport layer.

However, other more recent measurements have placed the conduction and valance bands of MoO_x at 6.7eV and 9.7eV, and the work function of around 6.8eV.[72,73] It should be noted that this is a change of approximately 4eV in the positions of the bands from what was considered previously to be the case.

The reason for such large variations in the measurements of the band energies is suggested to be contamination of the surface. Air contamination is shown to reduce the energy levels of MoO_x by approximately 1eV,[74] and residual water in devices has also been suggested to be responsible for the shift in the energy levels of the material.[72]

Methods of action of device improvement

The consideration of these new energy levels has led to a different suggestion for a model to explain the improvement seen through the use of MoO_x in a device. It has been proposed that hole injection is occurring at the interface between MoO_x and the organic material via the extraction of electrons to the conduction band of MoO_x.[73] This hopping process is possible due to the extremely low lying conduction band of MoO_x, and the presence of oxygen vacancies in the material giving rise to n-type behaviour with the Fermi energy lying close to the conduction band.[75]

However, this model has been challenged[42], as there are other oxides with conduction bands that are not deep enough for the hopping to occur, for example nickel oxide (NiO) on α-NPD, where the conduction band of the metal oxide is 2eV above the HOMO of the organic, yet an ohmic contact can still be obtained.

In addition to this, a further mechanism has been proposed as to the method of action of the MoO_3 layer, namely that of interfacial charge generation.[76] In this model, the offset between the conduction band of MoO_x and the organic layer is itself proposed to generate electron hole pairs thorough charge separation at the interface. The electron is then transported in the conduction band of MoO_3 to the anode, and the hole is transported in the organic layer to the recombination zone as normal. This mechanism is similar to the concept of interfacial carrier generation layers in stacked devices.[77] Evidence is suggested for this model in the improvement of current density of a device containing a hole blocking C_{60} layer at the ITO anode on the addition of MoO_x. The increase is attributed to the charge generation occurring at the MoO_x layer.

It can thus be seen that there are several models proposed for the action of MoO_3 in organic devices, and the method of this action remains poorly understood. In addition to this, although attempts have been made to investigate the widely varying energy level measurements, the effect of contamination and the deposition methods for MoO_x layers also remains poorly understood, offering an interesting opportunity for research.

Incorporation of MoO_x in OLED devices

The results discussed so far in this work have focussed on the use of metal oxides as a transparent conductive layer, and the modifications that can be made to such a layer to attempt to improve its

conductivity and thus lead to better functioning devices. However, metal oxides can also serve as useful layers for other functions in an organic electronic device, as has been discussed above.

A particular area of interest is that of carrier injection layers. Due to the deep HOMO levels of many organic semiconductors, for example Polyfluorene (PFO) at an energy of 5.8eV below vacuum,[78] the efficiency of a device is limited by the ability of ITO, with a work function of only around 4.8eV after oxygen plasma treatment,[79] to inject holes into the device. The use of PEDOT:PSS as an injection layer with a work function of 5.2eV[37] is the current standard layer used to improve the current injection of the device. The PEDOT:PSS layer also provides a smooth layer for deposition of further layers of the device structure. A schematic diagram of a typical green light emitting polymer light emitting diode (PLED) structure and the associated energy levels of the materials are shown in Figure 9.

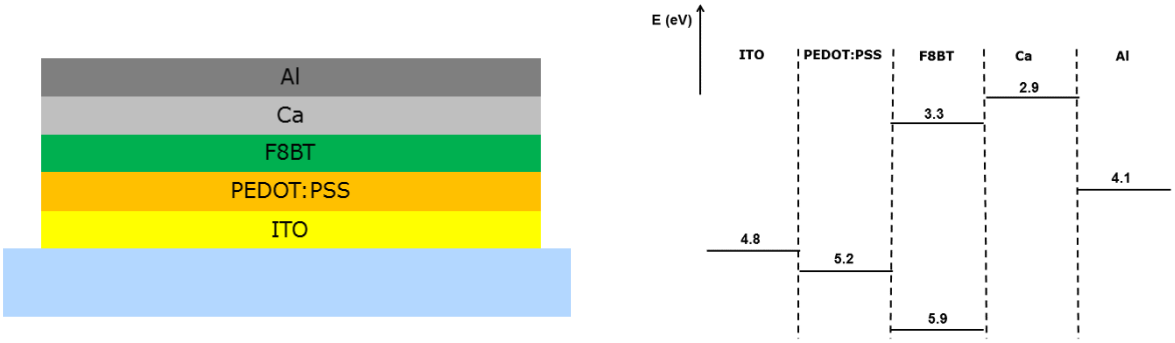

Figure 9: A schematic diagram (left) of the typical structure of a polymer organic light emitting diode. The thickness of each layer can vary depending on the materials used and the device concept. The energy levels associated with the materials are also shown (right). The emissive layer is Poly(9,9-dioctylfluorene-alt-benzothiadiazole) (F8BT)

It should be noted that PEDOT:PSS is generally used in polymer organic devices. This is due to the fact that when using small molecule organics, the range of materials available is larger due to the fabrication processes used. Evaporation techniques open the possibility of using metal oxides as injection layers[43], and indeed a thin evaporated layer of MoO_x has become the standard hole injection modification when evaporation techniques, and the associated high vacuum atmosphere that they provide, are available.[80] Evaporated MoO_x is attractive as a hole injection material due to its extremely low energy levels when maintained in a controlled environment.

It has also been shown that evaporated MoO_x can be utilised to improve injection to polymer organic semiconductors.[78] However, when considering the fabrication of working devices, using evaporation

techniques is not useful as the major advantage of polymer materials is their solution processablity, hence the continued reliance on PEDOT:PSS as material of choice.

Unfortunately, PEDOT:PSS does have disadvantages as a material. Its work function, although deeper than ITO, is still too low for ohmic injection into some polymer materials. In addition to this, the acidic nature of the material is a concern for the long term stability of devices.[81] It can thus be seen that alternative materials need to be investigated that retain the ability to be solution processed.

Solution processing of metal oxides has been investigated as a possible solution to these problems. Vanadium Oxide (V_2O_5)[82–84] and Molybdenum Oxide (MoO_x)[82–94] have both been investigated for this purpose. A number of different strategies were adopted in these investigations. Some use low temperature precursors that form metal oxide layers very easily but must be handled under a nitrogen atmosphere.[85] Some methods involve spin coating a solution of a precursor material after thermal[86,90] or chemical[83,87,88] treatment. As well as this, investigations have been performed using nanoparticle solutions.[89,93]

2.5 Conclusion

This chapter has intended to give the reader some of the context of the theoretical background of the project. To achieve this, three areas have been described.

The first section has described some of the basic physics surrounding the operation of organic semiconducting devices. This section described some of the fundamental material properties of organic semiconductors and compared these to their inorganic counterparts. The section went on to detail some of the consideration when interfaces are formed from these devices.

The second section of the background theory then described the considerations that result from these properties when fabricating actual devices from these materials. Basic device structure was described, along with some of the individual material properties that are desirable to achieve high efficiency organic devices.

The third and final section then went on to describe some of the materials that have been used to solve some of these issues in the actual fabrication of devices. The discussion of ITO and PEDOT:PSS is particularly important here, as they make up the standard contact that the later work in this project will be compared to. Finally, the concept of the inclusion of metal oxides into devices to improve their properties was introduced and two metal oxides that are the focus of this work, zinc oxide and molybdenum oxide, were discussed.

It is hoped that this chapter will have prepared the reader in full to understand the work presented in the remainder of the thesis, as well as understanding the general importance of the research on the development of contact materials for organic electronic devices.

3 Experimental Methods

3.1 Introduction

The next section of this thesis is focused on the main methods used for the deposition and characterisation of the contact materials studied in the project. It is divided into two major sections, discussing fabrication and characterisation respectively.

The first section deals with fabrication techniques used in the project. The second section then gives a brief description of each of the characterisation techniques used in the project. This section aims to describe what information can be obtained using each technique, along with some of the advantages and disadvantages of using them so that the results obtained can be understood in their full context.

When combined with the previous section, the reader should thus have full context for the interpretation of the results presented in the remaining sections of the thesis.

3.2 Fabrication Techniques

The method of the fabrication of the contact layers of a device has a large effect on the resulting properties.

Methods of fabrication can be divided into two major categories, based on either physical or solution deposition of the desired layer.

Physical deposition processes such as evaporation, sputter coating and pulsed laser deposition take place by evaporation or ablation of a source material through various physical methods. A key feature of these physical processes is that they are usually performed under vacuum to allow the atoms from the target to reach the substrate surface with sufficient energy to form a layer with the correct properties. This requirement for vacuum allows for good control of the fabrication atmosphere. However, the equipment required to produce these conditions limits the scalability of the process, particularly in the physical size of the substrate deposited on.

In addition to this, the high energy of the atoms reaching the deposition surface can become an issue if depositing onto a soft material, such as an organic layer, as the atoms may penetrate into a surface and cause changes to the behaviour of the interface. Physical methods remain the most common method for the deposition of the contact materials in most organic semiconducting devices. The anode, usually ITO, is sputter deposited onto the substrate, followed by the active layers of the device. The cathode, typically aluminium or calcium, is then evaporated onto the top of the device. These physical methods current remain the best way to produce contact layers with acceptable performance.

In contrast to this, solution methods, such as spin coating, spray pyrolysis and chemical vapour deposition usually involve depositing the layer in a solvent. As these techniques involve solvents or solvent vapour, no vacuum is present during the fabrication process. This greatly increases the flexibility of the technique in producing large area devices at lower cost. However if deposition environments are not maintained the possibility of contamination is increased.

In general, solution methods can be considered to be of lower energy than physical methods of deposition, in that molecules will not be arriving at the deposition surface with kinetic energy. This reduces the chance of penetration of lower layers or heating of the substrate. However, high temperatures may still be required for a deposition of materials with acceptable properties. In addition to this, the compatibility of solvents with the material to be deposited can cause significant problems.

Organic small molecule semiconductors are traditionally deposited using physical techniques such as evaporation. Organic polymer layers in contrast to this will usually be deposited by solution techniques, particular spin coating.

Substrate preparation

Both quartz and ITO substrates were used in this project. Both types of substrate were square and 12mm x 12mm in size. The ITO substrates were purchased with ITO deposited in a strip down the centre of the substrate with 1mm of space on each time. Substrates were cleaned in a clean room environment. All substrates used in the project were cleaned by wiping with acetone followed by sonication in acetone and iso-propyl alcohol for 30 minutes respectively. Substrates were then blown with nitrogen followed by drying in an oven for 10 minutes at 100°C.

Deposition by evaporation

Evaporating a material is one of the most common methods of vacuum deposition, along with that of sputter coating.

The technique involves the heating of a source of material in a vacuum environment, typically pressures of less than $1x10^{-6}$ Bar, although pressures of $1x10^{-9}$ Bar or less can be achieved in ultra-high vacuum systems. The low pressure of the chamber serves two purposes. The first of these is that the mean free path of molecules of material is increased to the order of the size of the chamber, meaning that atoms of the material to be deposited can travel from the source to the substrate without impacting air molecules. This allows the atoms to arrive at the substrate surface with enough energy to locate into ideal positions in the crystal lattice of the deposited layer and produce layers with higher quality then compared to solution processed methods.

This project required evaporated MoO_3 layers as a control layer to compare spray deposited MoO_x layers to. Evaporated MoO_3 layers were deposited at a rate of 0.3Å/s in a 5×10^{-7}mbar vacuum from MoO_3 powder purchased from Sigma Aldrich and used as received. OLED devices prepared in the project also used an evaporation deposited top contact of 20nm calcium followed by 200nm aluminium. Evaporated Ca layers were deposited at a rate of 0.3Å/s in a 5×10^{-7}mbar vacuum. Evaporated Al layers were deposited at a rate of 1nm/s in a 1×10^{-6}mbar vacuum. Both materials were purchased in pellet form and used as received in a nitrogen environment.

Deposition by Spin Coating

Spin coating, in contrast to evaporation, is the standard laboratory technique for solution processing of thin films of material. In a typical spin coating process, the desired material to be deposited is first dissolved in a suitable solvent. The solution is then dropped onto the deposition substrate which is rotating at high speed. This distributes a layer of the solution across the surface of the substrate, and a layer is deposited as the solvent evaporates.

Spin coating is typically performed in atmospheric conditions, although can be performed in a controlled environment if required. Substrates can also be heated prior to deposition, and will often be baked after the process to ensure all solvent has left the film.

PEDOT:PSS reference layers were obtained by spin coating solutions of AI-4083 which were purchased from Ossila and used as received. The solution was deposited onto the substrate, then spun at 1500rpm for 1 minute followed by heating at 110°C for ten minutes to produce layers of 60nm thickness. PFB, TFMO and TFB layers were prepared by dissolving the polymer to form 30mg/ml solution in p-xylene. The solution was then spin coated at 2000rpm for 1minute to produce layers 210nm, 165nm and 130nm thick respectively. F8BT emissive layers were prepared by dissolving the polymer to form 10mg/ml solution in p-xylene. The solution was then spin coated at 1500rpm for 1minute to produce layers 60nm thick.

Deposition by Spray Pyrolysis

An alternative solution based deposition method to spin coating is spray pyrolysis. In this method, a precursor to the desired material to be deposited is dissolved in a suitable solvent. A pressurised carrier gas is then used to spray this solution onto a deposition substrate, which will be held at a temperature high enough to induce thermal decomposition of the precursor into the desired final material. A diagram of the process is shown in Figure 10.

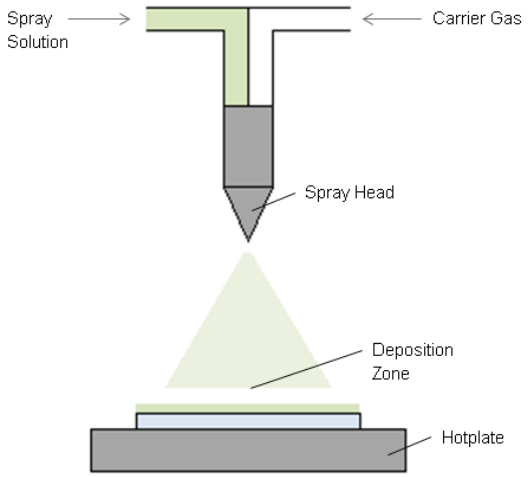

Figure 10: A schematic diagram of the spray pyrolysis technique. Precursor solution is sprayed onto a heated substrate using a pressurised carrier gas. The solvent evaporates and the precursor decomposes at the substrate surface to form the deposited layer.

Spray pyrolysis is an interesting technique due to the amount of control it provides over the deposition of the material involved. Fundamentally, the deposition process can occur in a number of ways:[95]

1. Solvent droplets reach the substrate surface and evaporate, leaving behind a solid that can further react in the solid state
2. The solvent evaporates before the droplet reaches the surface, leaving the dry solid to arrive at the surface where decomposition occurs.
3. The solvent vaporises and the solid then also melts and vaporises, the vapour then diffuses to the surface of the substrate where a vapour deposition process occurs.
4. The entire reaction takes place in the vapour phase.

To produce high quality crystalline films, process 3 is desirable, as it allows the effective vapour deposition of the product, preventing defects from evaporation of solvent but allowing the growth of the film at the substrate surface.

All precursors used for spray pyrolysis were purchased from Sigma Aldrich and used as received. were Zinc Acetate Dihydrate, Aluminium Nitrate Nonahydrate and Lithium Acetate Dihydrate as sources of

Zinc, Aluminium and Lithium in the deposited film respectively. Ammonium Molybdate Tetrahydrate and Bis(acetylacetonato)dioxomolybdenum(VI) were used in the deposition of MoO_x films.

All spray processes were performed using XL2000 0.4mm airbrushes. The airbrush was held vertically above a hot plate on which the substrates deposited on were present. For the results reported in chapters 5 and 6 of this thesis the spray distance was 30cm. The airbrush was provided with nitrogen gas at 2 bar pressure which was controlled using an electronic gas valve. The solvent used for all precursor solutions was methanol. Before and after the main spraying process 10ml of methanol solution was passed through the air brush to remove dust and clean the apparatus.

The spray process consists of repeated 5 second sprays followed by a 1 minute pause to allow the temperature of the substrate to be maintained. This process was repeated until a layer of the desired thickness was built up through the spraying of a selected amount of solution. This was 12ml for the depositions in chapter 5 and 5ml for the depositions in chapter 6.

Fabrication of devices

To investigate injection mechanisms, two types of devices were fabricated in this project.

Single carrier device were fabricated to investigate the performance of various injection layers. ITO substrates as cleaned above would then have the injection layer under study deposited onto them. Either PFB, TFMO or TFB would then be deposited on top of the layer as described above. Finally, a 5nm layer of MoO_3 followed by a 200nm layer of Al would be evaporated on top of the device through a mask to produce a contact pattern.

Luminescent devices were fabricated by the deposition of the relevant injection layer onto an ITO substrate. F8BT was then deposited onto the injection layer. Calcium and Aluminium were then evaporated on top of the layer as described above through an evaporation mask to provide contacts for the device.

3.3 Characterisation Techniques

Thermogravimetric analysis

Thermogravimetric analysis is a technique which involves the controlled heating of a sample of material. The temperature of the sample and its mass are monitored and compared to that of a reference.

As the temperature of the sample is increased, the monitoring of the temperature of the sample shows a differential. These differentials, along with the changes in mass of the sample can be used to determine changes occurring in the composition of the sample such as removal of water from the crystal or decomposition of the sample.[96]

The thermal analysis of the precursor materials was performed on a Stanton Redcroft STA 780 series simultaneous DTA/TGA instrument at a heating rate of 10°Cmin^{-1}.

Optical analysis

Optical analysis is a simple but very useful characterisation technique. The method is based on illuminating a sample with light of varying wavelengths. The light transmitted or reflected by the sample can then be collected and compared to a reference beam to determine its optical properties.

All UV-Vis spectra measured in this project were acquired on a Shimadzu UV-2600 Spectrophotometer.

Additional data was obtained from UV-vis spectra measured in this project using Tauc plots and by calculating the Urbach energy of films.

Tauc plots

A Tauc plot is an alternative plot of the absorption coefficient of a material, in which the photon energy is plotted against the quantity $(hv \propto)^{\frac{1}{r}}$ where $\propto$ is the absorption coefficient of the material and *r* is determined by the nature of the band gap of the material, equal to 0.5 for a direct band gap.[97] An example of a Tauc plot is shown in Figure 11.

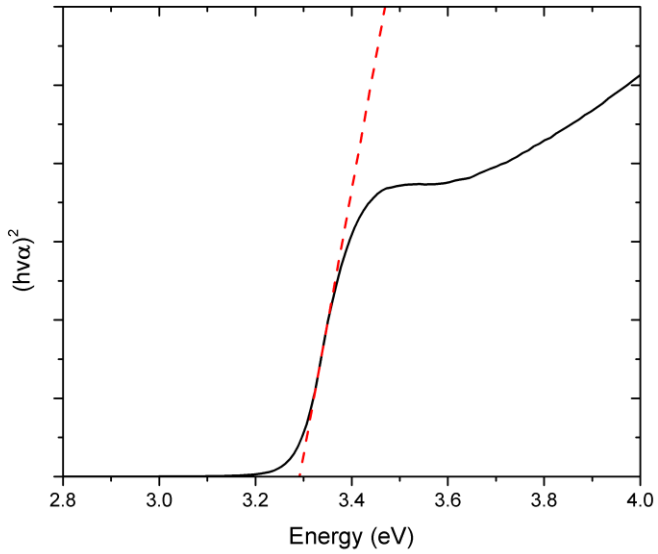

Figure 11: An example of a Tauc plot showing the linear regime of the absorption coefficient when plotted in this way. The linear regime can then be extended back to the energy axis to estimate the band gap of the material in question. The plot in this case if for a material with a direct band gap.

The purpose of the plot is to isolate the position of the band gap. At the absorption edge the relationship should be linear, with an absorption tail below this. By fitting the linear regime of the graph, the band gap energy can be estimated by calculating the intercept energy. In the case of the example figure this would be 3.29eV.

Tauc plots were performed for all of the films produced in chapter 5 of the thesis. The position of the slop was obtained by taking the first derivative of the curve obtained in the Tauc plot and taking a tangent at the point where the gradient of the curve was highest.

The Urbach energy

The behaviour of the absorption coefficient just below the band gap energy has empirically been measured to show an exponential tail off, known as the Urbach tail.[98] This takes the form:

$$\alpha(hv) = \alpha_0 exp\left(\frac{hv}{E_0}\right) \qquad \textit{Equation 7}$$

Where $\propto$ is the absorption coefficient of the material and α_0 and E_0 are material parameters. In particular, E_0 is a measure of the width of the exponential tail and has been suggested to be a measure of the structural disorder of the crystal.[99,100] A linear fit of the log of the absorption coefficient of a

material below the band energy can thus be used to extract the Urbach energy and provide an estimate of disorder in the crystal structure. The Urbach energy was calculated for all of the films produced in chapter 5 of the thesis.

Ellipsometry

Ellipsometry is another form of optical analysis. During the measurement, the sample of interest is illuminated with light of varying wavelength. The light incident on the sample is then collected onto a detector either in reflection or transmission. In the case of ellipsometry it is the polarisation state of the light collected from the sample that is used to determine information about the surface.

In the measurements performed in this project, two parameters were measured. These are Ψ, the ratio of the real reflected p and s polarisations of the reflected light, and Δ, the phase shift of the s polarised light relative to the p polarised component. These are related to the reflection coefficients r_p and r_s by:

$$\frac{r_p}{r_s} = tan\Psi e^{i\Delta} \qquad \textit{Equation 8}$$

The refractive indices of the material are contained in the reflection coefficients. In practice, this means that modelling is required to extract physical information about the material from the data obtained through ellipsometry. To facilitate this, Ψ and Δ are measured at multiple incidence angles and across many wavelengths. Modelling is then performed by building a set of ideal layers, calculating the associated Ψ and Δ values for the modelled system then comparing the modelled data to the measured data. By varying parameters such as the film thickness to improve the fit, information such as the refractive indices and thickness of layers in the measured system can be extracted.[101]

Materials can be modelled in a number of different ways. A standard model used for areas of the spectrum where a material is transparent is Cauchy's equation:

$$n(\lambda) = A + \frac{B}{\lambda^2} + \frac{C}{\lambda^4} + \cdots \qquad \textit{Equation 9}$$

Where n is the real refractive index of the material, λ is the wavelength of the incident light and A, B and C are the Cauchy coefficients of the material.

In this project, Ψ and Δ values were obtained using a J.A.Woollam Co VASE Ellipsometer at a wavelength range of 600nm to 1400nm at a 65°, 70° and 75° angle. Layers were then modelled using the first two

terms of the Cauchy equation to model their optical properties. The thickness of deposited layers were then estimated by comparison of these models to the Ψ and Δ values obtained in the measurement.

Surface profilometry and atomic force microscopy (AFM)

Both surface profilometry and AFM were performed on some layers in this project. Both techniques produce similar information on a material surface, but AFM provides surface information on a smaller scale than surface profile techniques.[102]

Surface profileometry was performed on the films using an KLA-Tencor alpha-step 200 surface profilometer. AFM measurements were performed using an Agilent 5500 system in close-contact tapping mode. The main purpose of the measurements was to calculate the surface roughness of the films.

Surface roughness in this project was calculated as the average deviation of the surface height, defined as R_a, or the root mean square average deviation, defined as R_{RMS}, where:

$$R_{a=} \frac{1}{n}\sum_{i=1}^{n}|y_i| \qquad \textit{Equation 10}$$

$$R_{RMS} = \sqrt{\frac{1}{n}\sum_{i=1}^{n} y_i^2} \qquad \textit{Equation 11}$$

Here y_i is the distance of any particular point of a surface from the average height of the surface.

Kelvin probe technique

The work function of the films was measured using a KP technology SKP5050 scanning kelvin probe system. A schematic diagram of the method is shown in Figure 12.

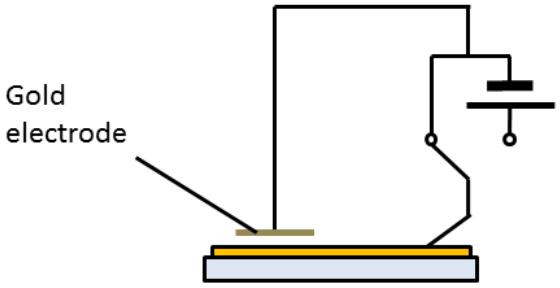

Figure 12: A schematic diagram of the operation of a kelvin probe. The exact layout of the components can vary, but the measurement involves bringing a reference electrode into close proximity to the surface and in some way measuring the induced potential between the surfaces.

A highly orientated pyrolysed graphite (HOPG) surface was used as a reference material to calculate the work function of the films.[103]

A Kelvin probe measurement records an average work function across the surface of the sample under the reference electrode, and can be performed under ambient conditions. These features result in a work function measurement performed under similar circumstances to that of the use of the layer in the fabrication of a device. However, the sample is required to be conductive, to perform the measurement.

Ultraviolet photoemission spectroscopy (UPS)

UPS scans were obtained using a He I source with an energy of 21.22eV with a -18.47V backing voltage. Analysis of the kinetic energy of the photoelectrons produces a spectrum of electron density with respect to energy. The work function of the films was determined by the position of the photoelectron cut-off in the spectrum.

UPS measurements require high vacuum. As this can affect the presence of contaminants on the surface of the material to be measured, the results obtained may differ from the properties of a material in atmosphere. The measurement is sensitive to the first 10nm depth of a material, as this is where the emission of photoelectrons will occur from. In addition to this, when used to measure a work function, due to the nature of the analysis of the spectrum, UPS will produce the absolute lowest magnitude work function of a surface, rather than an average value. There is also some evidence that the ultraviolet light used for the measurement can modify the work function of a surface.[104] These factors mean data obtained from a UPS measurement should be viewed in context with other analysis.

X-Ray Photoelectron Spectroscopy (XPS)

XPS scans were obtained using an Al monochromated X-ray source operated at 15kV, 5mA emission. The general survey scan was corrected to remove signal from a hydrocarbon contamination layer on the surface of the samples. The Mo ion ratos were obtained through fitting of the peaks associated with Mo 3d electrons to the $3d_{5/2}$ and $3d_{3/2}$ energies of the Mo^{+6}, Mo^{+5} and Mo^{+4} states

4-Point Probe technique

In the case of films intended to act as contact layers in a device, their conductivity is the most important factor. Conductivities in this project were measured using the four-point-probe technique, a schematic diagram of which is shown in Figure 13.

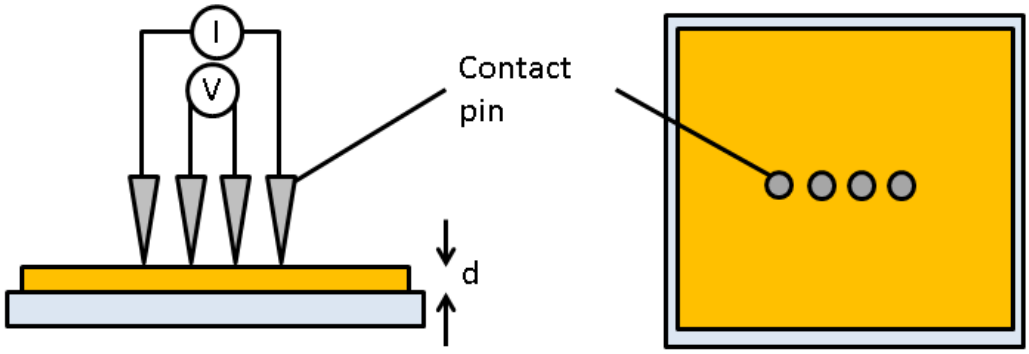

Figure 13: A schematic diagram of the four point probe technique, showing a profile (left) and plan (right) view. The technique is performed by bringing four equally spaced probes in a line into contact with the sample to be measured. A constant current is applied to the outer pair of needles, and a consequent voltage is measured across the inner pair. These values can be used to calculate the sheet resistance of the sample.

To perform an accurate measurement the spacing of the probes should be small with respect to the size of the samples. To calculate the sheet resistance of a sample, a geometric correction is also necessary. In the case of the samples used in this project, the sheet resistance $R_{\square}$ and resistivity ρ are calculated as follows:[105]

$$R_{\square} = \frac{\pi}{Ln2}\frac{V}{I} \qquad \rho = R_{\square}d$$

Where *d* is the thickness of the sample, usually measured in cm, and *I* and *V* are the current applied across and voltage drop measured across the pairs of contact pins. The probe spacing in the system using in this project was 0.5mm.

Measurement of devices

For luminosity measurements fully working devices were fabricated and a range of voltages applied and the current density and luminosity of the device were recorded. A schematic diagram of the measurement is shown in Figure 14.

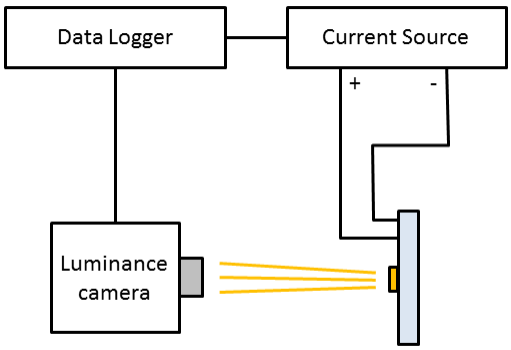

Figure 14: A schematic diagram of a luminance measurement of a light emitting device. The size of the sample device is not to scale. Samples sensitive to air or moisture may be contained within a sample chamber to perform the measurement.

The pixel of the device to be analysed is placed at the focal length of the luminance camera. Ambient light is minimized as much as possible during the measurement.

The data obtained can then be used to also calculate current and luminous efficiency of the device for comparison. Higher efficiencies imply improved carrier injection and blocking at the contact interfaces of the device, as well as better out-coupling of generated photons in the emissive layer.[106]

The luminous efficiencies of the prepared devices were measured in a N_2 environment in a sample holder using a Keithley Sourcemeter 2400 source measurement unit and a Minolta LS100 Luminance meter. The behaviour of the devices was measured from -5V to 10V in 0.2 V steps.

The rectification ratio of the devices was calculated as the ratio of current densities at identical forward and reverse voltages. 4V was used as a measurement voltage in this case.

Single carrier devices were analysed using an identical setup with no luminosity date being recorded.

3.4 Conclusion

This section of the thesis has intended to give the reader an overview of the experimental techniques, both in the fabrication of metal oxide layers and in the characterisation of layers produced.

The first section dealt with the various deposition techniques used.

The second half of the section then dealt with the various characterisation techniques that have been used in the project for the investigation of the films produced. Brief descriptions of each technique have been provided, along with some discussion of what is obtained from each measurement and some of the considerations that should be applied to the information received.

Understanding these techniques will then allow the reader to put the discussion of the thesis results into context in the next sections.

4 Development of the Spray Pyrolysis Process

4.1 Introduction

The general spray pyrolysis process has been discussed in the previous section. However, due to the number of deposition variables that can be changed, the process requires development of the particular precursors, solvents and technique used to produce various final layers.

In the case of zinc oxide, the basic deposition process has been studied in a reasonable amount of detail by previous work. Spray deposition of molybdenum oxide, however, has previously been studied in much less detail.

The first half of this section deals with the development of the spray pyrolysis process associated with the deposition of the zinc oxide film. Here, the decomposition processes associated with the precursors used for the study will be discussed. The basic observed properties of a zinc oxide film obtained through spray pyrolysis will then be considered. This will then allow the context of the changes to the film due to the doping process to be discussed in the main section on the doping of zinc oxide.

The second half of this section deals with the development of the spray process for the deposition of the molybdenum oxide layer. There is very little work in the literature on the spray deposition of molybdenum oxide, so this section deals with some of the basic experiments performed to obtain a layer of acceptable quality to perform a detailed study on. The decomposition of two possible precursors is considered, and test layers of molybdenum oxide are prepared with variations on several of the fundamental parameters of the spray pyrolysis process such as solution concentration and spraying distance. These experiments allowed a correct process to be determined to produce layers of a basic level of quality for further study.

This experimental section thus describes the optimisation of the spray pyrolysis process for the deposition of the two metal oxide layers, zinc oxide and molybdenum oxide.

4.2 Spray deposition of zinc oxide layers

Study of Precursors

The precursors are an important part of the spray pyrolysis process, as their decomposition is one of the key determining factors of the properties of the thin film that is achieved. The precursors used in this investigation were Zinc Acetate Dihydrate, Aluminium Nitrate Nonahydrate and Lithium Acetate Dihydrate as sources of Zinc, Aluminium and Lithium in the deposited film respectively. The chemical structures of the precursors are shown in Figure 15.

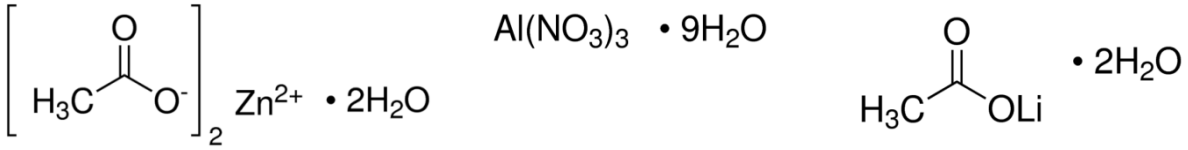

Figure 15: The three precursors used in this study: Zinc Acetate Hydrate (Left), Aluminium Nitrate Nonahydrate (Centre) and Lithium Acetate Hydrate. (Right)

Zinc acetate dihydrate has a molecular weight of 219g/mol and is readily soluble in methanol. Solubility can also be achieved in ethanol with the addition of 1% by weight of Ethanolamine. Aluminum nitrate nonahydrate has a molecular weight of 375g/mol and is readily soluble in methanol. Lithium acetate dihydrate has a molecular weight of 102g/mol and is readily soluble in methanol.

It should be noted that while the zinc and aluminium precursors are both soluble in methanol independently, it was found that after long periods in solution together a precipitate forms in the solution. To deposit films successfully the two solutions were thus prepared separately and combined to achieve the desired doping percentage immediately prior to the spray process.

Thermogravimetic analysis

The decomposition of the precursors is an important step in the spray pyrolysis process. Thermogravimetic analysis of the three precursor materials is thus presented in Figure 16.

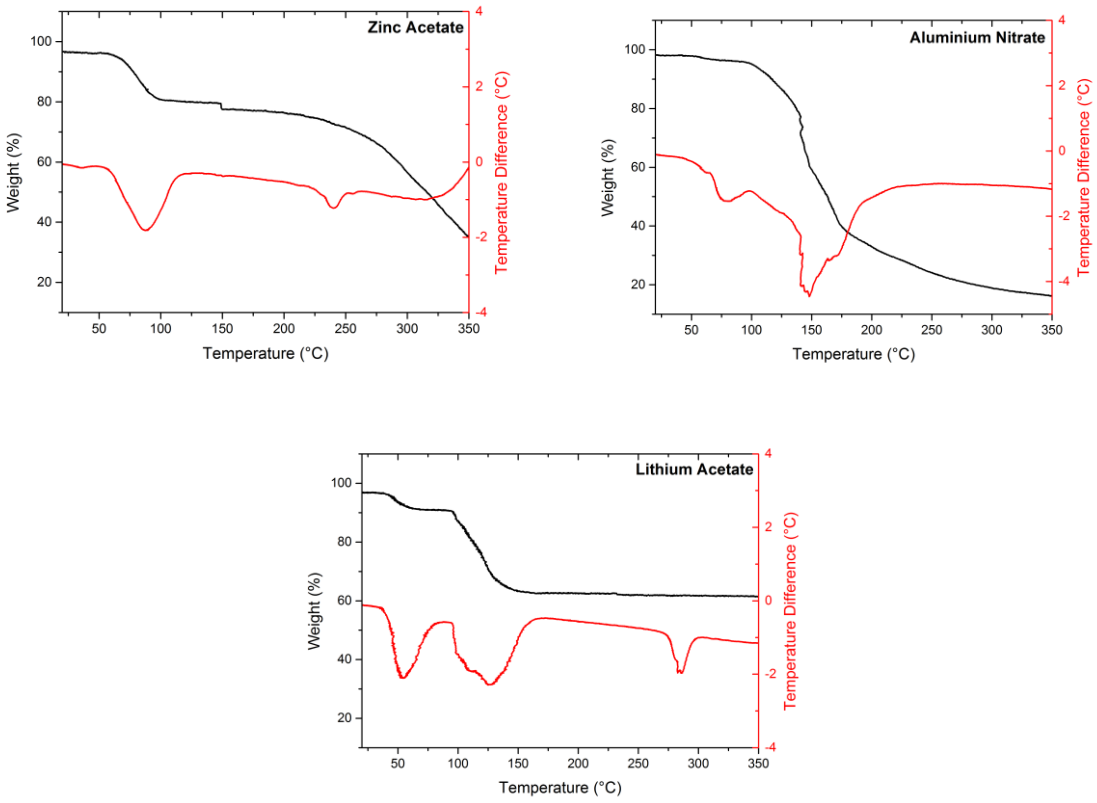

Figure 16: Thermogravimetric analysis scans of zinc acetate (top left), aluminium nitrate (top right) and lithium acetate (bottom). The scans were performed at a heating rate of 10°Cmin^{-1}.

The zinc acetate image shows an endothermic reaction and a 15% mass loss below 100°C. This is due to the evaporation of water from the crystal. A second endothermic process occurs at around 240°C and a second mass loss process begins to occur at a similar temperature. The endothermic process here is the melting of the precursor. The mass loss continues as the temperature is further increased to 350°C, and other studies have found this loss to be complete at 400°C.[107] This process is the conversion of the precursor into the zinc oxide final product. This suggests the conversion begins at 250°C, but may require higher temperatures to complete.

The aluminium nitrate image shows an endothermic process below 100°C, but there is no corresponding mass loss. This is the melting of the compound, found at 73°C. 60% mass loss of the sample then occurs between 100°C and 150°C in an endothermic process. This is the decomposition and conversion of the precursor into aluminium oxide. The mass loss does not appear to fully complete until a temperature of 350°C is reached.

The lithium acetate image shows three features. The first of these is an endothermic process associated with a small 5% mass loss beginning at 30°C. This is followed by a second endothermic process beginning at 100°C and completed at 150°C, associated with 25% mass loss. Finally an endothermic process with no associated mass loss occurs at 280°C. The processes at 30°C and 280°C are associated with the melting points of the hydrous and anhydrous lithium acetates respectively. The process occurring at 100°C may be the loss of water from the crystal.[108] If the peaks are assigned in this way, a decomposition process does not appear to occur below 350°C. Other studies have found lithium incorporation using the precursor at 400°C, however.[67]

The results presented in Figure 16 provide guidance on the range of temperatures that spray pyrolysis of zinc oxide layers may be achieved. The decomposition of zinc acetate hydrate would appear to be the limiting factor for the deposition of aluminium doped films, as the formation of zinc oxide appears to only begin at a minimum of 250°C, and may require higher temperatures to achieve good quality films. The decomposition of aluminium nitrate occurs at lower temperatures, so doping with aluminium would not be expected to be a problem. Incorporation of additional lithium into the film however, would seem to require a temperature of 400°C to be effective.

Initial spray experiments

The temperature at which the spray pyrolysis process is performed is an important variable when determining the properties of the as deposited films. Initial experiments involved the spraying of a non-doped zinc oxide film at various temperatures to determine the mechanics of the spray process. 0.1M concentration of zinc acetate solution in methanol at a spray distance of 15cm was deposited on quartz substrates, a method previously used for the spray deposition of zinc oxide.[49] Images of layers deposited at 200°C using the method described are shown in Figure 17.

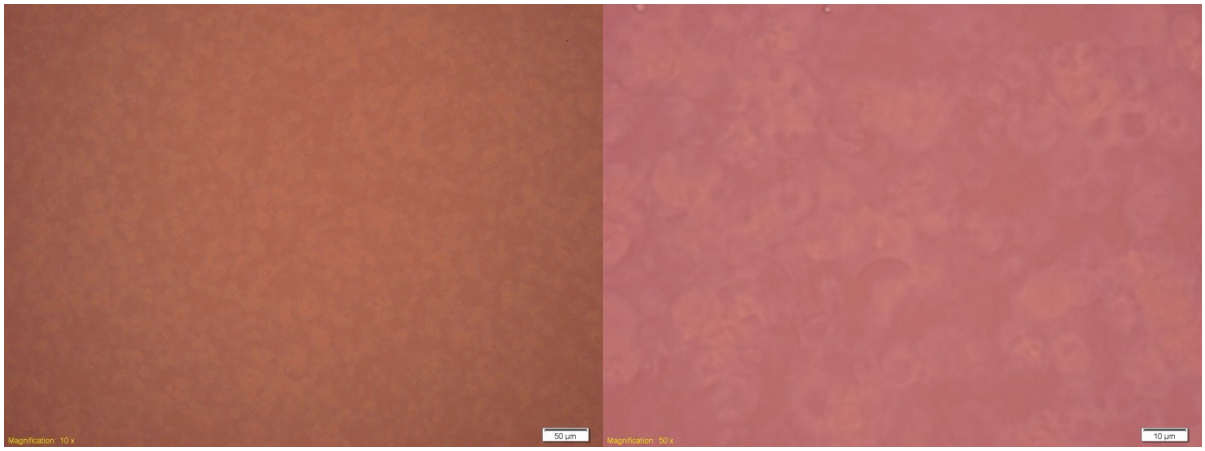

Figure 17: Zinc oxide layers deposited using the spray pyrolysis technique at 200°C. The left image has a scale bar of 50µm, whereas the right image shows a different area and has a scale bar of 10µm. The images are false colour.

It can be seen from the figure that although a layer has been formed across the surface of the substrate, the film has a textured appearance of small droplets. Due to the relatively low deposition temperature of these films, these structures are likely due to the slow evaporation of the solvent and only partial decomposition of the zinc acetate precursor used in the deposition process.

Images of layers deposited at a higher temperature are shown in Figure 18.

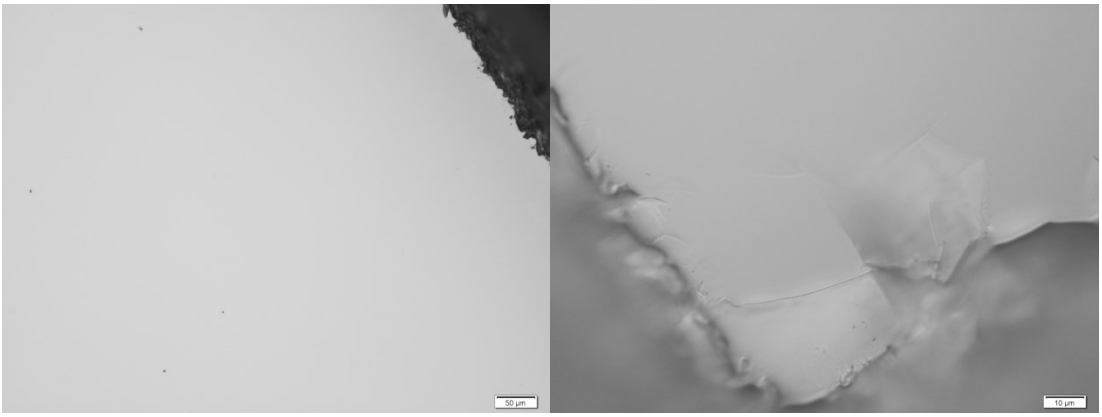

Figure 18: Zinc oxide layers deposited using the spray pyrolysis technique at 400°C. The left image shows the layer at a x10 magnification, whereas the right image shows a different area at x50 magnification

As can be seen in the figure, the spray deposition method at higher temperatures produces layers that are free of any defects or visible structure. In the right image of Figure 18, the edge of the zinc oxide film formed by the deposition process is visible due to the film not extending to the corner of the substrate.

As the layers are intended to act as transparent conductors, their light absorption is an important property that requires investigation. The transmission spectrum of the films also contains other useful information on the composition of the films. A measurement of the transmission spectrum of the pure zinc oxide films is shown in Figure 19.

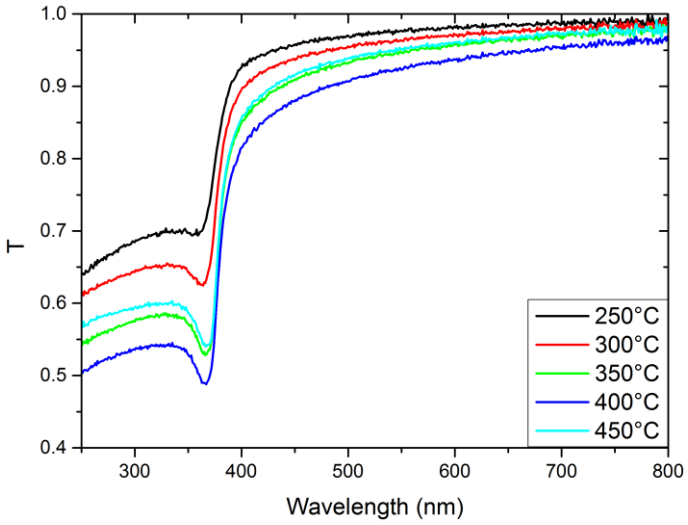

Figure 19: The measured transmission spectrum of zinc oxide films deposited using spray pyrolysis across a range of temperatures. The spectra have been corrected for the quartz substrate on which the deposition took place.

The basic form of the spectra shows that the films are largely transparent at energies below the band gap, although there is an reduction in transmission as the deposition temperature increases. All films then show an onset of absorption at 375nm, associated with zinc oxide's band gap energy, in this case calculated as 3.31eV. However, identification of the band edge absorption is complicated by the presence of an exciton resonance peak, located at 366nm or 3.39eV. As has already been discussed, zinc oxide has a large exciton binding energy of 60meV, and thus has measurable excitonic effects at room temperature. This peak is useful for determining the amount of crystalline order in the film, as its presence implies a high quality film is being formed. The absence of a visible peak at lower deposition temperatures where complete decomposition of the precursor is not necessarily occurring supports this.

Once into the absorption edge, the effect of the temperature of the deposition process is again more clear. The absorption of the films increases with increase in deposition temperature to a peak at 400°C, but then decreases for higher temperature depositions. The increased absorption of the films as the temperature is increased is due to the additional energy being available for precursor decomposition

and formation of the crystal lattice of the film. The decrease in absorption as the temperature is increased above 400°C is less well understood, but will be investigated in greater detail in the next section.

With this general understanding of the spray process for the formation of zinc oxide layers and the knowledge that high quality layers were being produced with the method, a detailed study of the doping process when other precursors were introduced to the spray mixture could go ahead. This study is reported in the next chapter of this thesis.

4.3 Spray deposition of molybdenum oxide

Precusors

As has previously been discussed, an important factor in the spray pyrolysis of any material is the precursor used for the deposition. For this investigation, two precursors were chosen as possible routes to achieving a layer of MoO_3. These precursors are Ammonium Molybdate Tetrahydrate and Bis(acetylacetonato)dioxomolybdenum(VI), and their chemical structures are given in Figure 20.

Figure 20: Ammonium Molybdate Tetrahydrate (Left) and Bis(acetylacetonato)dioxomolybdenum(VI) (Right), the two precursors investigated for deposition of MoO_3 by spray pyrolysis.

Ammonium Molybdate Tetrahydrate (AmMo) has a molecular weight of 1,234.86 g/mol. However, it can be seen that the basic molecular structure contains 7 molybdenum atoms. For a valid comparison between this and other materials, it is useful to consider concentrations of molybdenum ions/mol and thus divide relevant figures by 7. AmMo is readily soluble in water.
Bis(acetylacetonato)dioxomolybdenum(VI) ($Mo(acac)_2$) has a molecular weight of 326.15 g/mol, and is readily soluble in methanol.

Thermogravimetic analysis

The thermal decomposition of precursors is critical to the spray pyrolysis process, thus the investigation of the reaction of the precursor to heating is important. The TGA curves for the two possible precursors is thus shown in Figure 21.

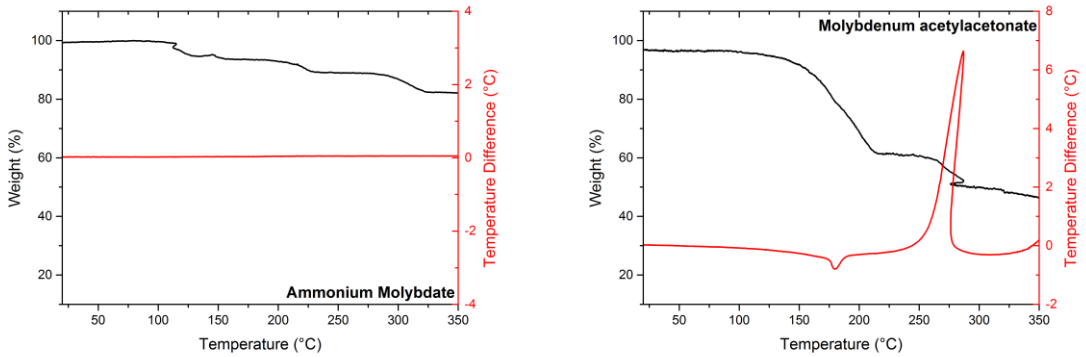

Figure 21: Thermogravimetric analysis of ammonium molybdate (left) and molybdenum acetylacetonate (right). The scans were performed at a heating rate of 10°Cmin^{-1}. The artefact in the right figure in the weight percentage curve at 260°C is likely due to the exothermic process occurring at the same point resulting in multiple data points at several temperature readings.

The left image shows that the AmMo precursor undergoes no apparent thermal processes when heated to 350°C. The compound does begin to lose mass at around 100°C, in a number of steps that results in a 15% mass loss when 350°C has been reached. The beginning of this loss at 100°C would suggest it could be the loss of water from the structure. This is similar to results obtained in other studies, and would suggest thermal decomposition of the precursor may not be taking place at these temperatures.[109] This would contradict previous studies which have suggested molybdenum oxide can be obtained from the annealing of aqueous AmMo without chemical processes if it is the case.[110]

The right image shows the decomposition of $Mo(acac)_2$. A 40% mass loss linked to a endothermic process occurs between 150°C and 200°C. The endothermic process is the melting point of the precursor at 184°C. However, the mass loss would suggest that the thermal decomposition of the precursor into molybdenum oxide may also be occurring around this temperature range. The second feature of the curves is an exothermic process occurring at 270°C. This feature is not seen in other studies of the material.[111] In this study, an exothermic peak is seen at a higher temperature of 510°C, which the authors suggest is the crystallisation of molybdenum oxide. The sol gel preparation of their material may have influenced its properties. The process here may be a crystal rearrangement, and could be associated with stoichiometric changes in the molybdenum oxide film.

The results presented in Figure 21 suggest that $Mo(acac)_2$ may be the more suitable material for the spray pyrolysis of molybdenum oxide films, and that 280°C may be a key temperature area for investigation.

Spectral analysis of precursor solutions.

The colour of precursor solutions used for solution deposition is discussed in literature, with some discussions reporting colouration[87,91], and others describing the solutions as colourless.[86] To investigate this, 0.1M solutions of AmMo and $Mo(acac)_2$ were prepared and their transmission spectra measured every 24 hours for the period of one week. Selected transmission spectra measured are shown in Figure 22. It is clear from the figure that little change has occurred in the spectra as the solutions have aged. Strong absorption onsets are evident beginning at 370nm for the AmMo solution and 435nm for the $Mo(acac)_2$ solution, as determined by the point where transmission drops below 0.9. These measurements suggest that the age of the solution is not a determining factor in the structure of the layer produced. This is encouraging for any applications as solution can be made up and used immediately or stored as required.

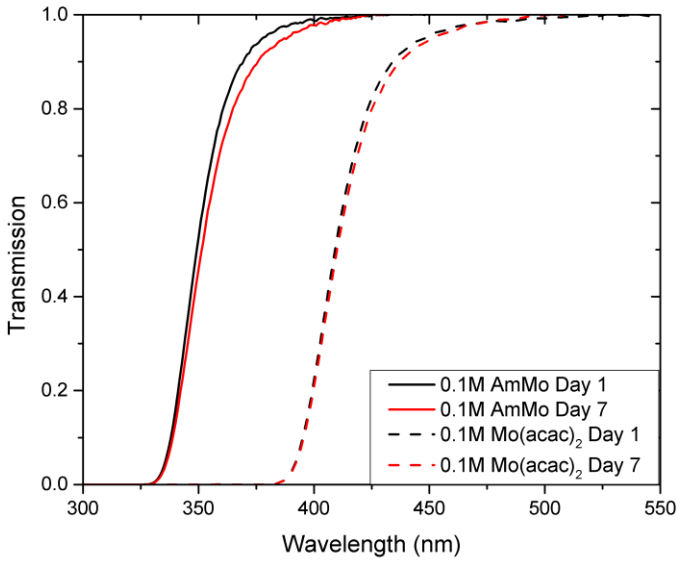

Figure 22: Transmission spectra of 0.1M solutions of AmMo and $Mo(acac)_2$ measured over a time period of 1 week. Only data from the first and final measurements are shown. Intermediate measurements show a gradual progression between these two curves. The spectra have been corrected for the absorption of the solvent.

Initial spray experiments

This section deals with the initial spray pyrolysis experiments with the two possible precursors. The carrier gas for the deposition was nitrogen in all cases, at a pressure of 2 bar. The depositions were

performed by spraying solvent for 3 seconds, then pausing for 1 minute, and repeating the process until the desired amount of precursor solution had been consumed. This process was followed to ensure that the substrate remained at the correct deposition temperature throughout the process.

To perform optimally as an injection layer, the MoO_3 should have as little optical impact as possible. That is, the layer should be non-absorbing and non-scattering to. It is also optimal for the layer to be as smooth as possible for the deposition of further layers. Optical microscopy of layers can give insight into these properties, as shown for example in Figure 23. The top left image shows a layer deposited with a relatively high precursor concentration at a close spraying distance. The roughness and non-uniformity of the layer are clear from the image, and it would be expected that this layer would perform poorly in terms of homogeneity as a hole injection layer. Its root mean square surface roughness, as measured by an alphastep profileometer, is 2µm, far too large for other layers to be deposited on top.

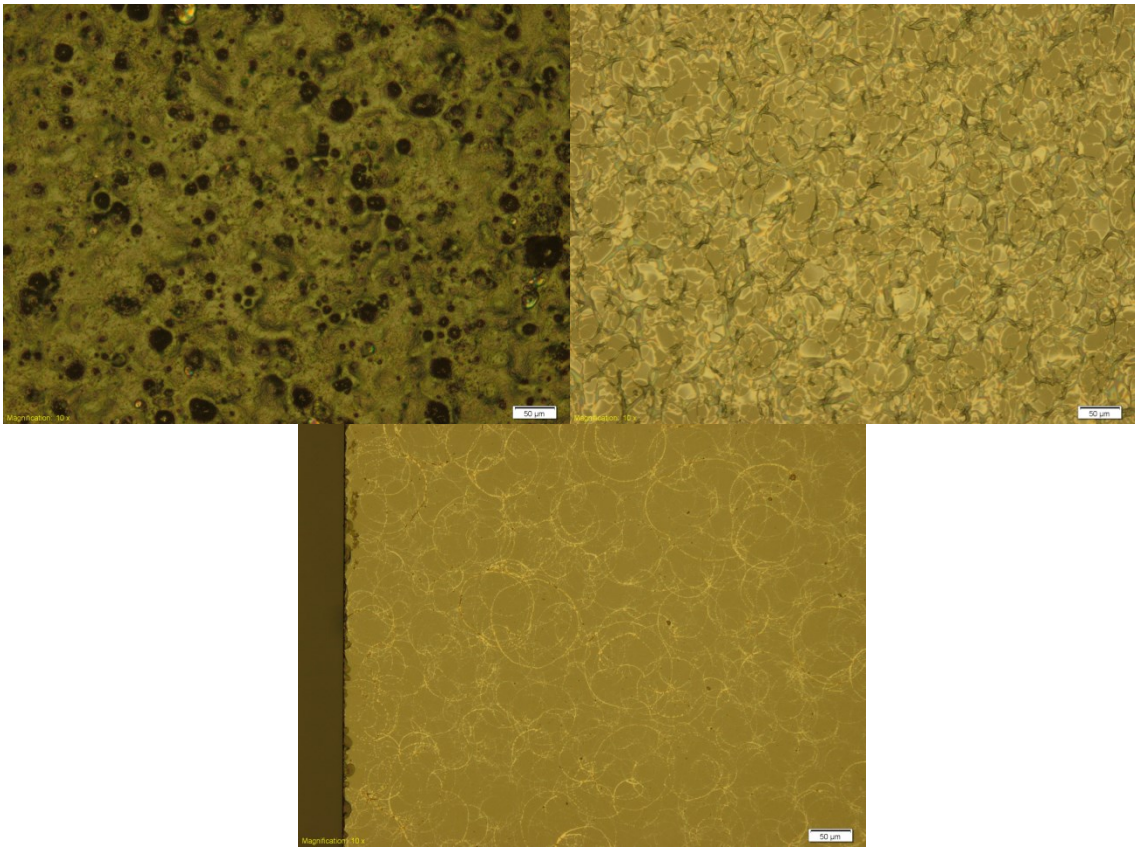

Figure 23: Optical microscope images of MoO_3 layers deposited using AmMo as a precursor material. The top left image shows a layer deposited at 350°C using 3ml of 0.0324M solution at a spray distance of 15cm. The top right image shows a layer deposited at 250°C using 3ml of 7×10^{-4}M solution at a spray distance of 15cm. The bottom image shows a layer deposited at 300°C using 5ml of 7×10^{-4}M solution at a spray distance of 30cm. The images are false colour.

The top right image of Figure 23 shows the effect of reduced precursor concentration on the deposited film. The image shows that the film now appears to be more uniform, with a lack of dark patches. However, it is clear that the film is cracking during deposition, and a measured root mean square roughness of 300nm indicates that the film is still too rough to use as an interlayer.

Finally, the bottom image in Figure 23 shows a layer deposited with an increased spray head to substrate distance. This image would suggest that under these conditions, solvent droplets are reaching the surface of the substrate before evaporating fully. This film has a root mean square surface roughness of 20nm. This surface roughness is still relatively high when considered for making good quality devices, as the surface roughness of PEDOT:PSS is usually measured to be 1-2nm. However, the images in Figure 23 illustrate the initial progress that was made to improve the quality of the thin film by adjusting some of the variables available in the process of spray pyrolysis, namely the distance of the spray head from the surface of the substrate.

It is clear in this case that the improvement in the quality of the layers is related to the rate of deposition of material at the surface of the substrate. A quicker rate of deposition, as a result of a higher precursor concentration or a shorter deposition distance, appears to be introducing too much material into the deposition area, leading to cracking of films or the possibility of un-decomposed precursor solution. A slower rate of deposition, through more dilute precursor solution deposited from a greater distance, appears highly desirable.

The solvent used for the deposition is also an important factor, as the rate of evaporation of the solvent used has an effect on the type of spray pyrolysis deposition occurring, as already discussed. [58] The use of $Mo(acac)_2$ as a deposition precursor allows the use of methanol as a solvent. The lower boiling point of methanol should result in higher quality deposition of MoO_3 layers, and images of initial experimentation are shown in Figure 24.

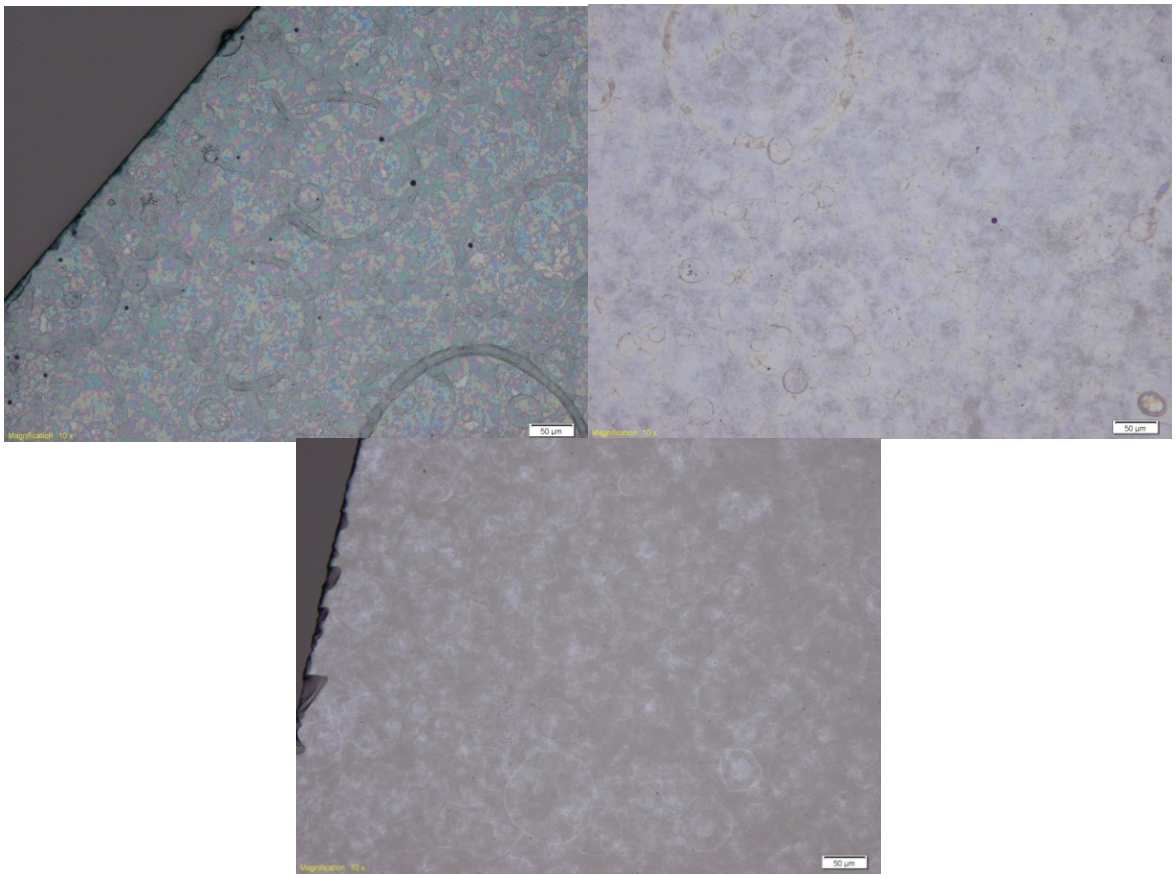

Figure 24: Microscope images of MoO_3 layers deposited using $Mo(acac_2)$ as a precursor material. Top left shows a layer deposited at 225°C using 5ml of 0.05M solution at a spray distance of 15cm. Top right shows a layer deposited at 250°C using 5ml of 0.01M solution at a spray distance of 15cm. Bottom centre shows a layer deposited at 250°C using 5ml of 0.005M solution at a spray distance of 15cm.

It is clear that a similar progression in the improvement of film quality is observed for the three images in Figure 24. The root mean square surface roughness decreases from 85nm in the top left image, to 15nm in the top right image and finally 5nm in the bottom image. These improvements in film quality are linked to a decrease in the rate of deposition of the film, as discussed in the previous paragraph. It can further be seen that the change in precursor and corresponding solvent from water to methanol has also increased the quality of the surface deposition, and the surface roughness of the final film has now reached a surface roughness that is appropriate for the incorporation of the layer into device structures.

The decision was made based on these results to perform more detailed experiments on layers deposited using $Mo(acac)_2$ as a precursor dissolved in methanol, due to the better film quality achieved.

The full study of the performance of the spray deposited molybdenum oxide layer deposited using this method is the subject of a later chapter.

4.4 Conclusion

In this chapter the development of the spray pyrolysis process for the deposition of the two materials under study for the rest of this work was discussed.

The first half of the section dealt with the development of the deposition process for the spray pyrolysis of aluminium doped zinc oxide layers with the addition of a lithium dopant. Thermal analysis of the precursors suggeted that the deposition will have to take place at temperatures of 350°C and above to achieve decomposition of the precursor materials to form final layers of an acceptable quality. This conclusion was supported by initial spray experiments which showed layers of visibly poor quality when deposited at lower temperatures.

Some of the basic optical properties of pure zinc oxide layers were then investigated to understand the effects of deposition at lower temperatures. This data again suggested lower quality layers are formed at lower temperatures. From these initial conclusions, it was decided to focus on deposition temperatures of 350°C and above for the more detailed investigations of aluminium and lithium doping in the main zinc oxide chapter.

The second half of the section dealt with the development of the deposition process for the spray pyrolysis of molybdenum oxide layers. As the existing literature for this process is very brief, here the investigation focussed on selecting a precursor and determining some of the basic spray conditions for the process. Here, molybdenum acetylacetonate was found to produce layers of the lowest roughness and best visual quality when sprayed at a concentration of 0.01M. Thermal analysis of the precursor suggested that the deposition process can begin at temperatures above 150°C, and that 280°C may be an area to investigate. This detailed temperature investigation is the main focus of the chapter describing the work on molybdenum oxide.

The investigation presented in this chapter thus laid the groundwork for the investigation in the next two chapters of the thesis.

5 Doping of Zinc Oxide for use as a transparent conductor

5.1 Introduction

This chapter discusses the spray deposition of doped zinc oxide films for the purpose of acting as transparent conductive films.

The study of spray deposition of the metal oxide begins with the characterisation of various aluminium doping levels of the zinc oxide film, and the effect of this on the physical, optical and electrical properties of the resulting sprayed layer.

The study then moves on to the effect of lithium doping on the already aluminium doped zinc oxide films. Two concentrations of lithium doping are considered. It is found that the resistivity obtained from the spray deposition of the doped layers is not acceptable for use as a transparent conductor, and the addition of lithium to the films does not improve this.

The study thus moves on to the annealing of the spray deposited films after their initial deposition. There is previously performed work suggesting that annealing under nitrogen or vacuum conditions can significantly lower the resistivity of spray deposited conductive layers, and this is also found to be true in this case. Here the lithium doping is found to have a positive effect on reducing the resistivity of the sprayed films, and a minimum resistivity of $5.02 \times 10^{-3}\Omega$cm was obtained for the 0.5% lithium doped 2% aluminium doped zinc oxide film.

5.2 Aluminium Doped Zinc Oxide

Doping of the layers was achieved by adding aluminium nitrate nonahydrate to the spray solution to achieve a desired percentage of aluminium. The solutions were then deposited by spray pyrolysis in a manner identical to that of the previous experiments. Using 4-point probe measurements, it was found that samples did not begin to display a measureable conductivity when deposited at temperatures lower than 350°C. When considered with the thermogravimetric analysis, it is likely that the aluminium precursor is not decomposing below these temperatures with enough energy remaining to achieve successful doping into the zinc oxide lattice. For the main sample sets discussed below deposition thus takes place at temperatures of 350°C and higher.

The initial investigation centred on the aluminium doping of Zinc Oxide films to provide a baseline of comparison for the further doping of films with lithium. The effect of various percentages of aluminium doping was thus investigated, and various physical properties of the films were measured.

Thickness and Roughness

The thickness of the films as measured by spectral ellipsometry and roughness as measured by profilometry are shown in Figure 25. The thickness of the deposited layers can may give information on the nature of the spray deposition process and minimizing the surface roughness of films for use in OLED structures is important, as has already been discussed.

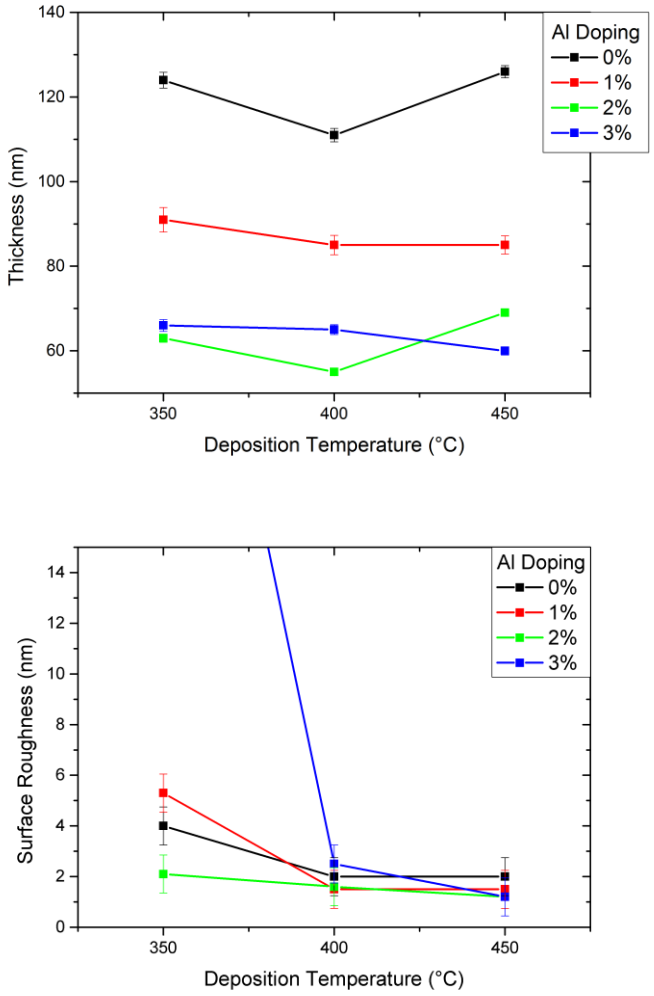

Figure 25: The thickness (top) and roughness (bottom) of zinc oxide films doped with varying concentrations of aluminium. The surface roughness is measured as the root-mean-square average. The data point for the roughness of a 3% Al film deposited at 350°C is off-scale at 34.8nm.

The top image indicates that there is no significant trend of thickness change of the deposited layer as the deposition temperature is increased above 350°C. This is in contrast to the lower temperature deposition where a thicker layer of non-decomposed precursor has been suggested to lead to an increased thickness of deposition. The slight variation in measured thickness of the layers gives an indication of the level of reproducibility of the spray pyrolysis process as performed. This variation is likely to be due to slight variations in substrate position when the spraying process is performed.

A clear trend is evident in the decrease in the thickness of the deposited films with an increase in the level of aluminium precursor in the solution. It is not clear why this would be the case. Thickness

variations associated with incomplete decomposition of precursors has been shown to occur, but in this case thicker layers were associated with less decomposition, and it is not clear how the addition of the aluminium precursor to the spray solution would lead to more decomposition. The thickness of the films deposited decreases to half its initial value as the aluminium dopant concentration reaches 2%, at which point no further decrease is observed as the doping level is further increased.

The bottom image of Figure 25 indicates that the measured surface roughness of the films decreases with increasing deposition temperature, appearing to saturate at an average surface roughness of 2nm. This compares to a standard surface roughness of 2.7nm for ITO.[112] It is expected that the surface roughness of the films would decrease as the deposition temperature increases, for two reasons. The increased temperature reduces the probability that any solvent reaches the surface of the substrate before evaporating, thus eliminating the presence of surface roughness due to the maragoli effect. In addition to this, the higher temperature of the deposition means a larger amount of energy is available for the incorporation of atoms into the crystal lattice, leading to a smoother film.

The 3% aluminium doped film deposited at 350°C measured an extremely high surface roughness of 34.8nm, as is not shown on the graph as it obscures the other data points. Some have suggested that the incorporation of aluminium into zinc oxide films has been suggested to reduce the diffusion of atoms during the film deposition process leading to higher surface roughness for aluminium doped films[113], whereas others have suggested the aluminium doping reduces the grain size of the deposited film leading to lower surface roughness.[114] All of these studies were performed using sputter coating as the deposition technique, however, so the conclusions may not apply to the spray deposition process. The effect here seems only to apply to the most doped sample at the lowest temperature, where the a reduction in the energy available as the film is deposited could be further increased by the presence of the aluminium atoms.

Optical analysis

Spectral analysis of the films was performed. The measured transmission and reflectance of the spray deposited films is shown in Figure 26.

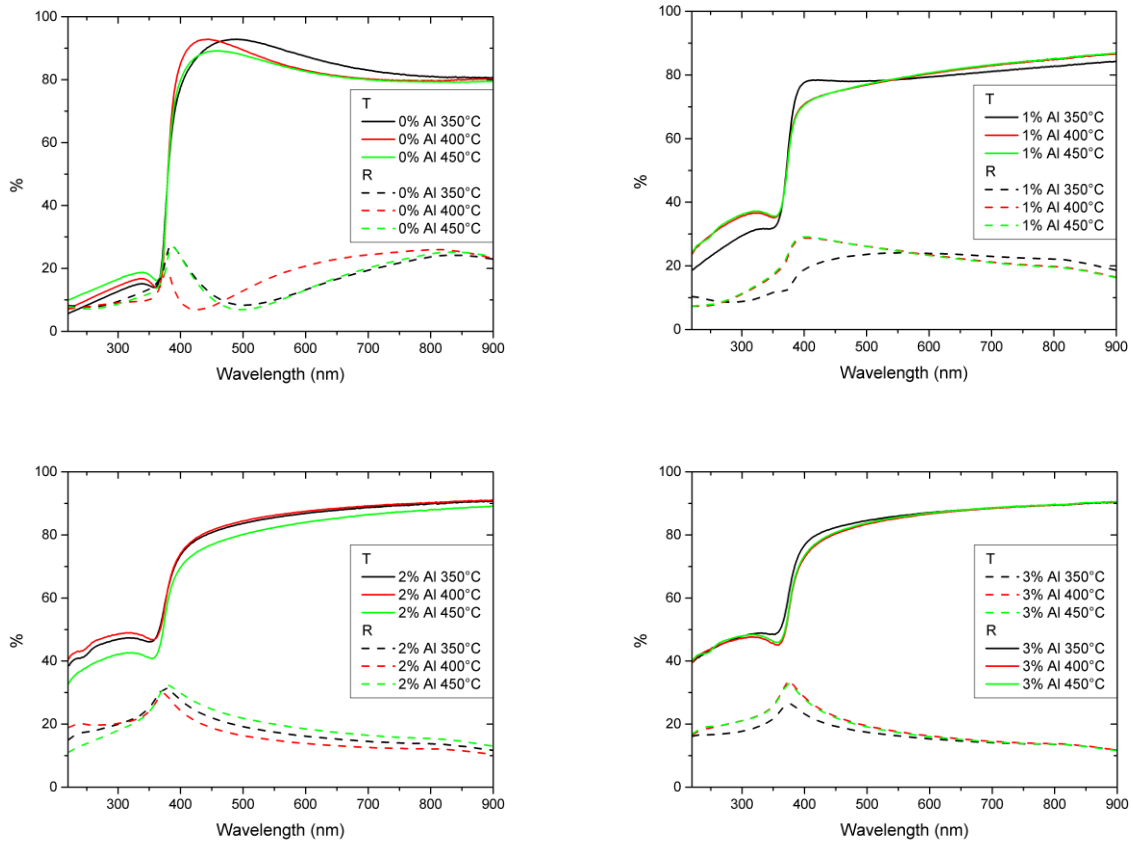

Figure 26: The measured transmission and reflectance of zinc oxide films doped with varying concentrations of aluminium and deposited at various temperatures.

The transmission of the films is the important property when considering their use as a transparent conductor. Here it appears that the transmission of the deposited films remains relatively constant with increased aluminium doping at wavelengths corresponding to an energy below the band gap of zinc oxide. The difference in the transmission and reflection spectra for undoped zinc oxide is due to interference oscillations beginning to become apparent due to the increased thickness of that layer when compared to the doped zinc oxide films. The low temperature 1% Al film also shows interference effects.

The spectral properties of the films can be combined with the thickness data to determine an absorption coefficient for each film, which can be used to interpret the physical characteristics of the layers. This data is presented in Figure 27.

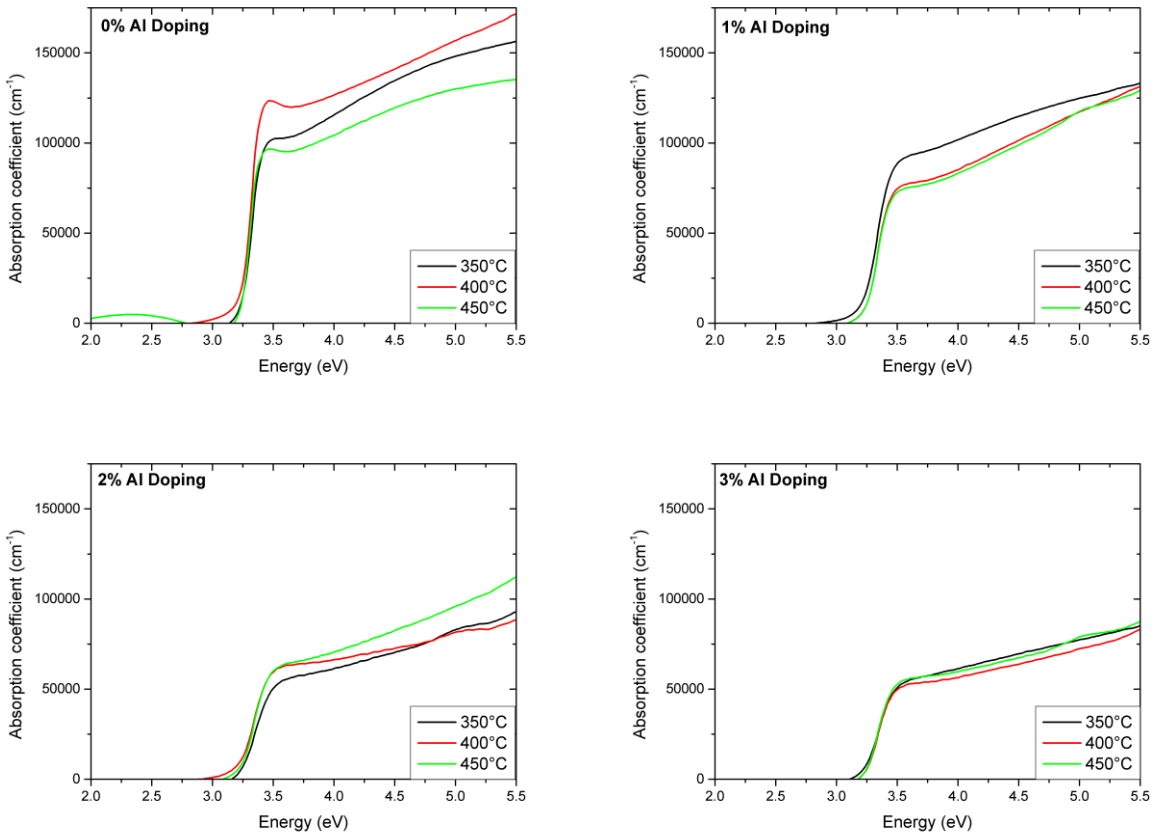

Figure 27: The calculated absorption coefficient of zinc oxide films doped with varying concentrations of aluminium and deposited at various temperatures. The absorption coefficients were calculated using the previously measured thicknesses in Figure 25 and the optical transmission and reflectivity of the films shown in Figure 26.

It is clear that for energies below the band gap, all of the deposited films are non- absorbing. This is the expected result, and confirms that any transmission losses from the film are due to reflection from the film or substrate surface.

The exciton peak of zinc oxide is a feature evident in Figure 27 in the top left image corresponding to undoped zinc oxide. The peak develops as deposition temperature is increased to 400°C, but decreases in magnitude for the film deposited at 450°C. The ratio of the exciton peaks to the local minimum at the higher energy is 1.03 for the 400°C peak and 1.01 for the 450°C peak. This would suggest that the crystal structure of the lattice becomes strained or otherwise disrupted, leading to a spreading out of the exciton peak until it is no longer visible.[115] This suggests the crystal quality of the film is highest for 400°C deposition.

In addition to this, the magnitude of the zinc oxide exciton peak is reduced by the introduction of aluminium to the lattice. The reduction in the exciton peak is likely due to the incorporation of aluminium disrupting the crystal structure of the aluminium and reducing the overall crystallinity of the film.

It is useful to summarise the optical analysis of the films. An analysis of the absorption of the deposited films above the band gap energy as well as Tauc analysis of the band gap data are shown in Figure 28.

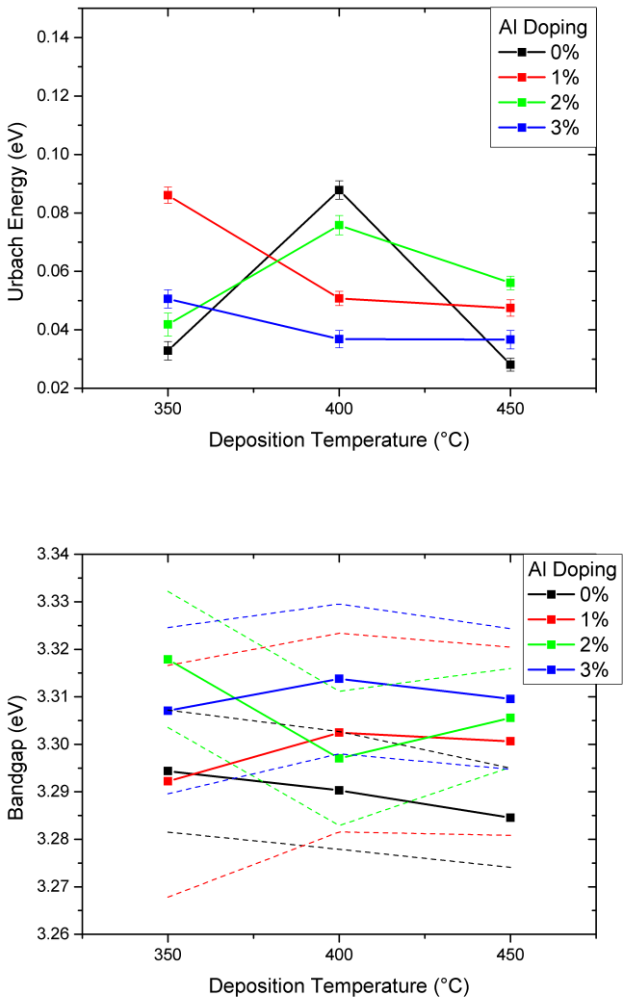

Figure 28: The calculated Urbach energy (top) and derived band gap (bottom) of zinc oxide films doped with varying concentrations of aluminium and deposited at various temperatures. The Urbach energy was extracted by fitting of the absorption coefficient below the band energy. The band gap of the films has been derived using Tauc analysis as described in the method section of the plots shown in Figure 27, and the error is indicated by the dashed lines.

The top image of Figure 28 compares the Urbach energy as a measure of the crystallinity of the films. The 1% and 3% aluminium doped films show a decrease in the parameter with increasing deposition temperature, as would be expected. The 0% Al doped film deposited at 400°C shows an unexpectedly high disorder, but the other points suggest the inclusion of aluminium into the film increases the crystal disorder. An increase in deposition temperature does not restore the lower parameter, suggesting that the 1% and 2% aluminium doping induces inherent disorder that is not annealed out by heating to 450°C.

The bottom image of Figure 28 shows the band gap of the deposited films, estimated using Tauc plots. The error in these plots is large and this error mainly results from the error in the reflectivity measurements of the films performed to determine their absorption to produce a Tauc plot. However, it is possible to determine trends in the data. The pure zinc oxide film has a band gap of 3.29eV at a deposition temperature of 400°C, which is lower than previously measured results of 3.37eV[54,116]. The deposition temperature of the films has a modest effect on the band gap of the material. For the undoped films the gap decreases slightly, where for the 1% and 3% Al doped samples the band gap increases with increased deposition temperature. For the 2% Al doped sample the gap energy is erratic. The aluminium doping may cause a small increase in the size of the band gap of the material, although there is clearly some uncertainty in the data. If this shift is a consistent effect, it is likely due to the Burstein-Moss shift that would be expected by the increase in carrier concentration that comes with the aluminium doping.[117] However, the magnitude of the shift is small, similar to other results with low levels of aluminium doping.[118]

Resistivity of films

The measurement of the resistivity of a transparent conducting layer is extremely important m to characterise its performance. Four point probe measurements were performed on the samples. This data is presented in Figure 29.

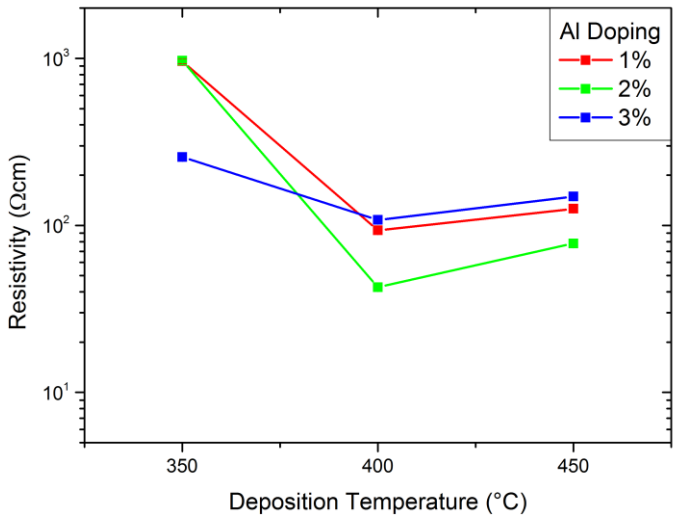

Figure 29: The measured resistivity of the zinc oxide films doped with various concentrations of aluminium deposited at various temperatures. The resistivity was calculated using the sheet resistance of the films as measured by four point probe and the thickness of the films shown in Figure 25. The estimated errors in the measured values are smaller than the points shown on the graph.

The resistivity of ITO is typically of the order of 10^{-3} Ωcm. It is clear that the measured resistivity of the spray deposited layers are significantly higher than this, with values ranging from 10^{2}-10^{3}, or many orders of magnitude higher. The lowest resistivity is obtained for the layer deposited at 400°C and doped with 2% aluminium. For lower deposition temperatures the increase in resistivity is likely due to not enough energy being available in the deposition process to incorporate the aluminium atoms into the lattice. Aluminum doping levels of 2% being an optimum level are consistent with other reports in the literature.[66]

It is clear that the deposition at this stage is not producing films of a high enough quality to be used as a transparent conducting layer in place of ITO. Annealing the films under certain conditions is known to improve the resistivity of the deposited films.[65] However, as has already been discussed it was hoped that the inclusion of lithium into the film in addition to the aluminium could improve these properties.

5.3 Doping with lithium

The main investigation of the effect of lithium doping was based on the concentrations found effective in increasing the measured mobility of zinc oxide films, which was found to be 1%.[67] Therefore, 0%, 0.5% and 1% doping concentrations were selected for investigation, along with aluminium doping concentrations of 0%, 1%, 2% and 3% based on the previous initial investigations suggesting the optimum aluminium doping concentration was 2%.

The films were prepared using a similar method to that in literature[67], which shows clear evidence of the effect of the lithium present in the film for both 0.5% and 1% doping concentrations through changes in the ZnO crystal lattice.

0.5% Li doping

Thickness and Roughness

The thickness of the 0.5% Li doped films as measured by spectroscopic ellipsometry and roughness as measured by profilometry are shown in Figure 30.

The trends observed here are similar to those shown in Figure 25 for the undoped zinc oxide film, and similar arguments would be expected to be true for the decrease in thickness with aluminium doping and decrease in roughness with increased deposition temperature. An effect of the lithium doping in improving the crystallinity of the layer could be expected to manifest as an increase in surface roughness due to an increase in crystal grain size. This effect may be visible in the 1% and 2% Al doped samples deposited at 350°C.

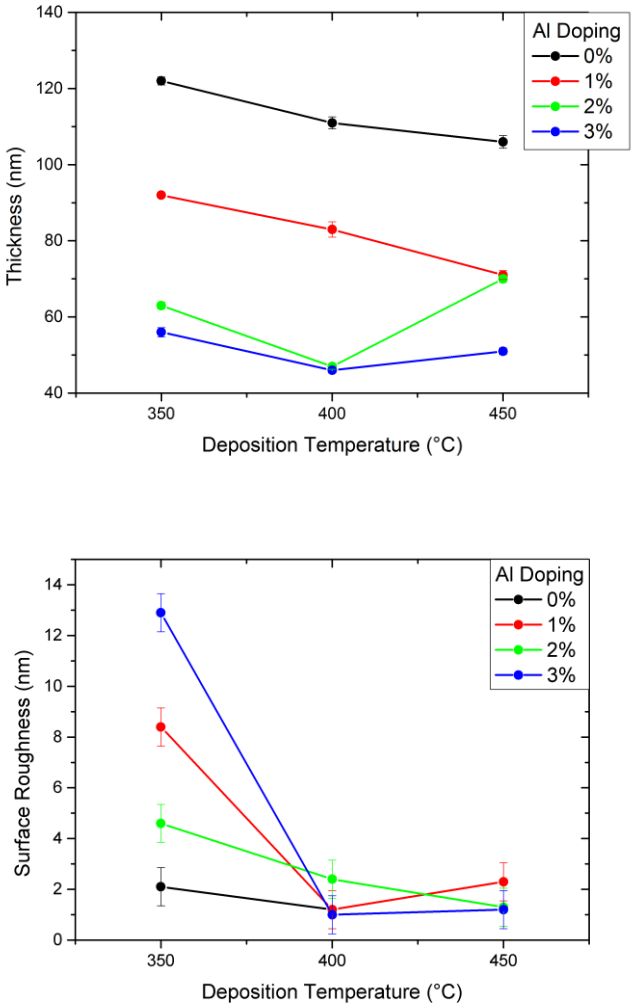

Figure 30: The thickness (top) and roughness (bottom) of 0.5% lithium doped zinc oxide films doped with varying concentrations of aluminium. The surface roughness is measured as the root-mean-squared average.

Optical analysis

Spectral analysis of the films was performed. The measured transmission and reflectance of the spray deposited films is shown in Figure 31.

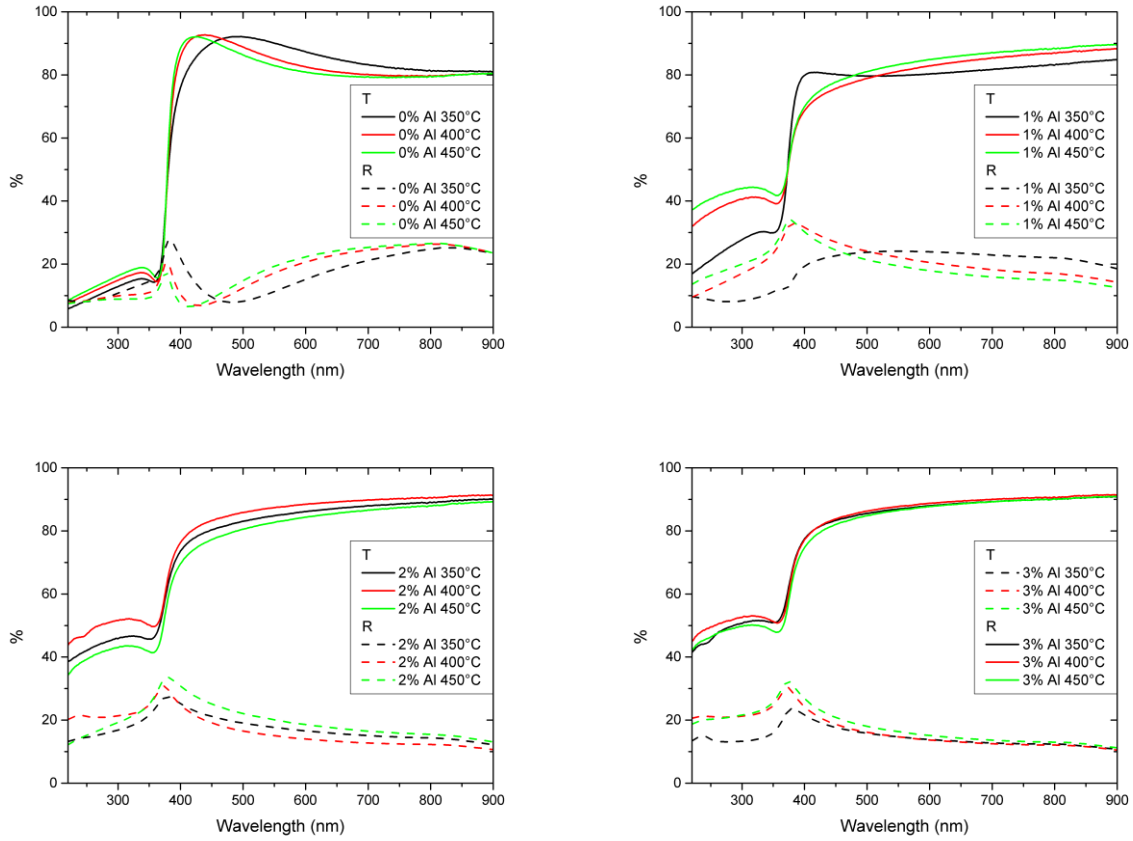

Figure 31: The measured transmission and reflectance of 0.5% lithium doped zinc oxide films doped with varying concentrations of aluminium and deposited at various temperatures.

The features shown in the figure are very similar to those shown for the non-lithium doped samples. Oscillations due to the thickness of the samples are most apparent in the top left image, which correspond with the samples with no aluminium doping being the thickest samples. The 1% aluminium doped sample deposited at 350°C shows an oscillation that would be associated with a thicker sample, but the sample was not measured to be significantly thicker than the samples deposited at a higher temperature. This effect is also seen in the reflection spectrum of the sample that lacks the peak that would be associated with the band onset absorption. As this feature is present in the equivalent non-lithium doped sample discussed in the previous section, it is unlikely to be an anomaly. The source of this feature is difficult to determine, although the index of the films or optical uniformity may contribute to the fringe visibility.

The measured transmission and reflectivity of the films can be combined with the thickness data to determine the absorption coefficient for each film. This data is presented in Figure 32.

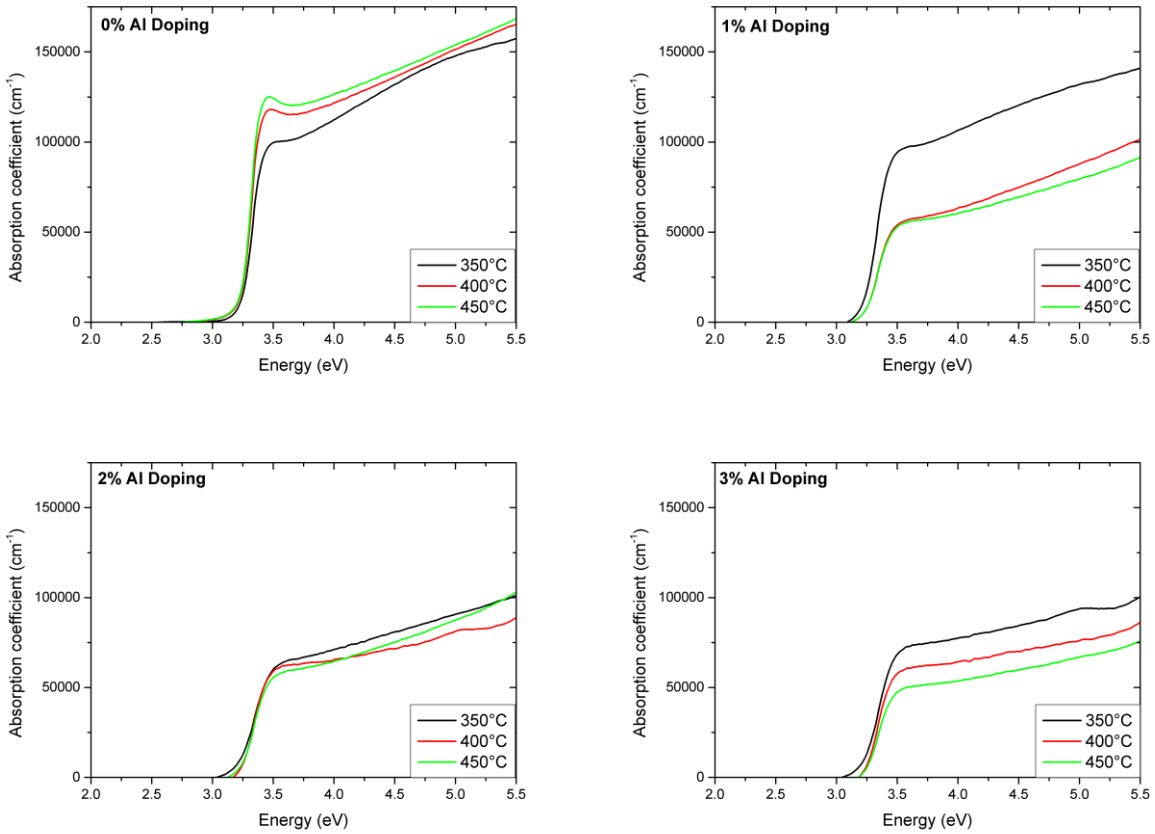

Figure 32: The measured absorption coefficient of 0.5% lithium doped zinc oxide films doped with varying concentrations of aluminium and deposited at various temperatures. The absorption coefficients were calculated using the previously measured thicknesses shown in Figure 30 and the optical transmission and reflectivity of the films shown in Figure 31

The absorption data for 0.5% lithium films shows a similar trend to that of the undoped films. The absorption of the films only doped with lithium in the band gap is of a similar level to the pure zinc oxide films discussed in the previous section. The 1% aluminium doped films show a similar feature to the corresponding non-lithium doped film deposited at 350°C in that absorption in the band gap is increased. This corresponds with the anomalous shape of the transmission and reflection curves for those films, and reinforces the suggestion that those films physically differ from the others.

The ratio of the exciton peaks to the local minimum at the higher energy is 1.02 for the 400°C peak and 1.04 for the 450°C peak. In contrast to the non-lithium doped films this would suggest that the highest deposition temperature here has produced the highest quality film.

As was done for the non-lithium doped film, it is useful to summarise the above data for comparison. The absorption at 4eV, above the band gap and the calculated band gaps of the 0.5% lithium doped sprayed samples are shown in Figure 33.

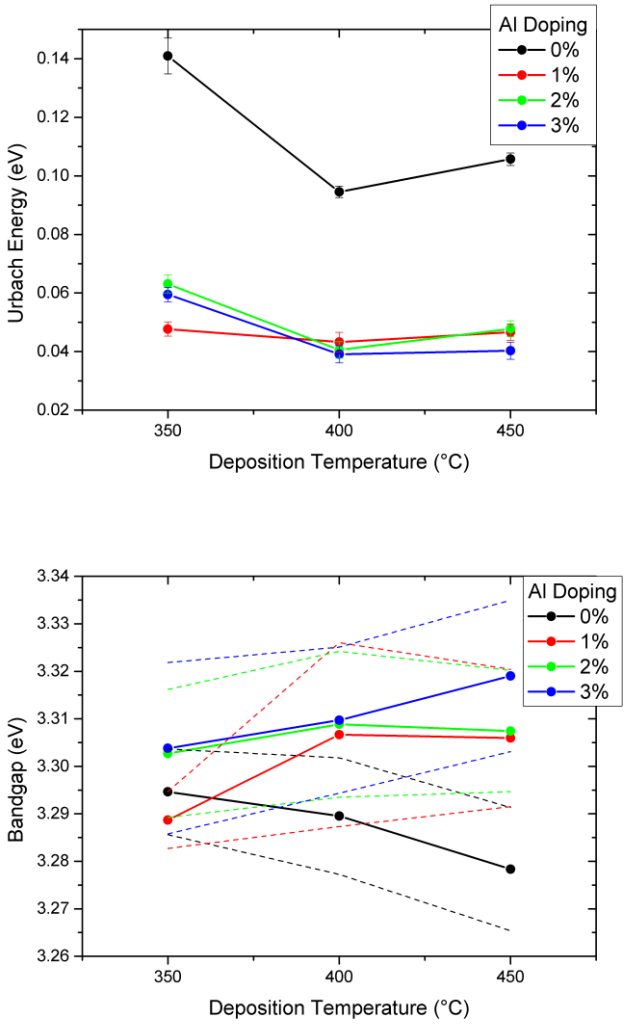

Figure 33: The calculated Urbach energy (top) and derived band gap (bottom) of 0.5% lithium doped zinc oxide films doped with varying concentrations of aluminium and deposited at various temperatures. The Urbach energy was extracted by fitting of the absorption coefficient below the band energy. The band gap of the films has been derived using Tauc analysis of the plots shown in Figure 32, and the error is indicated by the dashed lines.

The top image of Figure 33 shows the calculated Urbach energy of the various films. In comparison to the non-lithium doped samples, the disorder of the 0% aluminium doped zinc oxide films appears to have greatly increased, which would suggest the lithium doping is not improving the crystal structure of the film, and may be reducing it instead. The various aluminium doped films, however, show lower

Urbach energy here than for the non-lithium doped films with 1% and 2% aluminium doping. The aluminium doped films also show the expected reduction in disorder with increased deposition temperature.

The trend in the estimated band gaps by the Tauc method shown in the bottom image of Figure 33 is again similar to the non-lithium doped films, with no specific variations that can be attributed to the doping with lithium at the 0.5% level. However, the behaviour of the 2% Al doped film is here consistent with that of the 1% and 3% doped films. With Al doping the bandgap tends to increase with deposition temperature, whereas without doping it tends to decrease with deposition temperature.

Resistivity of films

The intent of the introduction of lithium doping is to decrease the measured resistivity of the films. The measured resistivity of the 0.5% lithium doped films is shown in Figure 34.

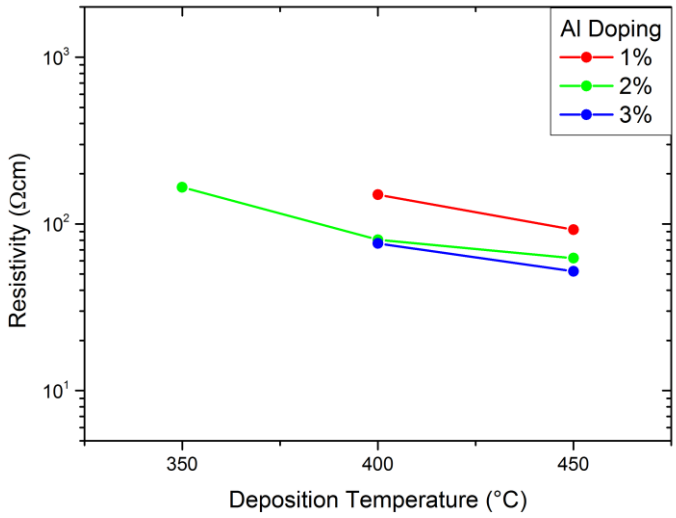

Figure 34: The measured resistivity of 0.5% lithium doped zinc oxide films doped with various concentrations of aluminium deposited at various temperatures. The resistivity was calculated using the sheet resistance of the films as measured by four point probe and the thickness of the films shown in Figure 30. For some films the resistivity was too high to be measured. The error in the measured values is smaller than the points shown on the graph.

It is evident that when compared to Figure 29, the resistivity of the deposited films has not been measurably improved by the lithium doping. The trend of decreasing resistivity when the deposition temperature is above 350°C is still present. However, the presence of lithium in the film does not appear

to have increased the resistivity of the films, implying that the incorporation of lithium has not reduced the increased carrier concentration through acceptor states.

It is clear that the lithium doping at this concentration has not significantly affected the properties of the film. However, further doping of the film and annealing of the films under nitrogen could still provide further change to the properties of the films.

1% Li doping

Thickness and Roughness

The thickness of the 1% lithium doped samples as measured by ellipsometry and the roughness as measured by surface profilometry are shown in Figure 35.

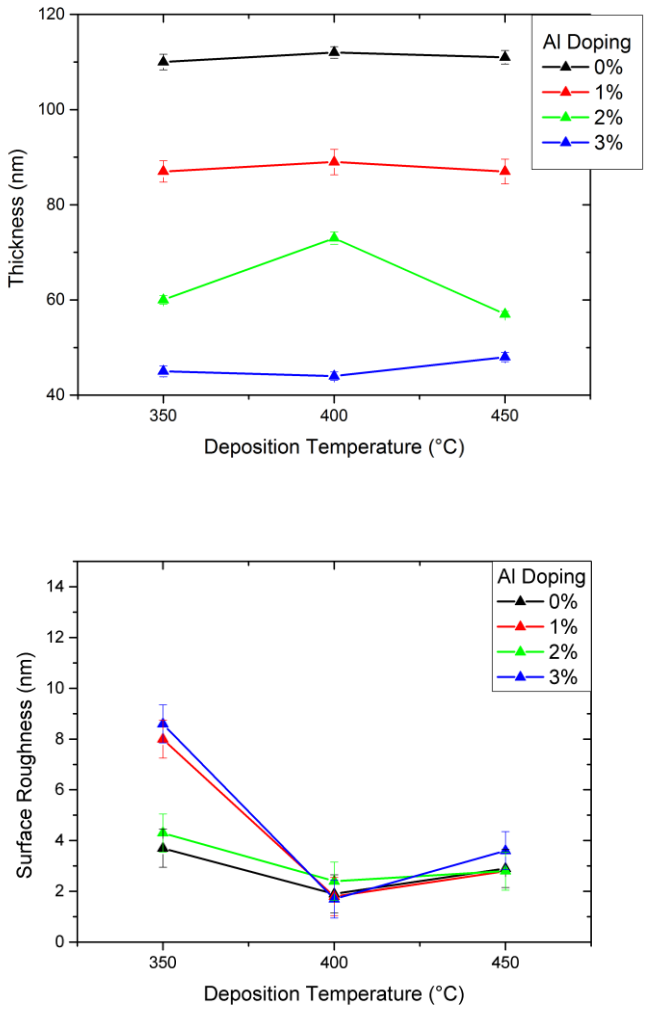

Figure 35: The thickness (top) and roughness (bottom) of 1% lithium doped zinc oxide films doped with varying concentrations of aluminium. The error in the thickness of the films is the error of the individual measurement. The surface roughness is measured as the root-mean-square average.

The measured thickness shows a similar trend with decreasing thickness for increasing aluminium doping, as with the previous 0% and 0.5% Li doped films. The thickness of the 1% lithium doped films appears to have decreased by a small amount when compared to the thickness of the non-doped films. This may be a continuation of a trend seen in the 0.5% doped films, although in that case the decrease is small compared to thickness variations in the film. This may be due to a similar effect to that for aluminium doping, or it may be the effect of the lithium doping increasing film density.

The measured surface roughness shows the expected trend of decreased roughness with increasing deposition temperature, although here the increasing deposition temperature to 450°C appears to slightly increase the surface roughness.

Optical analysis

Spectral analysis of the films was performed as before. The measured transmission and reflectance of the spray deposited films is shown in Figure 36.

General trends seen in the previous two sections are again repeated here. The most notable feature is the lack of change in properties as the deposition temperature in increased. The anomalous shape of the 1% aluminium doped sample deposited at 350°C observed in the previous two sections is no longer present in these samples. It is possible that the increased quantity of lithium doping is now resulting in more reproducible depositions, as other studies found that level of doping to be optimum for other properties.[67]

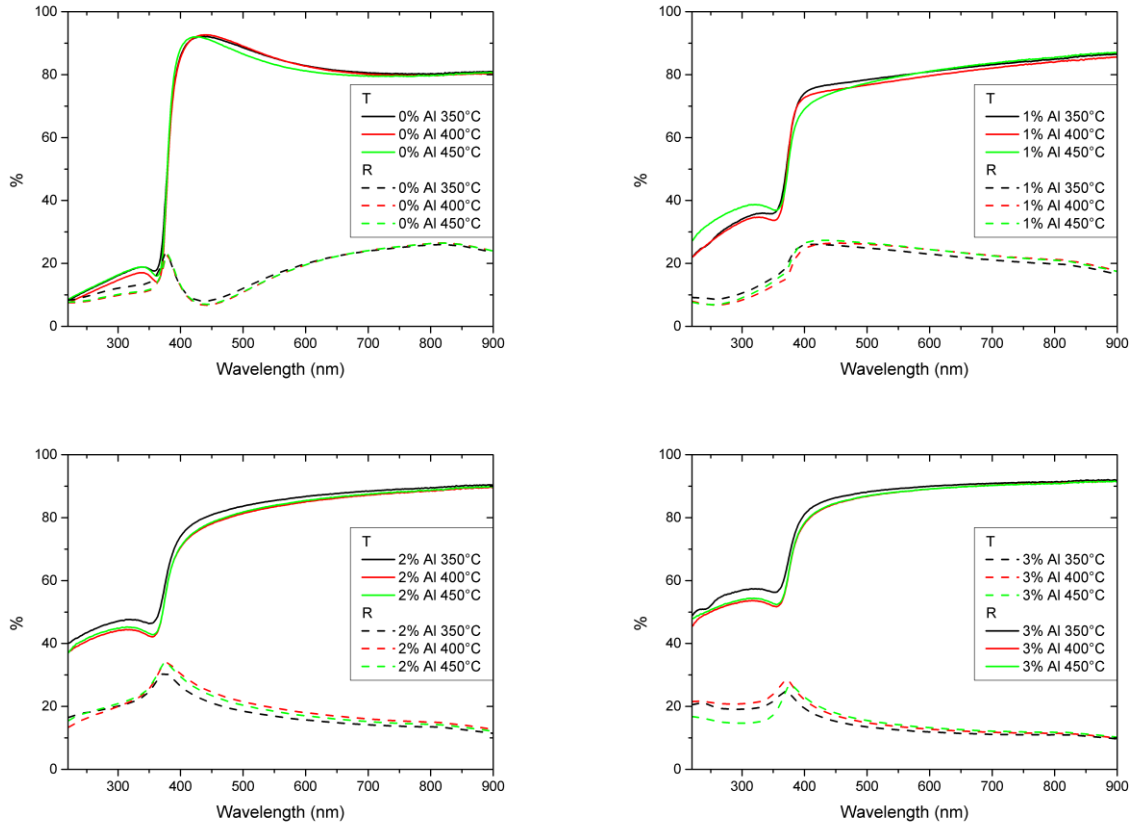

Figure 36: The measured transmission and reflectance of 1% lithium doped zinc oxide films doped with varying concentrations of aluminium and deposited at various temperatures.

The calculated absorption spectrum of the 1% lithium doped zinc oxide films is shown in Figure 37.

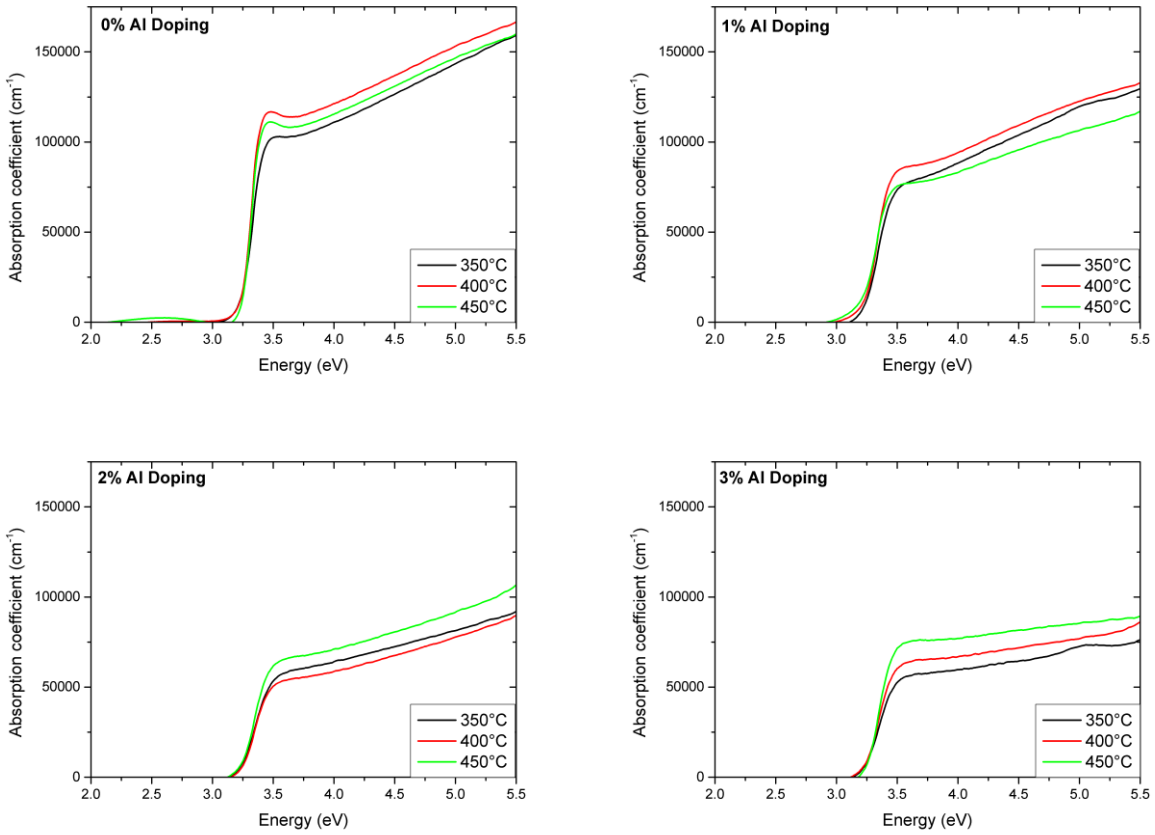

Figure 37: The calculated absorption coefficient of 1% lithium doped zinc oxide films doped with varying concentrations of aluminium and deposited at various temperatures. The absorption coefficients were calculated using the previously measured thicknesses shown in Figure 35 and the optical transmission and reflectivity of the films shown in Figure 36.

The absorption data again shows a similar trend to the other doping levels already investigated.

The ratio of the exciton peaks to the local minimum at the higher energy is 1.02 for the 400°C peak and 1.03 for the 450°C peak.

It is useful to summarise the optical data obtained from the films. The absorption of the 1% lithium doped films in the band gap and the size of the band gap as determined by Tauc analysis are shown in Figure 38.

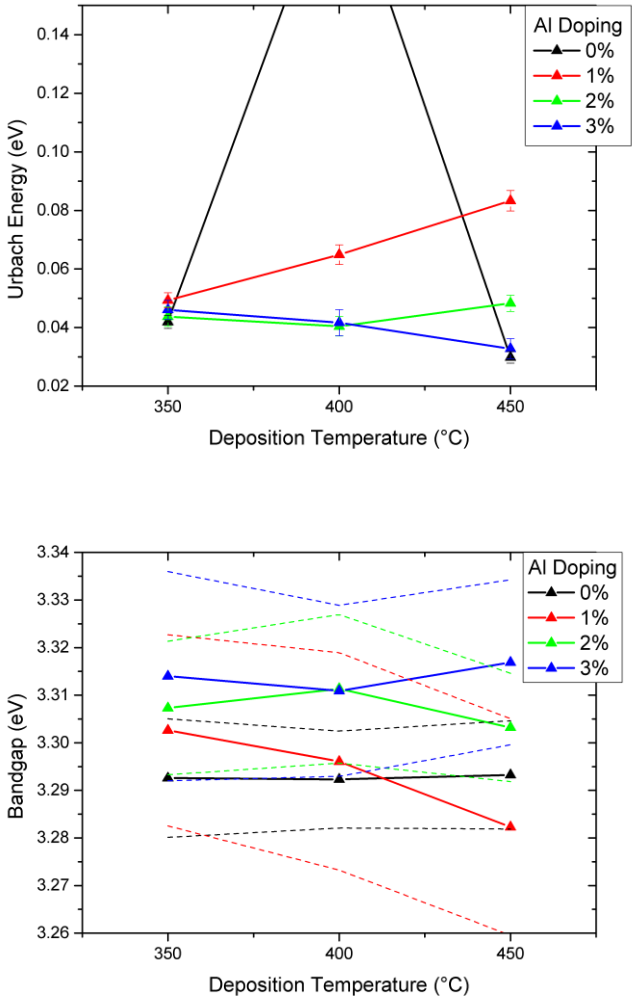

Figure 38: The calculated Urbach energy (top) and derived band gap (bottom) of 1% lithium doped zinc oxide films doped with varying concentrations of aluminium and deposited at various temperatures. The Urbach energy was extracted by fitting of the absorption coefficient below the band energy. The 0% Al doped sample deposited at 400°C has a Urbach energy of 0.2eV. The band gap of the films has been derived using Tauc analysis of the plots shown in Figure 37, and the error is indicated by the dashed lines.

The left image of Figure 38 shows the fitted Urbach energy of the various films. Here the 2% and 3% aluminium doped films show a similar low disorder to the 0.5% lithium doped samples, but the 1% al doped sample appears to have increased in disorder. The 0% aluminium doped samples show low values for deposition at 350°C and 450°C, whereas the sample deposited at 400°C shows a very high value similar to the corresponding non-lithium doped sample. These results thus show trends corresponding to both the 0% and 0.5% lithium doped sample sets, so there may be complex interactions between the various dopants occurring.

The trend in the calculated band gaps shown in the bottom image of Figure 38 here shows different behaviour to the 0% and 0.5% Li doped films. Here the 0% Al film shows no change in band gap as deposition temperature is increased, whereas the 1% and 2% AL films seem to show a downwards trend. The large error makes it difficult to determine the consistency of trends in the data.

Resistivity of films

The measured resistivity of the 1% lithium films is shown in Figure 39.

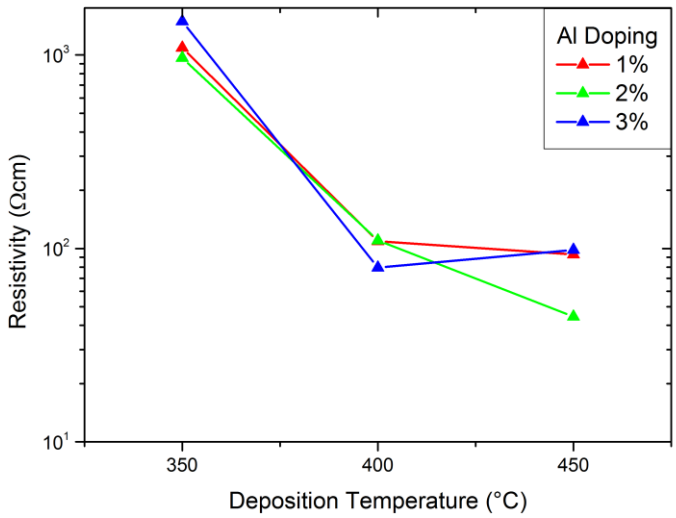

Figure 39: The measured resistivity of 1% lithium doped zinc oxide films doped with various concentrations of aluminium and deposited at various temperatures. The resistivity was calculated using the sheet resistance of the films as measured by four point probe and the thickness of the films shown in Figure 35. The error in the measured values is smaller than the points shown on the graph.

Again, when compared to the measured resistivity of the non-doped aluminium zinc oxide films shown in Figure 29, the addition of further lithium to the film has not decreased the resistivity of the films through the desired method of action in increasing the mobility of the ZnO film. It is possible that the further addition of aluminium to the films when compared to results in the literature disrupts the increase in mobility that was found when only deposition of the films though spray pyrolysis has been used.

However, it is known that annealing in a nitrogen environment has been found to significantly decrease the resistivity of aluminium doped zinc oxide films deposited by spray pyrolysis.[65] This was thus investigated as a method of improving the performance of the films.

5.4 Annealing

For the annealing of the films, the 2% aluminium doped zinc oxide films were selected for further investigation as the resistivity obtained from the spray pyrolysis at this aluminium level was generally lowest.

Some studies have found no effect when annealing aluminium doped zinc oxide films under any conditions,[119] whereas others suggest annealing under nitrogen has a positive effect.[65] As the studies where annealing has shown no effect were generally conducted on sputter deposited films, it is possible that the crystalline quality of the sputtered films was already high enough that further annealing would have little effect.

It was found in earlier work that the annealing process needed to be performed under nitrogen for any decrease in the resistivity of the films to be observed. This would tend to suggest that the decrease in resistivity that occurs is related to extraction of oxygen from the film. However, increase in grain size of the films being annealed may also be contributing to a decrease in resistivity.

The measured resistivity of 2% aluminium doped films also doped with varying amounts of lithium are shown in Figure 40.

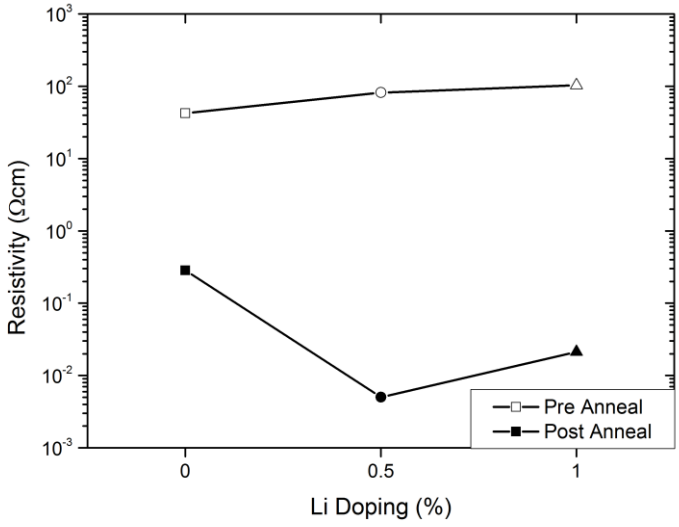

Figure 40: The impact of annealing the sprayed films with various lithium doping concentrations in a nitrogen environment. These films were all doped to 2% aluminium concentration and annealed for 1 hour at a temperature of 400°C. The error in the measured values is smaller than the points shown on the graph.

It is clear from the figure that the annealing process under nitrogen had a significant effect on the resistivity of the spray deposited films, resulting in a decrease in resistivity of several orders of magnitude. The decrease in resistivity is largest for the 0.5% lithium doped film, resulting in a measured resistivity of $5.02 \times 10^{-3}\Omega$cm, a relatively attractive value for device applications as it is in the range of resistivity values available with commercial ITO.

It is clear that the inclusion of lithium in the films had a significant effect on the annealing process of the films. As annealing of ZnO films has been shown to increase the grain size of the films[120], it is likely that the presence of the lithium in the film is assisting with this grain size increase in a similar fashion as has been shown for lithium doped pure zinc oxide films.[67] This increase in gran size leads to the decrease in the resistivity of the films due to decreasing the number of grain boundaries that carriers in the film need to cross.

Annealing of the non-lithium doped film led to a 2.2 orders of magnitude decrease in resistivity, whereas 0.5% and 1% lithium doping led to 4.2 and 3.6 orders of magnitude decrease. It would appear that the smaller amount of lithium doping leads to greater reduction in the resistivity of the films. It appears that the extra time associated with an annealing process allows the increase in crystallinity due to lithium acting as a sintering aid to more clearly manifest.

These experiments determined that 0.5% lithium doping was the optimal concentration for decreasing the resistivity of the aluminium doped zinc oxide films upon annealing. This was thus selected as the concentration to be used for further annealing experiments.

It is always a goal for fabrication of transparent conducting materials to reduce the temperatures associated with the deposition of the film. An investigation of varying the annealing temperature of the film is shown in Figure 41.

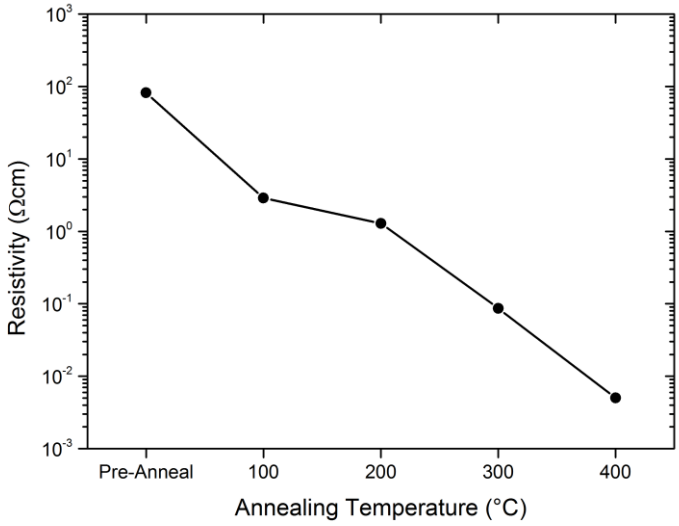

Figure 41: The effect of variation in the annealing temperature for 0.5% Li doped 2% Al doped sprayed ZnO films. The films were annealed for 1 hour under nitrogen atmosphere. The error in the measured values is smaller than the points shown on the graph.

It is clear from the figure that the annealing temperature of the process has a significant effect on the resulting resistivity of the film, with approximately order of magnitude decreases in resistivity as the annealing temperature is stepped up from 100°C to 400°C in 100°C intervals.

It is unsuprising that an increasing annealing temperature leads to a lower film resistivity. A higher annealing temperature leads to more energy being avalible for the filling of voids and increasing the grain size of the film. It appears that an annealing temperautre of 400°C is required to achieve film resistivities that are comparable to ITO. These annealing temperatures would also not be compatible with plastic substrates.

The spectral transmission of a film both before and after an annealing step is shown in Figure 42.

There are a number of interesting features in the figure. It is clear that the absorption of the films has not increased across the visible range after the film has been annealed. This is a promising result as the application of the films as transparent conductors depends on the films transparency, and the annealing process that decreases the resistivity of the film does not affect the absorption of the films.

There is also a clear decrease in wavelength, and thus increase in energy, of the onset of the band gap absorption of the film. Tauc analysis suggests that the band gap of the annealed film has increased to

3.58eV, compared to a band gap of 3.34eV for the non-annealed film. This increase in band gap is due to the Burstein Moss effect, as discussed when considering the optical spectrum of the non-annealed films. This indicates that the carrier concentration has been increased in the film, and it is thus unsurprising that a decrease in resistivity is observed.

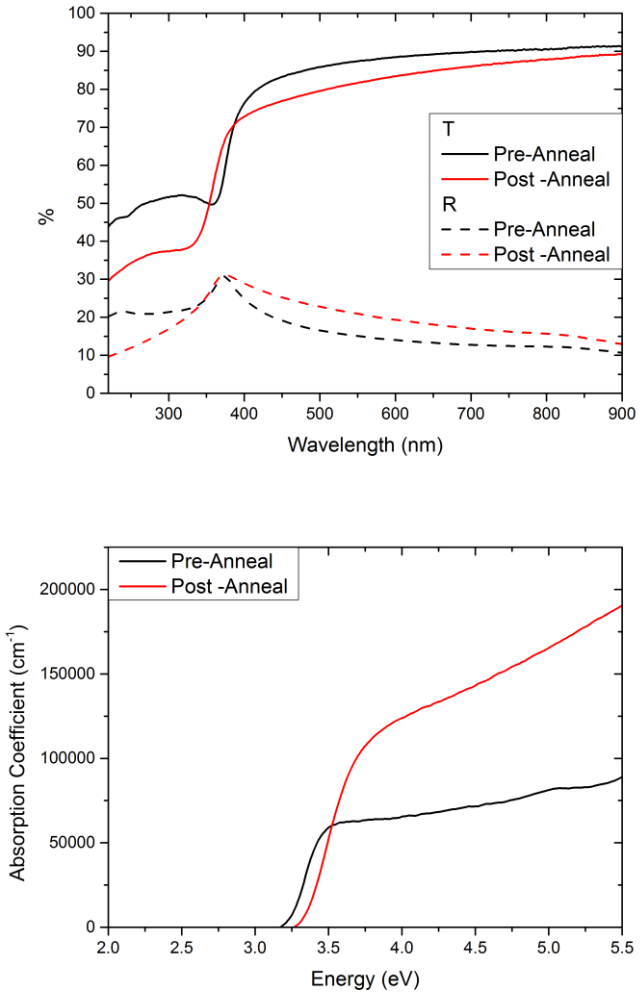

Figure 42: The change in the spectral transmission and reflection (top) and absorption (bottom) of the spray deposited films when annealed under nitrogen. The image shows the spectrum for a 0.5% lithium doped 2% aluminium doped zinc oxide film deposited at 400°C and annealed at 400°C for 1 hour. The absorption coefficient of the films is displayed against the energy of the incident light on the films.

As the layer is intended as an alternative to an ITO layer, it is useful to compare the optical properties of the 0.5% Li doped layer with that of ITO. This comparison is shown in Figure 43.

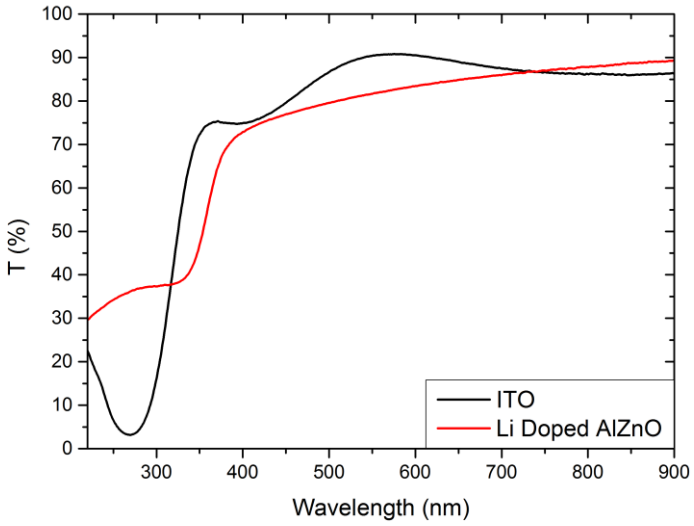

Figure 43: The measured transmission of an ITO layer and the 0.5% Li doped ALZnO layer. The ITO layer in this measurement was 140nm thick and the sprayed layer was 46nm thick.

It can be seen that in the visible range, the transmission of the two layers is of a similar magnitude. The ITO layer shows interference oscillations between 80% and 90% transmission, whereas the sprayed layer shows transmission decreasing from 90% to 75% across the visible range. The absorption onset occurs slightly earlier for the sprayed layer than ITO, with a band gap estimated using the Tauc method for ITO of 3.75eV, in agreement with prior literature,[121] compared to an estimate of 3.58eV for the sprayed film.

Figure 43 shows that the Li-Al doped ZnO layer would make a suitable alternative to ITO as the transmission of the layer remains above 75% for the entire visible light range. However, as the transmission of the layer is lower than ITO across this range, this would result in the efficiency of devices produced using the ZnO layer as a transparent conductor may be less efficient due to less of the generated light being transmitted from the emissive layer.

As the annealing process is performed under nitrogen, it is also necessary to determine if the performance of the annealed film degrades when exposed to atmosphere. A study of the resistivity of the films over time when exposed to atmosphere is thus shown in Figure 44.

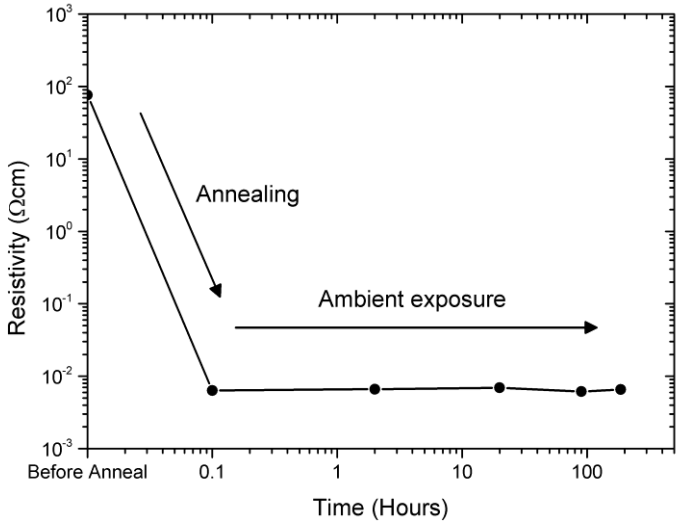

Figure 44: The performance of the annealed layer over an extended period of time. The image shows the measured resistivity of a 0.5% Li doped 2% Al doped zinc oxide film sprayed at 400°C and annealed for one hour under nitrogen at 400°C. The film was then exposed to normal atmosphere and the resistivity measured The error in the measured values is smaller than the points shown on the graph.

It is evident from the figure that the performance of the layer does not degrade when exposed to air. This implies that the structure of the film has been changed by the annealing process, as if the increased conductivity was solely due to the de-absorption of oxygen or moisture in the film then it would be expected that re-absorption would occur on exposure to air, leading the conductivity to decrease. This therefore supports the previous discussion that the annealing process has resulted in an increased grain size of the film, as this is a property that would not be affected by re-exposure to ambient atmosphere.

This figure also shows that the film would be suitable for application in ambient conditions as it retains its lower resistivity when removed from a nitrogen environment.

5.5 Conclusion

This chapter has dealt with the study of lithium doping of aluminium doped zinc oxide films. Initially, a study of aluminium doping of zinc oxide films was performed. The various physical, optical and electrical properties of the films were discussed, and a 2% doping concentration and a 400°C deposition temperature was determined to be optimal for the lowest resistivity of the films.

The effect of lithium doping on the films was then investigated. It was found that the inclusion of lithium into the film did not have very significant effects on the film properties, although it did seem to provide more systematic variations if the film properties with deposition temperature, perhaps suggesting better control of the deposition process. As the measured resistivity of the spray deposited films was also low, the investigation thus moved on to annealing of the films to increase performance.

It was found that annealing of the films in a nitrogen environment led to significant decrease in the measured resistivity of the films, and that this decrease was retained when the films were re-exposed to atmosphere. It was found that during annealing the lithium doping assisted in further decreasing the resistivity of the films when compared to the standard aluminium doped film. A minimum resistivity of $5.02 \times 10^{-3}\Omega$cm was obtained for the 0.5% lithium doped 2% aluminium doped films. This compares to a typical resistivity of $1 \times 10^{-3}\Omega$cm for ITO, so is thus approaching a competitive value.

6 Spray Pyrolysis of Molybdenum Oxide as a hole injection layer

6.1 Introduction

This chapter deals with the study of the spray pyrolysis of thin molybdenum oxide layers, and is divided into three parts.

The initial section describes some of the background of the material molybdenum oxide and why it has an application in organic semiconducting devices. Molybdenum oxide is a material particularly suited for application in the anode contact of such devices, and this section will also describe some of the previous work that has been performed in this area. Spray pyrolysis of molybdenum oxide remains a little investigated topic, emphasising the novelty of the work.

The second part of the chapter then focuses on a temperature study for deposition of the molybdenum oxide layer. Initial investigation in the previous section suggested that the temperature that the spray deposition is performed at may have a significant effect on the properties of the layer. The layer is thus deposited at various temperatures and a number of properties, such as the work function and molybdenum ion ratios in the layer are investigated. Finally, some simple test devices are fabricated, leading to the result that deposition of the layer at 225°C produces OLED devices of the highest emission efficiency, and that these devices operate at higher efficiencies than devices fabricated using both PEDOT:PSS and thermally evaporated molybdenum oxide injection layers.

Finally, the 225°C layer is incorporated into a majority solution processed high efficiency phosphorescent OLED device. The layer here again shows improved efficiency when compared to the traditional PEDOT:PSS hole injection layer, showing greatly improved switch-on voltage and reaching maximum efficiencies of 20 lm/W compared to 10 lm/W for an equivalent PEDOT:PSS hole injection layer device.

6.2 Background

Although it is clear that investigation of the solution processing of MoO_x has taken place, some common themes run through the work that has been performed. Almost all the prior work discussed has taken place on OPV devices, whereas OLED devices remain an under-explored area. This results in a lack of focus on the electronic properties of the MoO_x layer itself. In addition to this, all of the prior work uses spin coating as the deposition method of the layer. This limits the investigation possible on the effects of the thickness of the MoO_3 layer, which is especially important given the minimal thickness of the layer used.

Spray pyrolysis is a technique, on the other hand, that has not been used for the fabrication of these layers. The technique has been used to produce MoO_x layers[122–124], but was not investigated for deposition of layers in the organic electronics field. It was thus timely to perform a study of the spray pyrolysis of MoO_3 as a hole injection layer in OLEDs.

The investigation of the basic spray pyrolysis process has already been discussed in a previous chapter. This chapter deals with the investigation of the effect of one of the most important variables of the spray pyrolysis process, that of the temperature of the substrate during the deposition process. The investigation is divided into two parts. First, the thin film properties of the molybdenum oxide layer resulting from the deposition process is investigated. Then, the effect of incorporation of the layer into various forms of device is studied.

6.3 Investigation of MoO_x thin film

Initially, the film resulting from the spray deposition process was examined independent of any device structure. The chosen deposition temperatures begin at around the minimum that precursor decomposition would be expected to be taking place, as it is desirable to deposit the material at as low a temperature as is practical.

Thickness and surface roughness

The measured thickness and surface roughness of the spray deposited layers at various substrate temperatures is shown in Table 1.

Deposition Temperature (°C)	**180**	**225**	**255**	**300**	**340**
Thickness (nm)	71	73	68	38	20
Surface Roughness (nm)	15	20	15	7	5

Table 1: The measured thickness and surface roughness (R_a) of the spray deposited layers. The thickness has been determined by ellipsometry. The average surface roughness was determined using surface profilometry.

A clear trend evident in the date is that both thickness and surface roughness of the deposited films decreases with increased substrate temperature. This result is despite the fact that 5ml of precursor solution was used for each deposition, indicating that the deposited film is becoming more densely packed with increasing deposition temperature. This trend has been observed in the spray deposition of other materials.[125] This can be explained by the atoms of the precursor material having more energy at the substrate surface to incorporate into the crystal lattice of the layer. At lower temperatures, incomplete evaporation of the precursor solvent will also contribute to surface roughness of the film due to the Marangoni effect[126] , film thickness variations resulting from varying solvent evaporation rates at different points on a droplet on a substrate.

It is notable that at lower temperature deposition, the surface roughness of the films is significantly higher than would normally be expected for an efficient interlayer in a luminous device[127], and thus the

layers deposited at a lower temperature would be expected to perform less efficiently. This point will be considered further when the performance of devices incorporating the layers is discussed.

Optical analysis of films

As the film is being incorporated in an optical structure, the transmission characteristics of the film as deposited are important to understand. The optical transmission and reflection of films deposited at various temperatures and a 60nm PEDOT:PSS film, as well as their calculated absorption, is shown in Figure 45.

In terms of the device performance the transmission spectra of the films as deposited in a device structure are most important. The PEDOT:PSS reasonably transparent across the entire visible spectrum, although the transmission of the layer drops towards 80% in the near infrared. In contrast to this, the spray deposited layers deposited below 350°C have a broad absorption across the red and near infrared region of the spectrum, which is also visible as a green tint in the colour of the films. The position of the band will lead to lower efficiencies for red light emitting diodes and solar cells, due to the absorption of some photons emitted from the emissive layer. However, any efficiency losses compared to other injection layers are better considered when measuring their overall performance in emissive devices, and thus will be examined later in the chapter.

The bottom image in Figure 45 shows the absorption of the deposited films. It would be expected that pure MoO_3 films would show no absorption at energies below the band gap. The spray deposited layers, however, display a broad absorption centred at 817nm. The strength of this absorption increases slightly, peaking for the sample deposited at 225°C and then decreases with increasing deposition temperature. This absorption has been linked to a $Mo^{+5} \rightarrow Mo^{+6}$ inter-valance charge transfer transition, suggesting an increasing proportion of Mo^{+5} ions as the absorption increases .[128]

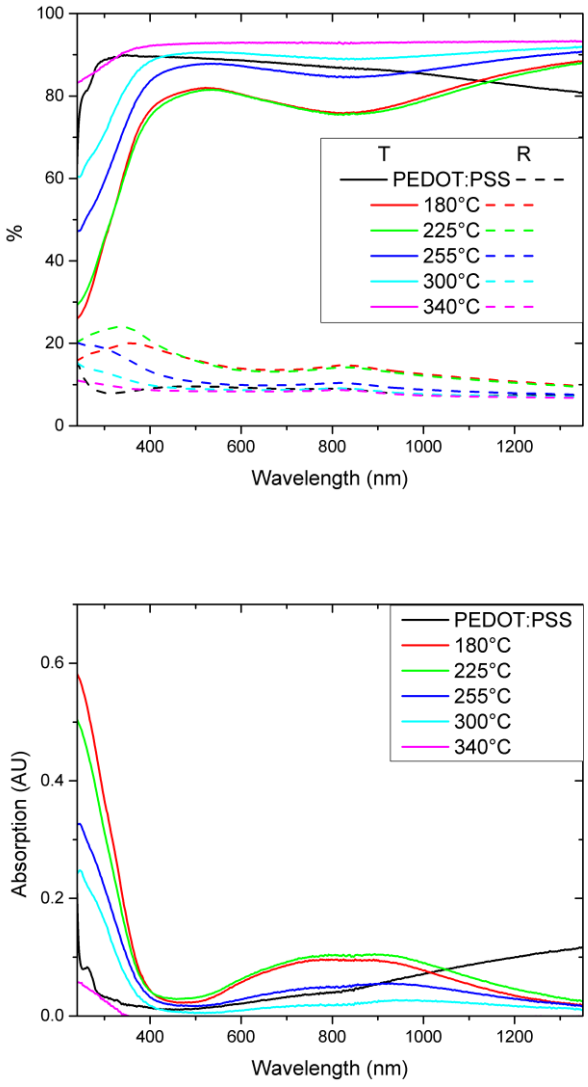

Figure 45: The measured transmission and reflection spectra (top) and absorption (bottom) of the MoO_x films deposited by spray pyrolysis, as well as a 60nm PEDOT:PSS layer.

Work function measurement by Kelvin Probe

The work function of the deposited layers as measured by the kelvin probe method is shown in Figure 46.

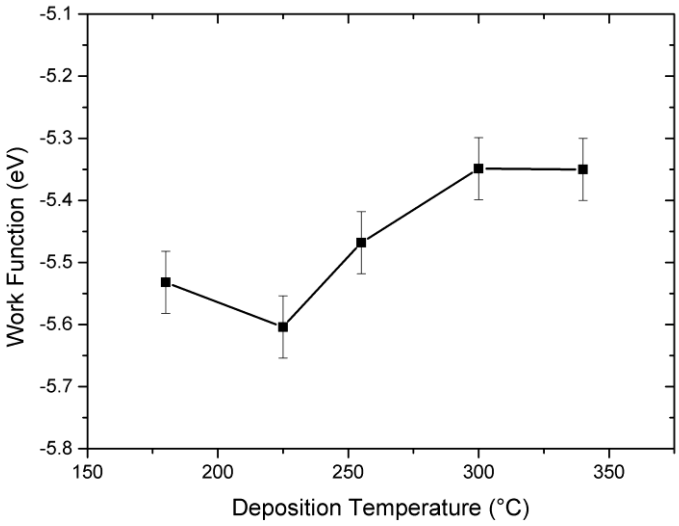

Figure 46: The work function of the spray deposited MoO_x films as measured by the Kelvin probe method.

The work function of the spray deposited films has a value of -5.54eV for 175°C deposition, reaching a peak of magnitude -5.6eV at 225°C before increasing to -5.35eV as the temperature of deposition is further increased. This is in all cases a significantly larger work function value than that of PEDOT:PSS at -5.2eV, suggesting that all of these layers should achieve a more favourable hole injection energy level alignment in a typical organic device than PEDOT:PSS.

Other work has suggested a work function value of -5.4 to -5.6eV for MoO_x either fabricated in air or exposed to air after vacuum deposition.[92,129] This is clearly in agreement with the results presented here. Previous work has also suggested that thermal annealing under vacuum of as deposited films leads to a decrease in the measured work function of MoO_x films due to increases in the number of oxygen vacancies in the film.[130,131] A similar trend of reduction in work function is observed here, although as the deposition has taken place in air and spray pyrolysis is not analogous to thermal annealing, this is not necessarily evidence of increasing oxygen vacancies, as will be discussed in the next section.

UPS measurements

Ultraviolet photoelectron spectroscopy (UPS) provides an alternative method of determining the work function of the films to compliment the kelvin probe measurement. UPS scans performed on the spray deposited films as well as an ITO reference substrate is shown in Figure 47.

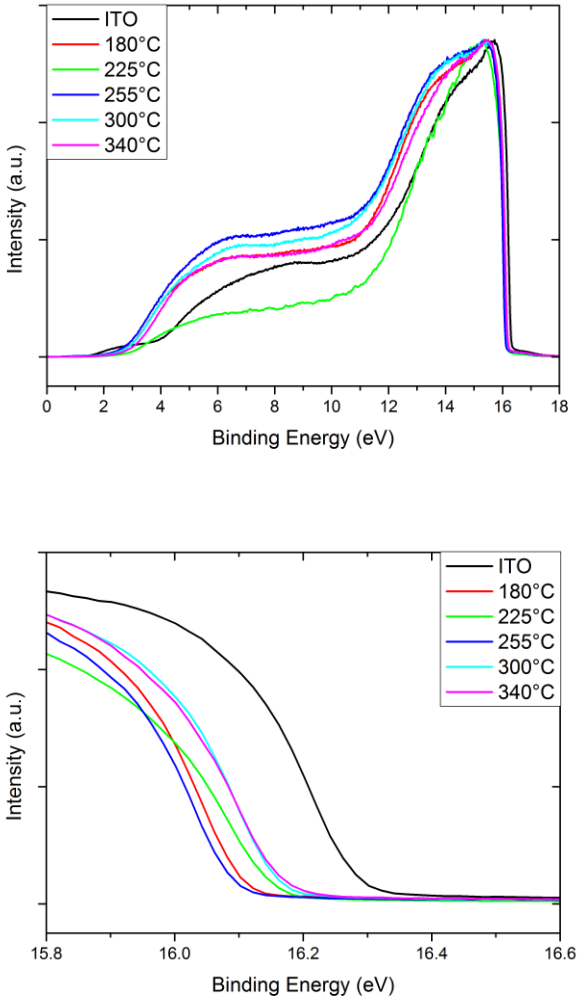

Figure 47: UPS scans of the deposited MoO_x layers. The top image shows the entire scan and the bottom image shows the photoemission cut off. The spectra were acquired using a light source of energy 21.22eV.

The UPS scan provides information on the electron density of the films at various energies. The work function of the films can be obtained by subtracting the point of photoemission cut off of the spectrum from the energy of the incident light on the sample, in this case 21.22eV. The results of this calculation are shown in Figure 48.

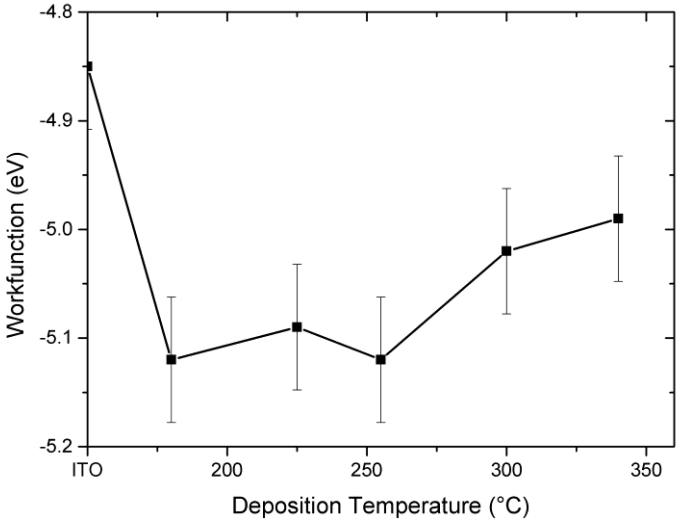

Figure 48: The work function of the deposited MoO_x layers as calculated from UPS measurements. The value is obtained by subtracting the photoemission cut off of the measured spectra from the energy of the incident ultraviolet light.

When compared to the work function of the films as measured by Kelvin prove in Figure 46, it is clear that although the general trend of first decreasing then increasing work function with increased deposition temperature is still present, the absolute values of work function measured by UPS are lower. For example, the film deposited at 225°C had a work function value of 5.6eV from Kelvin probe measurements, but a value of 5.1eV from UPS. In the literature it is generally noted that work function values as measured by UPS are lower in magnitude than those measured by kelvin probe.[132,133] This is attributed to the high vacuum conditions of a UPS measurement causing desorption of molecular species from the surface of the sample before the measurement takes place, which can have a large effect on the measured work function. It is also suggested that the fact that UPS measures the lowest magnitude work function possible whereas a kelvin probe measurement gives an average value can be responsible for the observed deviations.

In this case, the value of the work function measured via Kelvin probe is considered to be more relevant. This is due to the fact that the deposition of further layers on the MoO_x layer takes place in ambient at atmospheric pressure, the same conditions under which the Kelvin probe measurement takes place.

XPS measurements

X-ray photoelectric spectroscopy (XPS) was performed on the deposited samples. An example of a curve produced by this measurement is shown in Figure 49.

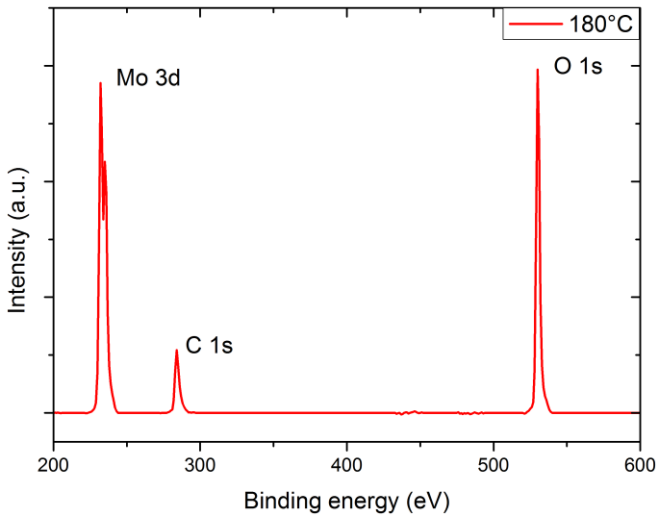

Figure 49: An example of a XPS survey scan of one of the deposited MoO_x films. The measurement produced similar curves for all deposition temperatures. The curves have been corrected for the measured background. The origin of the peaks visible in the spectrum has been indicated.

The XPS measurements produced curves that are very similar for all samples, so data are only presented here for a single deposition temperature as an example. The carbon peak suggests the presence of a hydrocarbon contamination layer, which attenuates the other peaks. After correction for this,[134] the ratio of the remaining Mo 3d and O 1s peaks can be used to determine the O:Mo ratio of the deposited films. The results of this calculation are shown in Figure 51.

In addition to this, the specific oxidation states of Mo ions present in the film can be determined by performing a high resolution scan of the Mo 3d peaks in the spectrum and fitting these peaks with respect to contributions from the individual ionic states as determined from the literature.[135] The results of these scans are shown in Figure 50.

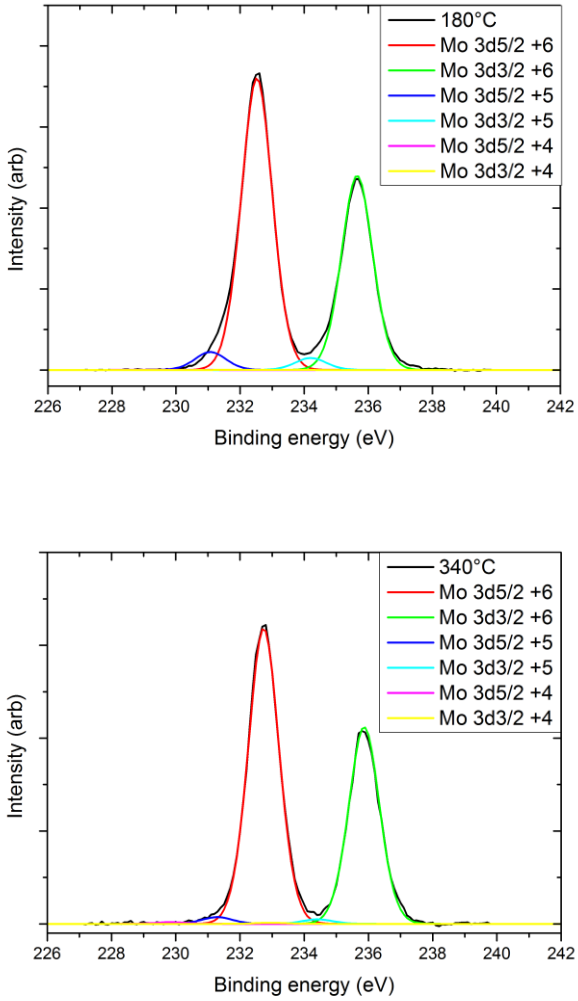

Figure 50: Examples of high resolution XPS scans of the Mo 3d peak for the MoOx films deposited at 180°C (top) and 340°C (bottom). The peak is a superposition of the contribution from the three possible Mo ion states of +4, +5 and +6, each split into pairs due to spin-orbit coupling. The top figure shows a contribution almost entirely from the +6 state, whereas a more significant fraction of the +5 state is present in the bottom figure.

The shape of the Mo 3d peak is determined by the contributions from the three Mo ion states present in the film. These are the +4, +5 and +6 states. Each contribution is split into two peaks due to spin orbit coupling. The positions of each of the peaks have been determined from literature.[136] Analysis of the area of each of the peaks can then be used to determine the ion ratios present in the film.

The information derived from the XPS survey and high resolution scans can then be summarised. This information is presented in Figure 51.

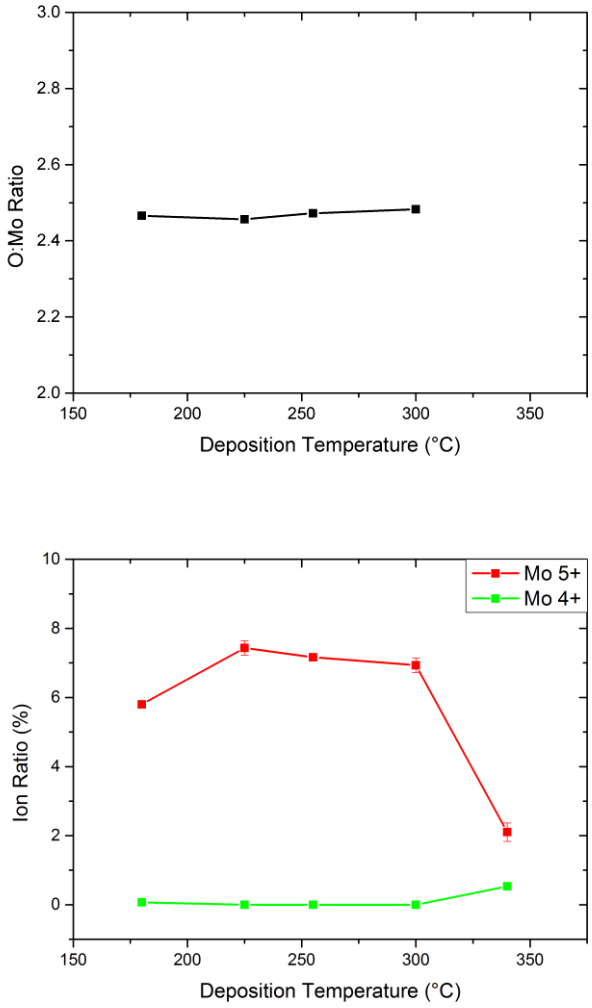

Figure 51: Data derived from XPS analysis of the deposited films. The top image displays O:Mo atomic ratios as determined by a XPS general survey scan. The ion ratio for the film deposited at 340°C could not be calculated due to the presence of the underlying ITO film in the data. The bottom image displays data derived from analysis of high resolution scans of the Mo 3d peaks. Where error bars are not visible they are smaller than the data point.

A calculated ratio for the film deposited at 340°C is not present. This is due to the fact that the XPS scan indicated a contribution from the ITO present underneath the film. This suggests that either the film was thinner than the survey depth of the XPS measurement, approximately 10nm, or that complete coverage of the substrate had not been achieved. The presence of other ITO-based contributions meant that the stoichiometry of the MoO_x film could not be extracted. Data derived from the survey scan in the top image of Figure 51 for the remainder of the films shows that the molybdenum to oxygen atom ratio is unaffected by the deposition temperature of the spray process, measuring close to 2.46 for all the

films. This is in agreement with the values reported in some literature for evaporated MoO_x[129], but other reports place the ratio at no lower than 2.7, even after annealing the film.[131]

The bottom image in Figure 51 shows that for the films deposited at lower temperatures, around 7% of the film consists of the Mo^{+5} state, with the remainder of the film made up of the Mo^{+6} state. Once the deposition temperature reaches 340°C, the proportion of the film consisting of the Mo^{+5} state significantly drops to 2%, and a small proportion of the Mo^{+4} state appears, making up 0.5% of the film. This data is consistent with the wide absorption band shown in Figure 45 in which the strength of the $Mo^{+5} \rightarrow Mo^{+6}$ inter-valance charge transfer transition decreases significantly for the film deposited at 330°C.

It is clear that for all deposition temperatures, the spray process produces films with a large number of oxygen vacancies, as the O:Mo ratio would be expected to be much higher when considering the measured ion ratio if the films were stoichiometric. Recent discussion of the inclusion of MoO_x films in organic devices has suggested that the presence of oxygen vacancies is fundamental to their efficient operation in organic devices.[130,137] It would therefore be expected that films deposited by spray pyrolysis should also improve the efficiency of devices as there appears to be a significant number of oxygen vacancies in the deposited films when compare to stoichiometric MoO_3.

6.4 Incorporation of MoO_x film into semiconductor devices

The previous section dealt with the investigation of spray deposited MoO_x films. For the results obtained to be discussed in context, however, it is necessary to incorporate the layers into organic devices so their performance can be investigated. This section thus incorporates the sprayed layers into devices. The first study reported deals with the investigation of the electrical properties of the layers by incorporating them into hole only devices with various semiconducting layers. The second study then deals with the incorporation of the layers into light emitting diodes to investigate their performance.

Hole only devices

As has already been discussed, single carrier devices allow the investigation of the behaviour of an injection contact by only allowing the injection of one carrier. Based on the expected work function of the MoO_x layers as determined through previous measurement, a variety of semiconducting polymers can be chosen for investigation of the injection properties of the layer. For this investigation, 3 materials were selected. These polymers were Poly(9,9- dioctylfluorene-co-bis-N,N-(4-butylphenyl)-bis- N,N-phenyl-1,4-phenylenediamine) (PFB), poly(9,9- dioctylfluorene-co-N-(4-methoxyphenyl)diphenylamine) (TFMO)and poly(9,9-dioctylfluorene-co- N-(4-butylphenyl) diphenylamine) (TFB) and were supplied by the Sumitomo Chemical Company. The chemical composition of the materials used are shown in Figure 52, and the structure and energy levels of the resulting hole only devices fabricated are shown in Figure 53.

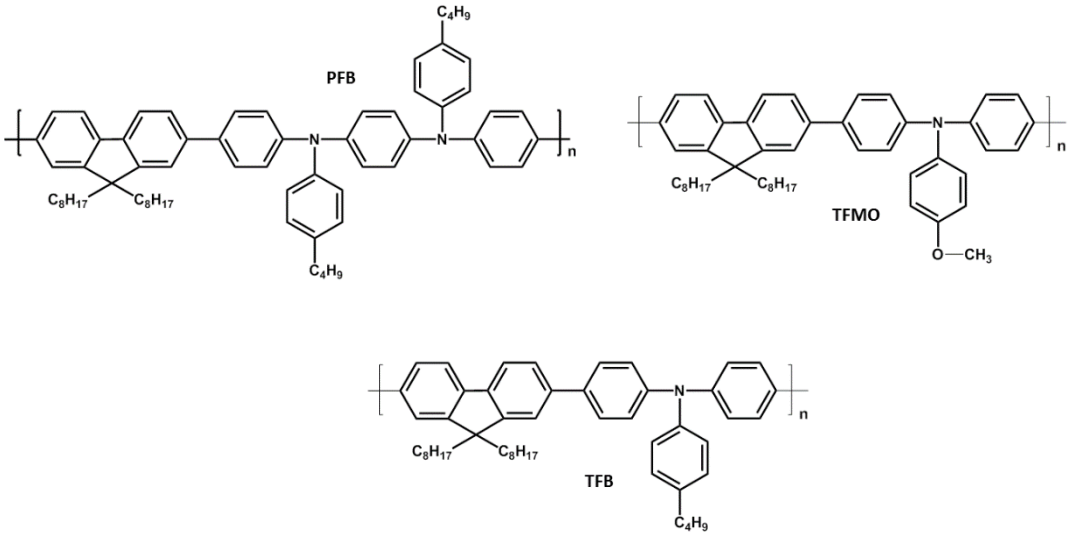

Figure 52: The three materials used for the fabrication of hole only devices. Poly(9,9- dioctylfluorene-co-bis-N,N-(4-butylphenyl)-bis- N,N-phenyl-1,4-phenylenediamine) (PFB) (left), poly(9,9- dioctylfluorene-co-N-(4-methoxyphenyl)diphenylamine) (TFMO) (right) and poly(9,9-dioctylfluorene-co- N-(4-butylphenyl) diphenylamine) (TFB) (bottom) are all relatively high mobility hole transporting polymers.[138]

The presence of evaporated MoO_3 in the structure of the devices is suitable to block any electron injection into the device. These particular hole transport materials were selected for the position of the HOMO levels in each. PFB has a HOMO level at 5.1eV[138], TFMO at 5.2eV[139] and TFB at 5.3eV.[138] From previous work function measurements performed, the work function of the sprayed MoO_x layers is expected to be of similar levels, so changes in the injection behaviour occurring at the boundary can be observed.

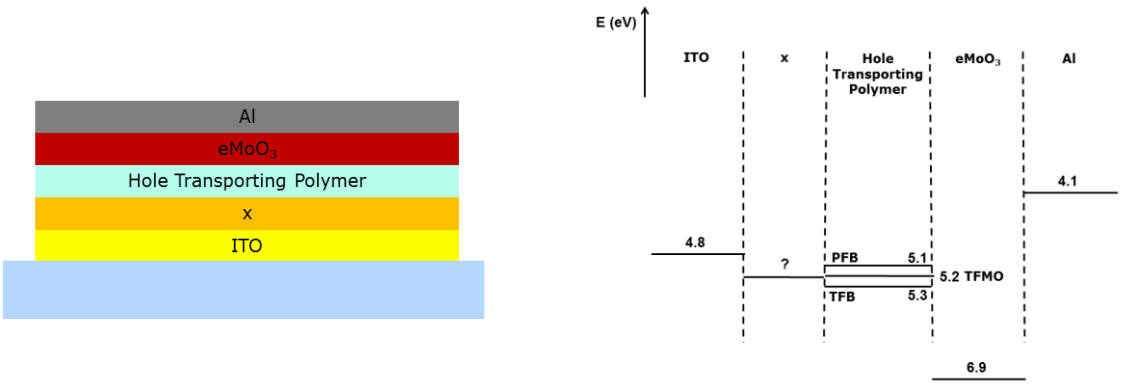

Figure 53: The device structure (left) and relevant energy levels (right) of the hole only devices fabricated for investigation of the sprayed MoO_x layers. The layer labelled 'x' represents the sprayed MoO_x layer or a different hole injection material for comparison.

Devices of the structure shown in Figure 53 were fabricated for using the spray deposited MoO_x layers as hole injection layers for the three hole transport materials discussed. Devices were also fabricated with no hole injection layer present, with ITO in contact with the hole transport layer, as well as devices using PEDOT:PSS and an evaporated MoO_3 layer for comparison. The measured electrical properties of these devices are shown in Figure 54 and Figure 55.

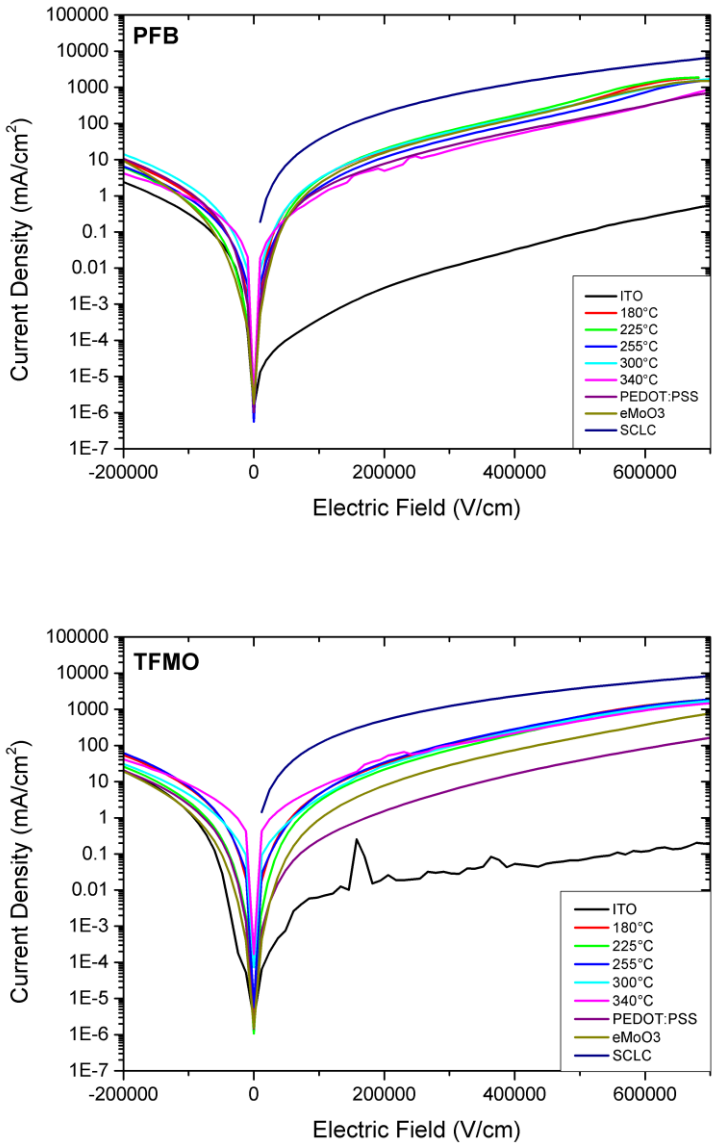

Figure 54: The electrical properties of hole only devices fabricated using various hole injection layers. The top image shows devices fabricated with PFB and the bottom with TFMO. The SCLC current density has been calculated using literature values for the mobilities of the polymers. The electric field was determined by dividing the applied voltage by the thickness of the polymer layer.

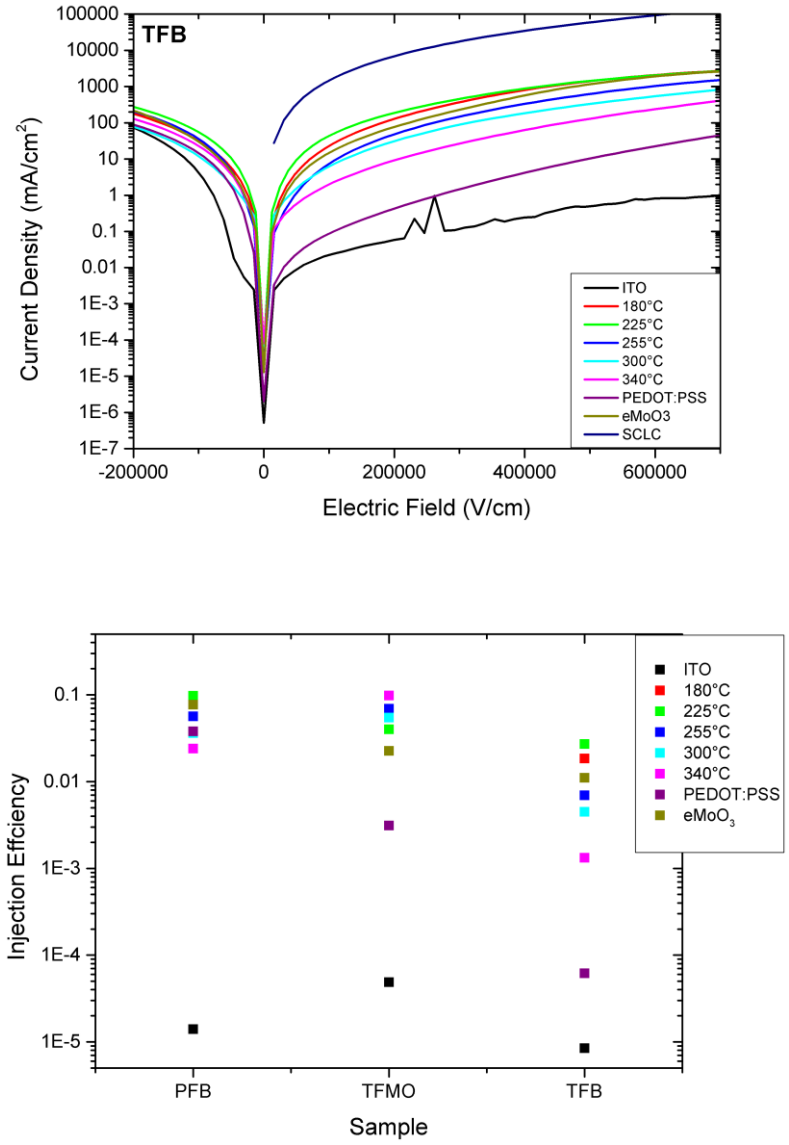

Figure 55: The electrical properties of hole only devices fabricated using various hole injection layers. The top image shows devices fabricated with TFB. The SCLC current density has been calculated using literature values for the mobilities of the polymers. The electric field was determined by dividing the applied voltage by the thickness of the polymer layer. The injection efficiency of the devices (Bottom) is calculated as the ratio of the current density of the device to the modelled SCLC at 200000 V/cm.

The theoretical SCLC current for each material in Figure 54 and Figure 55 has been calculated using Poole-Frenkel coefficients for each polymer as determined from literature. These shown in Table 2.[139,140]

	μ_0 ($\times 10^{-3}$ $cm^2V^{-1}S^{-1}$)	β ($\times 10^{-3}$ $cm^{0.5}V^{-0.5}$)
PFB	0.1	2.5
TFMO	4.5	0.75
TFB	4	1.6

Table 2: Poole-Frenkel coefficients for each polymer used in the study as determined from literature.[139,140]

For all of the devices in Figure 54 and Figure 55, it is clear that the magnitude of the current densities measured is lower than the modelled SCLC current density. This is a feature that is commonly seen in hole only devices when fabricated with materials that should be able to form an ohmic contact and thus achieve ohmic injection.[141] This is suggested to be due to the fact that vacuum level alignment may not be achieved in the device structure. However, the data from the spray deposited devices can still be compared with respect to the various reference layers that have also been used.

The top image of Figure 54 shows hole only devices fabricated with PFB as the hole transporting material which has the highest HOMO level of 5.1eV. All of the spray deposited MoO_x layers, as well as both the PEDOT and evaporated MoO_3 layer show similar injection properties, suggesting that the injection barrier at the interface has been minimised for all layers. The device with no injection layer, however, shows current densities approximately 4 orders of magnitude lower that the other layers. This result is to be expected when considering the work function of the layers involved. The work function of ITO, 4.8eV, is lower than the HOMO level of PFB at 5.1eV, and carrier injection is clearly being limited by an injection barrier at the interface. None of the other layers have a work function of less than 5.2eV, and therefore would not be expected to be injection limited.

The bottom image of Figure 54 shows hole only devices fabricated with TFMO which has the intermediate HOMO level of 5.2eV. The spray and evaporation deposited molybdenum oxide devices show similar properties to the PFB devices with these layers, as does the device with no injection layer. The PEDOT device, however, shows a decrease in current density of approximately an order of magnitude compared to the molybdenum oxide devices. As PEDOT:PSS is considered to have a work function of 5.2eV, it would not be expected to be injection limited in this device. It is suggested that the energy level alignment at the PEDOT:PSS interface must produce an unfavourable dipole which is limiting carrier injection to some extent, or that the interaction between the layers is modifying the PEDOT:PSS properties. Chemical interactions between the various polymer layers and injection layers may also be having an effect on the behaviour of the devices.[142]

The top image of Figure 55 shows hole only devices fabricated with TFB which has the lowest HOMO level of 5.3eV. The ITO device continues to be injection limited, and as for TFMO the performance of the PEDOT:PSS device is notably poor. In addition, the spray deposited MoO_x devices now begin to show differences in performance. The films deposited at 180°C and 225°C continue to show minimum injection barrier properties. The films deposited at higher temperatures, however, show decreases in current density, with a larger magnitude decrease as the deposition temperature increases. As the work function of the deposited films was found to decrease with increasing deposition temperature, this is the expected result as the injection barrier increases and the device moves away from minimised injection barriers.

The bottom image of Figure 55 shows the injection efficiencies for the various layers into the various hole transport materials. These values have been calculated as a fraction of the modelled SCLC current, which is the maximum theoretical current that could be achieved in each device. This image can be considered to be a summary of the other images in the figure, and shows the same observations. It is notable that even in the case of the best performing MoO_x layers, which from their measured work function could be expected to show ohmic injection, the ratio to the theoretical SCLC calculation is still far lower than one. This is likely due to the mobility of the layers used for these experiments being lower than the literature values used for the calculation. There is also evidence that other factors prevent the achievement of true ohmic injection at interfaces that would be expected to.[141]

It can also be useful to consider the electrical properties of single carrier devices on a log-log plot. The data shown in Figure 54 and Figure 55 is thus re-plotted in Figure 56.

Log scales of single carrier devices can be useful for determining the type of transport occuring. If the hole transport material is considered to contain no traps, The current density gradient on a log-log scale should be constant in the case of ohmic injection where the current is space charge limited,[143] and the modelled SCLC shows this.

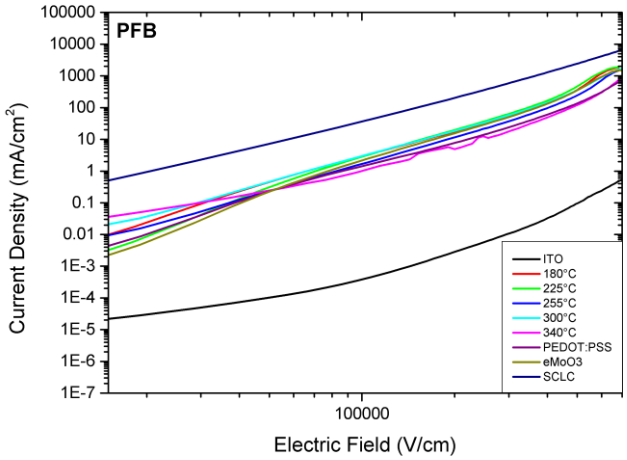

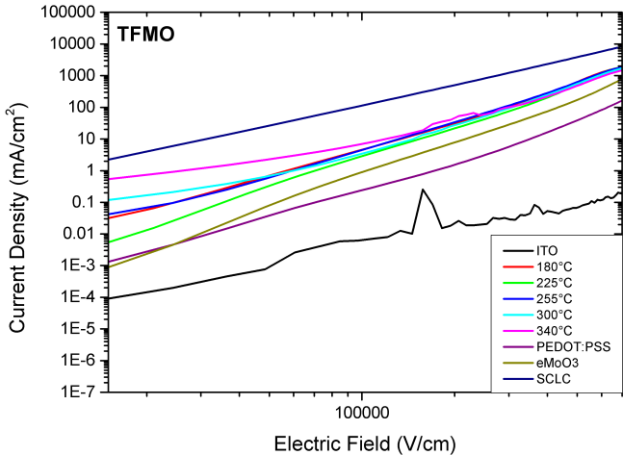

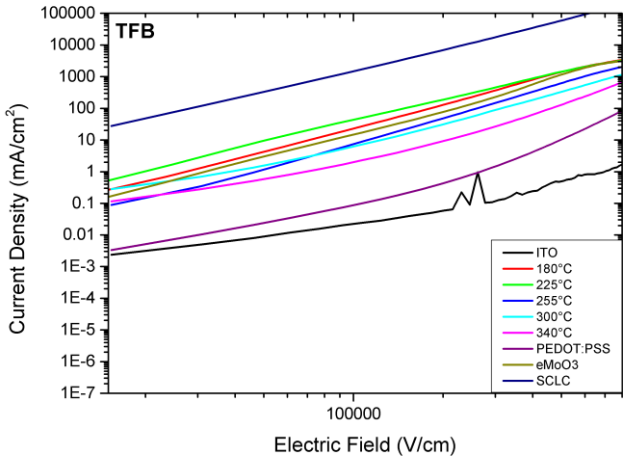

Figure 56: The data shown in Figure 55, re-plotted on a log-log scale.

Behaviour differing from a linear nature suggests the presence of traps in the material.[144] However, the shape of the various curves in Figure 56 appears to remain constant across the different hole transport materials used. For example, the single carrier devices fabricated by spray deposition at 250°C appear to show a linear response on the log-log figure with a gradient of 2 for all three transport materials, whereas the deposition at 330°C shows an initial gradient lower than 2 for all three materials. This would suggest it is the interface at the injection contact that is responsible for these variations, perhaps suggesting that variations in the deposition method of the charge injection layer can cause variations in the trap density of the organic semiconducting material deposited on top.

OLED performance using MoO_x as a hole injection layer

The final step in the investigation of the sprayed molybdenum oxide layers is the fabrication of luminescent devices to investigate the effect of the deposited layers on device performace. Luminescent devices were prepared using the spray deposited MoO_x layer and several reference layers using F8BT as the emissive layer of the device. The basic structure of the devices prepared is shown in Figure 9 consisting of the injection layer, shown in the figure as PEDOT:PSS deposited on ITO, followed by the emissive layer and a calcium/aluminium top contact. This is one of the simplest structures possible, and thus allows for the properties of the injection layer to be better understood.

The current density response of the fabricated devices is shown in Figure 57. The top image in Figure 57 shows the current density response of devices fabricated with the sprayed molybdenum oxide layer deposited at various temperatures. The devices with a layer deposited at 180°C and 225°C show very low leakage current, which then increases drastically as the deposition temperature is further increased. This increase in current density would be expected to partially arise from the reduced thickness of the sprayed layer as the deposition temperature is increased. It is unlikely that the increase is due to reduced electron blocking at the interface as the increased current is symmetrical in both forward bias (before switch on) and reverse bias. As the roughness of the sprayed film decreases with increasing deposition temperature it is unlikely that the increase in current is due to incomplete coverage of the emissive layer. It is possible that as the deposited layer becomes thinner, pinholes are appearing in the film, and that these could increase the leakage current of the device.

The switch on voltage of the devices occurs between 2.2-2.4V for all of the measured devices, independent of the leakage current density. The low temperature 180°C and 225°C spray deposited devices also show a minimum current density that is significantly offset for the 0V, unlike the higher

temperature devices where the current density has a sharp minimum at 0V. This is likely due to the presence of traps in the emissive layer which are known to produce this feature. The apparent larger leakage current for the devices containing layers deposited at a higher temperature may then be masking the appearance of this feature in those layers.

The bottom image of Figure 57 shows the current density response of devices fabricated with the 225°C spray deposited MoO_x layer compared to a PEDOT:PSS injection layer and two thicknesses of evaporated molybdenum oxide layer. All the reference devices show low leakage current, although the thinner evaporated molybdenum device shows an increased reverse bias current. As the evaporated molybdenum layer is exposed to oxygen during the fabrication process, degradation of the layer is expected to arise from interactions with moisture and oxygen.[129] The performance of the thinner layer would be expected to be more affected by this exposure.

The switch on of all the reference devices occurs between 2.2 and 2.4V.

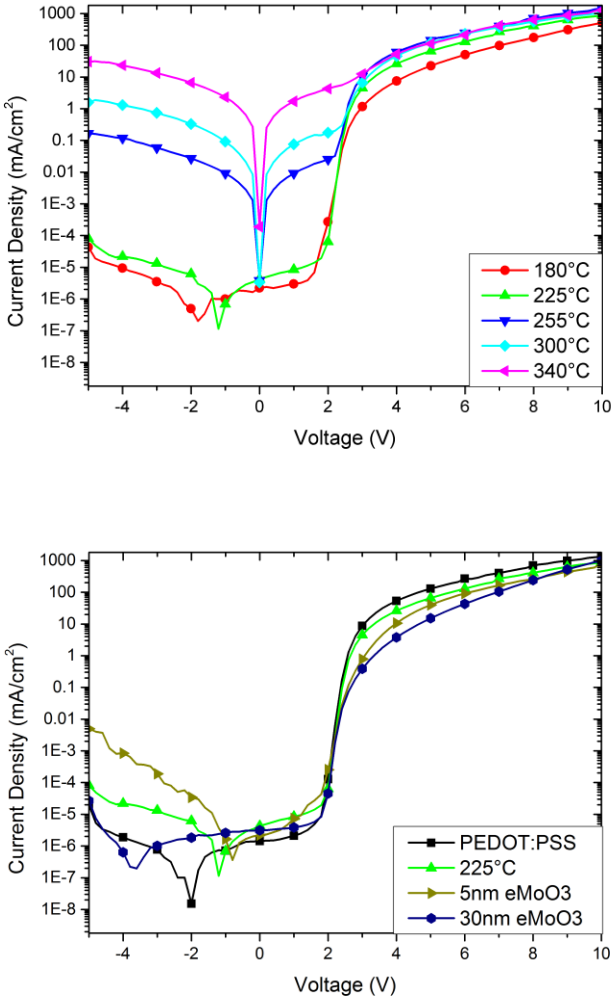

Figure 57: The measured current voltage response of luminescent devices fabricated using spray deposited molybdenum oxide injection layers as well as various reference layers. The top image shows the effect of the variation of the deposition temperature of the spray pyrolysis process. The bottom image displays a comparison of the sprayed MoO_x layer deposited at 225°C with several reference layers.

The measured luminance of the fabricated devices is shown in Figure 58.

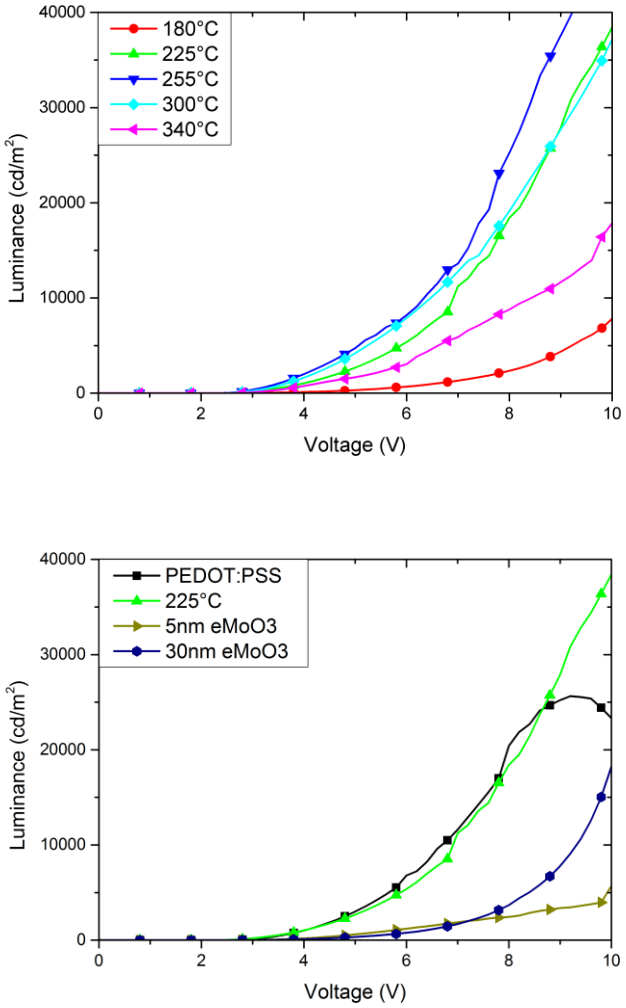

Figure 58: The measured luminance response of luminescent devices fabricated using spray deposited molybdenum oxide injection layers as well as various reference layers. The top image shows the effect of the variation of the deposition temperature of the spray pyrolysis process. The bottom image displays a comparison of the sprayed MoO_x layer deposited at 225°C with several reference layers.

The top image of Figure 58 shows the measured luminance of the spray deposited layers. There are clearly large variations in luminance as the deposition temperature is varied. The device containing the layer fabricated at 180°C shows a low luminance. As the deposition temperature increases, the luminance of the device increases up to a peak for the device containing the layer deposited at 255°C. The luminance of the device then decreases as the deposition temperature of the hole injection layer is further increased. The luminance of each of these devices continues to increase for the entire measurement range up to 10V and in the case of the 225°C, 255°C and 300°C deposited MoO_x layers exceeds 35,000 cd/m^2

The bottom image of Figure 58 shows the luminance of devices fabricated with the 225°C spray deposited MoO_x layer compared to the reference layers. Here, the sprayed layer device shows similar performance to the PEDOT:PSS layer until relatively high voltages are reached, where the performance of the PEDOT:PSS device begins to break down. This is likely due to the acidic nature of the PEDOT:PSS damaging the ITO surface, which then causes further break down when the device is exposed to higher temperature associated with high voltage operation.[145] The luminance of the two evaporated molybdenum oxide layers is significantly lower than the sprayed layer. This is likely due to the evaporated layers sensitivity to oxygen and moisture.

The current density and luminance data obtained can then be combined to produce data on the current efficiency and power efficiency of the devices. This derived data is shown in Figure 59.

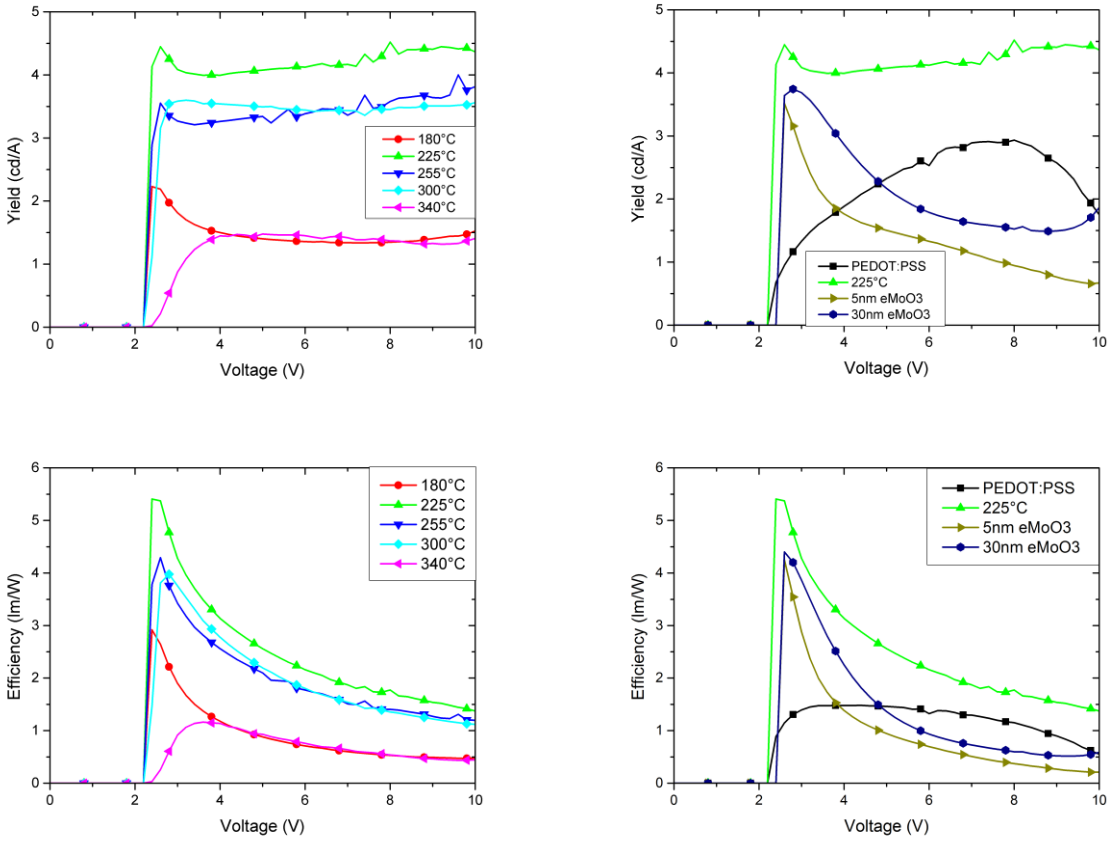

Figure 59: The measured current efficiency (top) and luminous efficiency (bottom) of devices fabricated using various hole injection layers with respect to voltage. The left images display the measured luminous efficiency of the spray deposited layers. The right images display the measured efficiency of the sprayed MoO_x layer deposited at 225°C with several reference layers.

The left images in Figure 59 display that the luminous efficiency of devices prepared using the sprayed layers is initially low for low temperature deposition, but quickly rises to a peak efficiency of 5.4lm/W for the film deposited at 225°C. As the deposition temperature is further increased, the efficiency drops, with the device prepared with 330°C MoO_x having the lowest peak efficiency of all the measured devices. This efficiency roll-off is usually attributed to triplet-triplet annihilation.[146] These results are fully representative for devices prepared using the spray pyrolysis method. The right images of Figure 59 display the performance of the device containing the MoO_x layer deposited at 225°C in comparison to devices with other reference layers. The device incorporating a 60nm PEDOT:PSS layer shows a peak efficiency of 1.45 lm/W, and devices containing both 5nm and 30nm evaporated MoO_x layers peak at 4.2 lm/W and 4.4 lm/W respectively. It can be seen that the spray deposited layer thus produces devices with higher luminous efficiencies in than for either PEDOT:PSS or evaporated MoO_3 injection layers.

It can also be useful to view efficiency data plotted against the luminance of the devices. This is shown in Figure 60.

The thin film results can now be discussed in the context of this measured device performance. As the efficiency of the devices decreases for films deposited above 225°C, it is clear that the surface roughness of the films as shown in Table 1 is not the primary determinant of device performance here, as an increase in deposition temperature leads to smoother films. The lack of a significant change in performance when the thickness of the eMoO_x reference layers is varied suggests that the change in thickness of the spray deposited layers is also unlikely to be a source of performance variation in the devices.

The film deposited at 225°C has both the deepest work function and highest proportion of Mo^{+5} state, as shown in Figure 46 and Figure 51. It would thus appear that the measured work function of the film is the most important factor when determining device performance, as would be expected as a deep work function provides the most favourable energy level alignment to the HOMO of the emissive polymer.

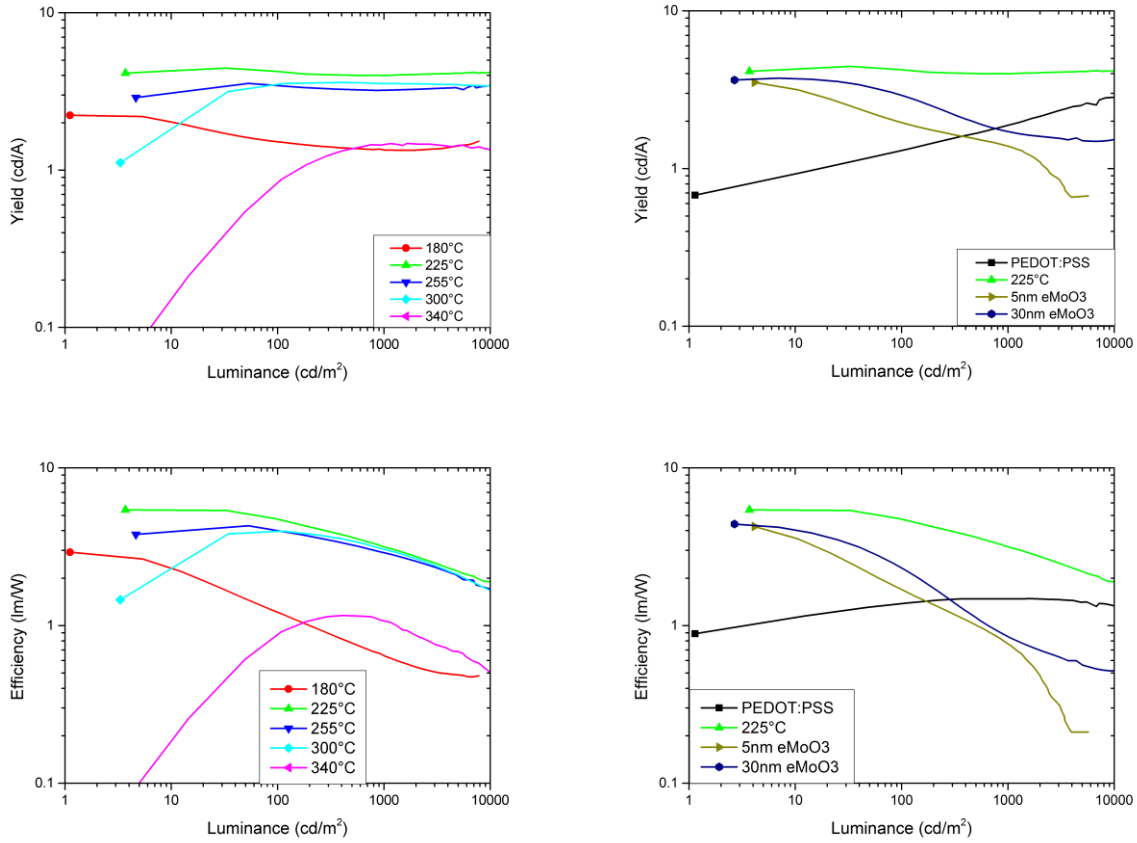

Figure 60: Efficiency data similar to that shown in Figure 59, plotted against luminance on a log-log scale to illustrate the performance of the various layers at both low and high luminance values.

6.5 Incorporation into higher efficiency OLED devices

The investigation in the previous section has shown that spray deposition of an optimised molybdenum oxide hole injection layer can achieve an increase in the device efficiency when compared to standard layers. However, the main study performed in the previous section was performed with a very basic device structure for a relatively less efficient emissive layer.

For a more in depth investigation of the spray process, it was determined that it would be useful to investigate the performance of the layer in a higher efficiency device stack as well. The layer deposited at 225°C, as the best performing in the temperature study, was selected to be used I ourn further investigation.

Surface characterisation of MoO_x layer

Atomic force microscopy scans compliment information obtained from profilometry data that was discussed earlier in the chapter. AFM scans performed on a MoO_x layer spray deposited at 225°C are shown in Figure 61.

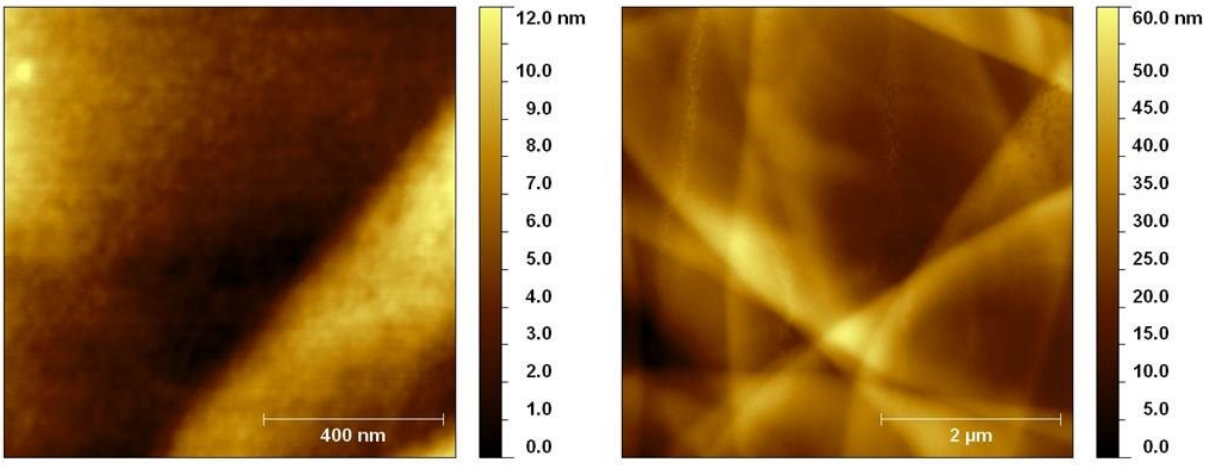

Figure 61: AFM scans of a MoO_x layer deposited using spray pyrolysis at 225°C on a ITO coated glass substrate. The left image shows a 1×1µm area in the centre of the 5×5µm area of the right image.

The figure shows two different sized areas of the sample. The left image shows a $1\times1\mu m^2$ portion of the sample. The root mean square roughness of the area was measured to be 2.6nm. The right image shows a $5\times5\mu m^2$ area of the sample. The root mean square roughness of this area was measured to be 8.9nm.

These images are an indication of the effect of spray deposition on the surface profile of the sample. The large scale image shows ridges present in the sample most likely due to the Marangoni effect of

evaporating droplets at the surface of the sample, as has already been discussed. The surface structure in this image correlates with the surface profilometry data discussed previously.

The left image, however, details the surface structure on a smaller scale where the large droplets are no longer a factor. Here, the surface roughness is much decreased, and approaches figures that have been reported for molybdenum oxide prepared through other methods. This would suggest that the surface of the layer on the nanoscale is suitable as an injection layer. However the larger scale non-uniformity results in some patterning that is visible at low luminance when the device turns on. Efforts to improve the spray pyrolysis technique further could reduce this effect.

Fabrication of higher efficiency devices

The 225°C layer was then incorporated into higher efficiency devices. The emissive layer of the devices was a guest-host blend with 5 wt% of the guest phosphorescent green emitter Bis(2-phenylpyridine)(acetylacetonate)iridium(III) ((PPy) 2 Ir(acac)) dispersed in a 60:40 volume blend of 2,6-Bis(3-(9H-carbazol-9-yl)phenyl)pyri- dine (26DCzPPy) and 4,4’,4’’-tris(N -carbazolyl) triphenylamine (TCTA) as host. Details of the general structure and preparation of these devices are presented elsewhere.[10] The sprayed molybdenum layers were incorporated in these devices as an alternative hole injection layer. It was also postulated that the thickness of the sprayed molybdenum oxide layers may be reducing the efficiency of devices incorporating the layer due to the shunt resistance introduced into the device by a thicker insulating layer, but attempting to reduce the thickness led to inconsistent device performance.

As a possible solution to this problem a thin sprayed MoO_x layer was deposited at 225°C onto PEDOT:PSS. As the PEDOT:PSS layer should remain stable at these temperatures, it was hoped that the presence of the PEDOT:PSS layer might stabilise the device performance, allowing a thinner sprayed MoO_x layer to produce efficient devices through assisting with hole injection. The measured current voltage and luminance data of the various devices is presented in Figure 62.

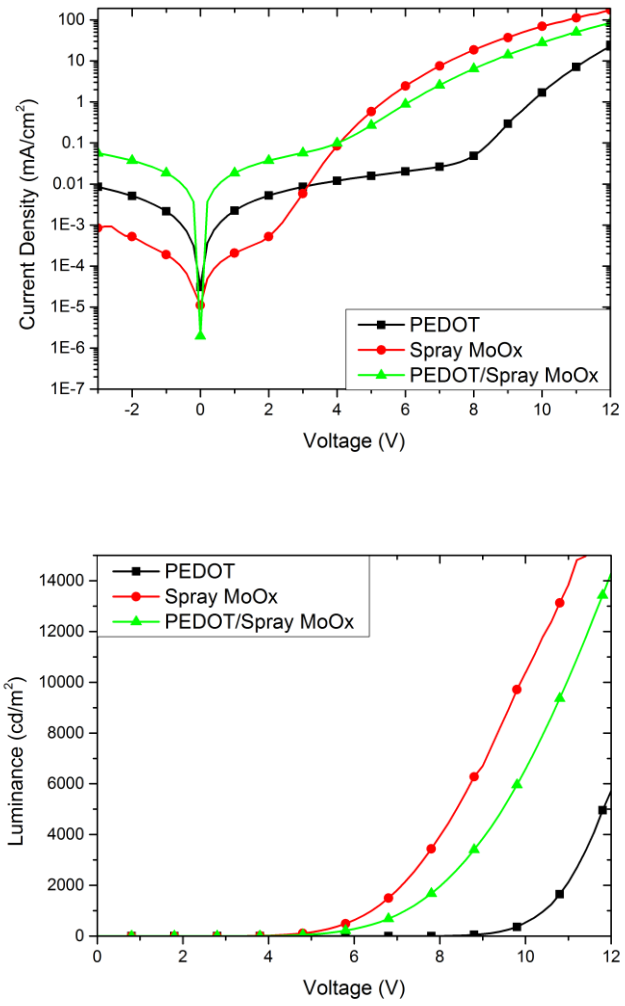

Figure 62: The measured current voltage response (top) and luminance (bottom) of devices fabricated using spray deposited molybdenum oxide injection layers, a PEDOT:PSS layer, or a sprayed molybdenum oxide layer deposited on top of a PEDOT:PSS layer.

The top image shows the current density response of the three types of device. The superior performance of the device containing the spray deposited molybdenum oxide layer when compared to the device containing PEDOT:PSS is evident in the reverse current and the switch on voltage of the devices.

The current in reverse bias for the MoO_x device is an order of magnitude lower than that of the PEDOT device. This implies improved blocking of reverse carriers, which would improve the efficiency of the device, and is likely due to the deeper valence band of MoO_x when compared to PEDOT:PSS. The switch on voltage of the MoO_x device has been reduced significantly, down to approximately 2 volts from 8

volts for the PEDOT device. Operation at a lower voltage again leads to more efficient emission, and is explained by the deeper work function of the MoO_x layers noted above leading to a decrease in injection barrier for holes into the device.

The combined PEDOT:PSS/MoO_x shows an interesting mix of properties. The reverse current of the device is an order of magnitude higher than the PEDOT:PSS reference device. The switch on voltage, however, occurs at around 4 volts, an improvement on the control device.

A possible explanation of these properties is that the spray deposition of the molybdenum oxide damaged or washed away a substantial portion of the PEDOT:PSS layer. As the deposited MoO_x layer is thin, it is likely that incomplete coverage of the device has occurred. The MoO_x that is present has improved the switch on voltage of the device, but the incomplete coverage results in short pathways and an increased reverse current. This would tend to suggest that the efficiency of the resulting device should be reduced.

The bottom image of Figure 62 shows the measured luminance of the devices. The onset of emission from the devices occurs as would be expected from the current density response already discussed. It is noteworthy that both devices containing the sprayed MoO_x layer reach a luminance of 10,000 cd/m^2, whereas the PEDOT:PSS device reaches only 6000 cd/m^2 in the measurement range.

The data shown in Figure 62 can be used to calculate the yield and luminous efficiency of the device under study. This data is shown in Figure 63.

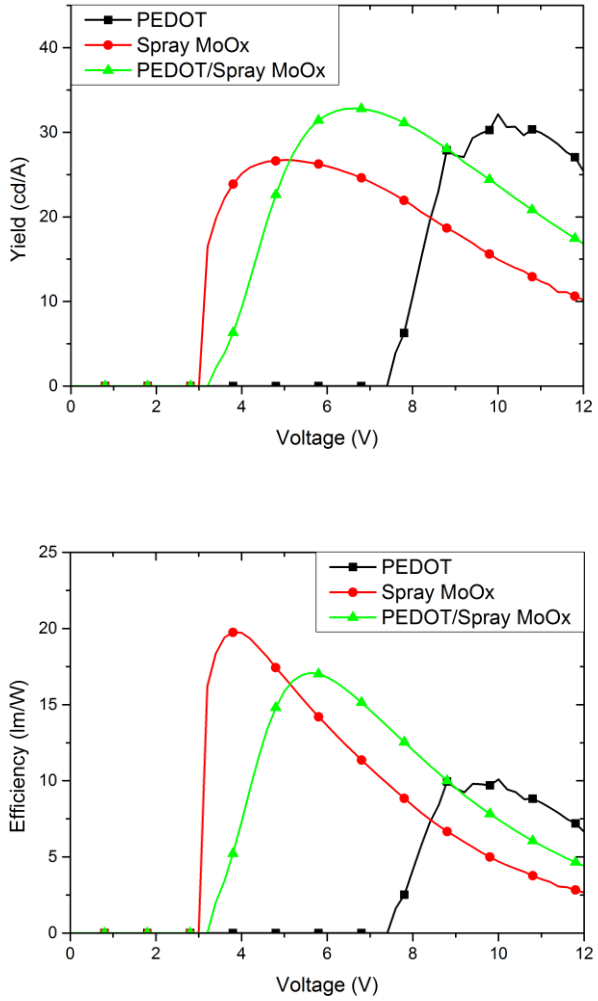

Figure 63: The measured yield (top) and efficiency (bottom) of devices fabricated using a spray deposited molybdenum oxide injection layers, a PEDOT:PSS layer, or a sprayed molybdenum oxide layer deposited on top of a PEDOT:PSS layer.

The top image shows the yield of the devices. It is interesting that here the maximum yield is achieved by the combined PEDOT:PSS/MoO_x device at 33cd/A, followed by the PEDOT:PSS reference device at 30cd/A and the MoO_x device at 26cd/A. The combined and control devices here achieve better peak yields as the current efficiency value is not dependent on the voltage that the device is operating at. This means that although the switch on of each of these devices is higher than that of the device only containing MoO_x, the lower current flows during emission for the other devices lead to higher yields, albeit at higher operation voltages. The injection layers in each case are of a similar thickness, so this should not result in any variation in device performance due to varying thickness.

When the power efficiency is considered, shown in the bottom image, the advantages of the spray deposited MoO_x become clear. The device reaches a peak efficiency of 20 lm/W at 3.8V. This is twice the peak efficiency reached by the PEDOT:PSS containing device, which peaks at around 10 lm/W at 10V. The combined PEDOT:PSS/ MoO_x device reaches a peak efficiency of of 17 lm/W at 5.6V.

It is useful to examine the efficiency of the devices with respect to the luminance levels they can achieve. These plots are shown in Figure 64.

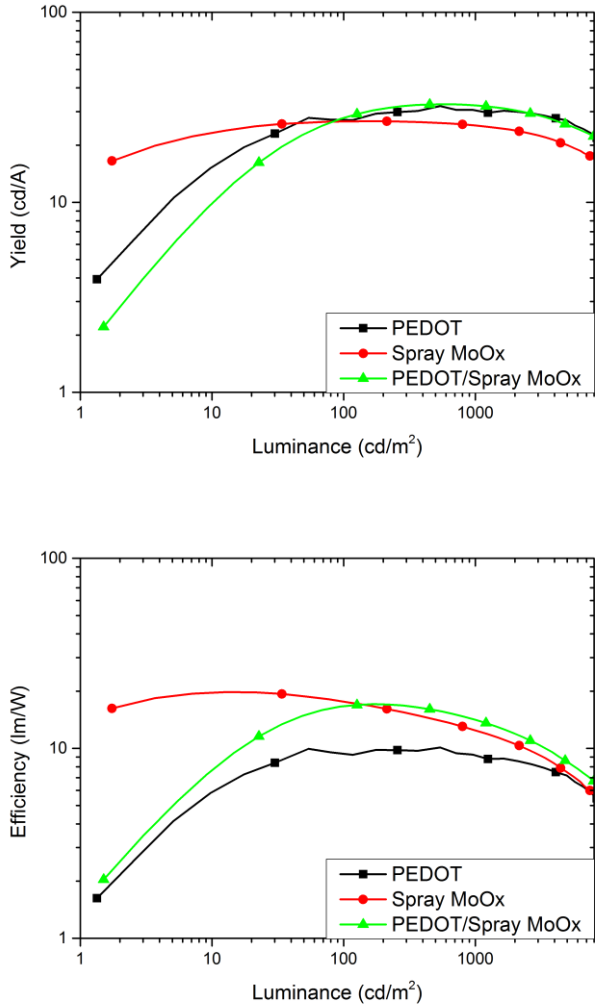

Figure 64: The efficiency data for the devices shown in Figure 63, plotted against luminance on a log-log scale.

The figure shows that for luminance levels up to 100 cd/m^2, the spray deposited MoO_x device shows superior performance when compared to the two other devices. In addition to this, in terms of luminous

efficiency, the bottom image shows that the spray deposited MoO_x device shows superior performance to the PEDOT:PSS device across all luminance values.

These studies have shown that the spray deposited MoO_x layer can provide an injection layer which improves the performance of a solution processed OLED device. The superior performance achieved is likely due to the same reasons as performance improvements were seen in the temperature study of the material, in that the deeper work function of the spray deposited layer when compared to that of PEDOT:PSS leads to better hole injection at the interface.

There is some suggestion that a combination of PEDOT:PSS with the sprayed MoO_x layer may be able to produce a superior device to either material alone, but it is clear the deposition process would need to be modified to be more compatible with PEDOT:PSS. It is possible that alternative solvents could be used to achieve this.

6.6 Conclusion

In this section, the fabrication of molybdenum oxide (MoO_x) layers using the method of spray pyrolysis has been investigated. A brief discussion of the current understanding of how molybdenum oxide can improve the performance of organic devices, along with previous work on depositing the layer was given.

The composition of the sprayed films, as well as their optical and electrical properties was then investigated. The compactness and roughness of the layers appears to be less important to their performance when incorporated into a device. The superior performance of the sprayed MoO_x devices is ascribed to their deep work function, which allows better energy level alignment with the emissive layer.

Devices using Poly[(9,9-di-*n*-octylfluorenyl-2,7-diyl)-*alt*-(benzo[2,1,3]thiadiazol-4,8-diyl)] (F8BT) as an emissive layer have been fabricated incorporating the sprayed MoO_x as a hole injection layer which show good performance in comparison to both devices using Poly(3,4-ethylenedioxythiophene):poly(styrenesulfonate) (PEDOT:PSS) and evaporated MoO_x as injection layers. A peak efficiency of 5.4lm/W has been achieved with the sprayed layer, more than three times that of the PEDOT:PSS device of the same material.

Finally, the best performing layer deposited at 225°C was selected and incorporated into a higher efficiency solution processed OLED device. Here, a peak efficiency of 20 lm/W was achieved, around double that of the device fabricated with PEDOT:PSS. The switch on voltage of these devices was also reduced to 2V from 8V by incorporating the MoO_x layer.

This section has thus shown that the spray deposition of molybdenum oxide is a feasible method for reducing the complexity of the deposition of the device stack and determined the optimal temperature for doing so.

7 Conclusion

The aim of this work has been the investigation of the spray pyrolysis process for the deposition of various metal oxides. Before discussing the final conclusions, it is useful to consider some of the further work that could be performed in each of the studies that form part of this thesis.

7.1 Further Work

The first area of study for this project was the general spray pyrolysis process. There are a number of improvements which could lead to improved film deposition using the process. Ultrasonic spray heads, which involve the fast vibration of the head to improve atomisation of the solution,[147,148] lead to smaller droplets of solution and thus less energy required for the evaporation of the solution as the deposition takes place. This should reduce the surface roughness of the films deposited, particular evident in the spray deposition of molybdenum oxide in this work.

Another technique that might be explored is the inflight heating of the spray solution to encourage decomposition. This can be achieved by infra-red heating of the droplet stream.[149] This approach can allow the temperature of the deposition substrate to be reduced, perhaps opening the way for deposition at plastic compatible temperatures, particularly for the deposition of the zinc oxide films.

Both of these methods would require significant changes to the spray apparatus used here, so were not investigated in this project. However, they could lead to a reduction in deposition temperature, one of the most important goals of any deposition technique being used in conjunction with plastic electronics.

The second area of study was the deposition and doping of zinc oxide films as a transparent conductive layer. Here, one of the more interesting areas for study would be the introduction of other precursors. As the deposition temperature was limited in part by the requirements for the decomposition of the zinc acetate precursor, using a more volatile precursor could result in achieving conducting layers at lower deposition temperatures.

Diethyl Zinc is an extremely volatile precursor, so volatile that exposure to air results in the formation of zinc oxide. This makes the material difficult to work with, but the material has been used to spray deposit zinc oxide layers.[150] It is possible that combining this material with other spray precursors could lead to much lower temperature deposition.

In addition to this, there are other possible dopants that may be able to be used as sintering aids in the spray deposition process. An example is yttrium, which has been suggested to improve the crystallinity of zinc oxide layers when co-deposited together.[151] This might lead to improvements in the conductivities of the deposited films in a similar manner to that for lithium doping as used in this work. There may also be other sintering aids that could serve a similar purpose.

The final area studied was the deposition of molybdenum oxide films as hole injection layers. Here, there is interesting work to be performed on the doping of the layer to manipulate its work function. Aluminium doping has been suggested as a method of reducing the work function of the molybdenum oxide layer to make it suitable for use in the cathode of a device as an electron injection layer,[152] given that the material is n type. Initial experiments were performed to investigate this process using the spray deposition technique, but have not progressed to the point where the data can be presented as wholly reliable. However, this is an interesting area for further investigation. Caesium doping has also been suggested as a route to manipulating the work function of the layer.[153]

Finally, moving into the more general possibilities there are a number of other metal oxides with applications as contact layers. Zinc oxide has undergone a large amount of investigation as an electron injection layer in organic devices.[154–156] Vanadium[110,157] and tungsten oxide[158,159] are possibilities for hole injection or extraction. Although the bulk materials have been studied in some detail, spray pyrolysis allows for the co-deposition and doping of these various materials, which may lead to interesting combinations of properties and superior device performance.

These various prospects would all provide interesting scope for further work to be performed in the area of study for this thesis.

7.2 Final Conclusions

This project has aimed to study the spray deposition of various metal oxides for use in the contacts of organic electronic devices.

The thesis began with an introduction to some of the context of organic devices in terms of the physics involved in the materials, with a focus on the injection mechanics that are found at boundaries in organic electronic devices. This was followed by a discussion of the deposition and characterisation techniques used during the project. The aim of both of these chapters was to provide the reader with a broad context of the area in which the work of the project was being performed, as well as discussing the reasoning behind the use of spray pyrolysis as a deposition technique and the various characterisation techniques employed.

The next chapter dealt with the initial spray experiments and the optimisation of the deposition of the various layers. As the spray deposition of zinc oxide has been studied in some detail previously, the investigation here focussed on some of the properties likely to be observed in the main doping investigation. One of the main discoveries here was that the doping of zinc oxide with aluminium did not show measurable conductivity below a deposition temperature of 350°C, so the investigation in the next chapter focused on temperatures above this. The initial optimisation of the molybdenum oxide spray process suggested minimum deposition temperatures above 150°C, and that 280°C appears to be a point at which the properties of the film may change.

The next chapter then involved the main study of the spray deposition of aluminium doped zinc oxide and further doping with lithium. The first half of this chapter gave a summary of the physical, optical and electrical properties of various aluminium and lithium dopings of the sprayed zinc oxide films. The aluminium doping produced moderate levels of conductivity in the zinc oxide, but still at orders of magnitude too low to be used as an electrode in a device. In addition to this, the addition of lithium did not appear to improve the measured conductivity of the devices. This investigation thus moved on to annealing the films under a nitrogen environment. This was found to significantly improve the conductivity of the deposited layers, and here the lithium doping was found to further increase the conductivities of the layers. A resistivity of $5.02 \times 10^{-3}\Omega$cm was obtained for the 0.5% lithium doped 2% aluminium doped film.

In the final experimental chapter, the spray deposition of molybdenum oxide and its inclusion as a hole injection layer in organic electronic devices was investigated. Detailed physical and electrical characterisation was performed on layers deposited at a variety of temperatures. It was expected from previous work performed that the ion ratio in the films would be an important factor, but this was found not to be the case. However, the stoichiometry of the films suggests that the presence of large numbers of oxygen vacancies is important to the performance of the films. It is the measured work function of the films, however, that best correlated with device performance. The sprayed molybdenum oxide layers were then incorporated in a high efficiency solution processed organic light emitting diode, achieving a peak efficiency of 20 lm/W was achieved, around double that of an equivalent device fabricated with PEDOT:PSS.

The intent of this project has been to both show that spray pyrolysis is a versatile technique for use in organic electronics, as well as to investigate the inclusion of metal oxide materials in organic devices. The project has shown that the method can be applied to deposit a transparent conducting layer and hole injection layers, showing the variety that can be achieved with the technique as well as the improvements in the field that the inclusion of metal oxides in device structures can provide.

Publications

Wang, X., Levermore, P. A., Ramon, M. C., Voigt, M., Belton, C., Lofts, E., Cheung, C., Stavrinou, P., Nelson, J. and Bradley, D. D. C. (2013), Paper No P33: Large-Area Printed Transparent Electrodes for Flexible Organic Light-Emitting Diodes. SID Symposium Digest of Technical Papers, 44: 112–114. doi: 10.1002/sdtp.43

Lofts E., Perumal A., Faber H., Wang, X., T. D. Anthopoulos and Bradley, D. D. C., Preparation of Molybdenum Oxide Kayers by various Solution Processing Methods to enhance Hole Injection in Organic Light Emitting Diodes (in prep)

Lofts E, Mclachlan M, Wang, X. and Bradley, D. D. C., Effect of substrate temperature on the spray deposition of Molybdenum Oxide Layers for use in Organic Light Emitting Diodes (in prep)

Talks

Spray Pyrolysis of MoO_x Layers for Incorporation in the Anode Contact of Organic Electronic Devices, 2014 MRS Fall Meeting, Symposium P – Hybrid Oxide/Organic Interfaces in Organic Electronics

References

1. Kryj, P., Kruit, M. & Moore, P. Freeimages.com.
2. McNeil, R., Siudak, R., Wardlaw, J. H. & Weiss, D. E. Electronic Conduction in Polymers. *Aust. J. Chem.* **16,** 1056–1075 (1963).
3. Ekimov, A. I. & Onushchenko, A. A. Quantum size effect in three-dimentional microscopic semiconductor crystals. *JETP Lett* **34,** 345–348 (1981).
4. Walzer, K., Maennig, B., Pfeiffer, M. & Leo, K. Highly Efficient Organic Devices Based on Electrically Doped Transport Layers. *Chem. Rev.* **107,** 1233–1271 (2007).
5. Hwang, J., Wan, A. & Kahn, A. Energetics of metal–organic interfaces: New experiments and assessment of the field. *Mater. Sci. Eng. R Reports* **64,** 1–31 (2009).
6. Burroughes, J. H. *et al.* Light-emitting diodes based on conjugated polymers. *Nature* **347,** 539–541 (1990).
7. Jenekhe, S. a. Polymer semiconductors: a fast mover with a bright spark. *Nat. Mater.* **7,** 354–355 (2008).
8. Günes, S., Neugebauer, H. & Sariciftci, N. S. Conjugated polymer-based organic solar cells. *Chem. Rev.* 1324–1338 (2007). doi:10.1021/cr050149z
9. Cai, M. *et al.* High-efficiency solution-processed small molecule electrophosphorescent organic light-emitting diodes. *Adv. Mater.* **23,** 3590–3596 (2011).
10. Perumal, A. *et al.* High-Efficiency, Solution-Processed, Multilayer Phosphorescent Organic Light-Emitting Diodes with a Copper Thiocyanate Hole-Injection/Hole-Transport Layer. *Adv. Mater.* n/a–n/a (2014). doi:10.1002/adma.201403914
11. Pope, M. & Swenberg, C. E. *Electronic Processes in Organic Crystals and Polymers*. (Oxford University Press, 1999).
12. Yersin, H. *Transition Metal and Rare Earth Compounds III*. *Springer* (2004). doi:10.1017/CBO9781107415324.004
13. Baldo, M. A. *et al.* Highly efficient phosphorescent emission from organic electroluminescent devices. *Nature* **395,** 151–154 (1998).
14. Kulkarni, A. P., Tonzola, C. J., Babel, A. & Jenekhe, S. A. Electron Transport Materials for Organic Light-Emitting Diodes. *Chem. Mater.* **16,** 4556–4573 (2004).
15. Sze, S. M. & Ng, K. K. *Physics of Semiconductor Devices*. (John Wiley & Sons, 2007).
16. Meerheim, R., Furno, M., Hofmann, S., Lüssem, B. & Leo, K. Quantification of energy loss mechanisms in organic light-emitting diodes. *Appl. Phys. Lett.* **97,** 25–28 (2010).
17. Haynes, W. M. *CRC Handbook of Chemistry and Physics*. (CRC Press/Taylor and Francis, 2012).
18. Minami, T. Transparent conducting oxide semiconductors for transparent electrodes. *Semicond. Sci. Technol.* **20,** S35–S44 (2005).
19. Fortunato, E., Ginley, D., Hosono, H. & Paine, D. C. Transparent Conducting Oxides for Photovoltaics. *MRS Bull.* **32,** 242–247 (2007).
20. Wang, Z. B. *et al.* Optical design of organic light emitting diodes. *J. Appl. Phys.* **109,** 053107 (2011).
21. Lawson, R. P. W. & Carter, G. The Desorption of Mercury and the Work Function of Polycrystalline Gold. *Appl. Phys. Lett.* **9,** 85 (1966).
22. DuBridge, L. The photoelectric and thermionic work functions of outgassed platinum. *Phys. Rev.* **31,** 236 (1928).
23. Tokmoldin, N., Griffiths, N., Bradley, D. D. C. & Haque, S. a. A Hybrid Inorganic-Organic

Semiconductor Light-Emitting Diode Using ZrO 2 as an Electron-Injection Layer. *Adv. Mater.* **21,** 3475–3478 (2009).

24. Hatton, R. a., Willis, M. R., Chesters, M. a. & Briggs, D. A robust ultrathin, transparent gold electrode tailored for hole injection into organic light-emitting diodes. *J. Mater. Chem.* **13,** 722–726 (2003).
25. Lyons, P. E. *et al.* High-Performance Transparent Conductors from Networks of Gold Nanowires. *J. Phys. Chem. Lett.* **2,** 3058–3062 (2011).
26. Präzisions Glas & Optik. ITO-Coatings on High Quality Glass Substrates. at <http://www.pgo-online.com/intl/katalog/ito.html>
27. Park, Y., Choong, V. & Gao, Y. Work function of indium tin oxide transparent conductor measured by photoelectron spectroscopy. *Appl. Phys. Lett.* **68,** 2699–2701 (1996).
28. Sugiyama, K., Ishii, H., Ouchi, Y. & Seki, K. Dependence of indium–tin–oxide work function on surface cleaning method as studied by ultraviolet and x-ray photoemission spectroscopies. *J. Appl. Phys.* **87,** 295 (2000).
29. U.S Geological Survey. *Mineral Commodity Summaries: Indium*. (2012).
30. Sun, Y. & Rogers, J. a. Inorganic Semiconductors for Flexible Electronics. *Adv. Mater.* **19,** 1897–1916 (2007).
31. Reddy, V. S., Das, K., Dhar, A. & Ray, S. K. The effect of substrate temperature on the properties of ITO thin films for OLED applications. *Semicond. Sci. Technol.* **21,** 1747–1752 (2006).
32. Boehme, M. & Charton, C. Properties of ITO on PET film in dependence on the coating conditions and thermal processing. *Surf. Coatings Technol.* **200,** 932–935 (2005).
33. Groenendaal, B. L., Jonas, F., Freitag, D., Pielartzik, H. & Reynolds, J. R. Poly(3,4-ethylenedioxythiophene) and Its Derivatives: Past, Present and Future. *Adv. Mater.* **12,** 481–494 (2000).
34. Kim, J. S. *et al.* Indium–tin oxide treatments for single- and double-layer polymeric light-emitting diodes: The relation between the anode physical, chemical, and morphological properties and the device performance. *J. Appl. Phys.* **84,** 6859 (1998).
35. Huang, J., Miller, P. F., De Mello, J. C., De Mello, A. J. & Bradley, D. D. C. Influence of thermal treatment on the conductivity and morphology of PEDOT/PSS films. *Synth. Met.* **139,** 569–572 (2003).
36. Carter, S. A., Angelopoulos, M., Karg, S., Brock, P. J. & Scott, J. C. Polymeric anodes for improved polymer light-emitting diode performance. *Appl. Phys. Lett.* **70,** 2067 (1997).
37. Nardes, A. M. *et al.* Conductivity, work function, and environmental stability of PEDOT:PSS thin films treated with sorbitol. *Org. Electron.* **9,** 727–734 (2008).
38. Scott, J. C., Carter, S. A., Karg, S. & Angelopoulo, M. Polymeric anodes for organic light-emitting diodes. *Synth. Met.* **85,** 1197–1200 (1997).
39. Levermore, P. a., Chen, L., Wang, X., Das, R. & Bradley, D. D. C. Fabrication of Highly Conductive Poly(3,4-ethylenedioxythiophene) Films by Vapor Phase Polymerization and Their Application in Efficient Organic Light-Emitting Diodes. *Adv. Mater.* **19,** 2379–2385 (2007).
40. Kiebooms, R., Aleshin, A., Hutchison, K., Wudl, F. & Heeger, A. Doped poly(3,4-ethylenedioxythiophene) films: Thermal, electromagnetical and morphological analysis. *Synth. Met.* **101,** 436–437 (1999).
41. Mäkinen, A. J., Hill, I. G., Shashidhar, R., Nikolov, N. & Kafafi, Z. H. Hole injection barriers at polymer anode/small molecule interfaces. *Appl. Phys. Lett.* **79,** 557 (2001).
42. Greiner, M. T. *et al.* Universal energy-level alignment of molecules on metal oxides. *Nat. Mater.* **11,** 76–81 (2012).

43. Tokito, S., Noda, K. & Taga, Y. Metal oxides as a hole-injecting layer for an organic electroluminescent device. *J.Phys. D Appl. Phys.* **29,** 2750–2753 (1996).
44. Chu, C.-W., Li, S.-H., Chen, C.-W., Shrotriya, V. & Yang, Y. High-performance organic thin-film transistors with metal oxide/metal bilayer electrode. *Appl. Phys. Lett.* **87,** 193508 (2005).
45. Morii, K. *et al.* Encapsulation-free hybrid organic-inorganic light-emitting diodes. *Appl. Phys. Lett.* **89,** 183510 (2006).
46. Mang, A., Reimann, K. & Rübenacke, S. Band Gaps, Crystal-Field Splitting, Spin-Orbit Coupling, and Exciton Binding Energies in ZnO under Hydrostatic Pressure. *Solid State Commun.* **94,** 251–254 (1995).
47. Bagnall, D. M. *et al.* Optically pumped lasing of ZnO at room temperature. *Appl. Phys. Lett.* **70,** 2230 (1997).
48. Nomura, K. *et al.* Room-temperature fabrication of transparent flexible thin-film transistors using amorphous oxide semiconductors. *Nature* **432,** 488–92 (2004).
49. Adamopoulos, G. *et al.* Structural and Electrical Characterization of ZnO Films Grown by Spray Pyrolysis and Their Application in Thin-Film Transistors. *Adv. Funct. Mater.* **21,** 525–531 (2011).
50. Chopraa, K. L., Majora, S. & Pandya, D. K. Transparent conductors—A status review. *Thin Sol. Fil.* **102,** 1–46 (1983).
51. Wang, Z. L. & Song, J. Piezoelectric nanogenerators based on zinc oxide nanowire arrays. *Science (80-.).* **312,** 242–6 (2006).
52. Shalish, I., Temkin, H. & Narayanamurti, V. Size-dependent surface luminescence in ZnO nanowires. *Phys. Rev. B* **69,** 1–4 (2004).
53. Minami, T., Miyata, T. & Yamamoto, T. Work function of transparent conducting multicomponent oxide thin films prepared by magnetron sputtering. *Surf. Coatings Technol.* **108-109,** 583–587 (1998).
54. Janotti, A. & Van de Walle, C. G. Fundamentals of zinc oxide as a semiconductor. *Rep. Prog. Phys.* **72,** 126501 (2009).
55. Xu, Y. & Schoonen, M. A. A. The absolute energy positions of conduction and valence bands of selected semiconducting minerals. *Am. Mineral.* **85,** 543–556 (2000).
56. Hausmann, A. & Utsch, B. Oxygen Ion Vacancies as Donors in Zinc Oxide. *Z. Phys. B* **220,** 217–220 (1975).
57. Hutson, A. R. Hall Effect Studies of Doped Zinc Oxide Single Crystals. *Phys. Rev.* **108,** 222 (1957).
58. Zeng, Y. J. *et al.* Identification of acceptor states in Li-doped p-type ZnO thin films. *Appl. Phys. Lett.* **89,** 042106 (2006).
59. Tsukazaki, A. *et al.* Repeated temperature modulation epitaxy for p-type doping and light-emitting diode based on ZnO. *Nat. Mater.* **4,** 42–46 (2004).
60. Joseph, M., Tabata, H. & Kawai, T. p-Type Electrical Conduction in ZnO Thin Films by Ga and N Codoping. *Jpn. J. Appl. Phys.* **38,** 1205–1207 (1999).
61. Minami, T., Nanto, H., Takata, S. & Tadatsugu, M. Highly Conductive and Transparent Aluminium Doped Zinc Oxide Thin Films Prepared by RF Magnetron Sputtering. *Jpn. J. Appl. Phys.* **23,** 280–282 (1984).
62. Minami, T., Sato, H., Imamoto, H. & Takata, S. Substrate Temperature Dependence of Transparent Conducting Al-Doped ZnO Thin Films Prepared by Magnetron Sputtering. *Jpn. J. Appl. Phys.* **31,** 257–260 (1992).
63. Chrisey, D. B. & Hubler, G. K. *Pulsed Laser Deposition of Thin Films*. (Wiley, 2003).
64. Merchant, J. De & Cocivera, M. Preparation and Doping of Zinc Oxide Using Spray Pyrolysis.

Chem. Mater. **7,** 1742–1749 (1995).
65. Xu, J. *et al.* Low temperature growth of highly crystallized ZnO:Al films by ultrasonic spray pyrolysis from acetylacetone salt. *Mater. Sci. Eng. B* **167,** 182–186 (2010).
66. Manouni, A. *et al.* Effect of aluminium doping on zinc oxide thin films grown by spray pyrolysis. *Superlattices Microstruct.* **39,** 185–192 (2006).
67. Adamopoulos, G. *et al.* Spray-deposited Li-doped ZnO transistors with electron mobility exceeding 50 cm^2/Vs. *Adv. Mater.Mater.* **22,** 4764–9 (2010).
68. Hong, J.-P., Lee, J., Kim, J. & Heo, Y. Doping of Nitrogen in Li-Al doped ZnO by RF Magnetron Sputtering. *J. Korean Phys. Soc.* **54,** 1293–1296 (2009).
69. Ravichandran, C., Srinivasan, G., Lennon, C., Sivanathan, S. & Kumar, J. Investigations on the structural and optical properties of Li, N and (Li, N) co-doped ZnO thin films prepared by sol–gel technique. *Mater. Sci. Semicond. Process.* **13,** 46–50 (2010).
70. Reynolds, K. J., Barker, J. a., Greenham, N. C., Friend, R. H. & Frey, G. L. Inorganic solution-processed hole-injecting and electron-blocking layers in polymer light-emitting diodes. *J. Appl. Phys.* **92,** 7556 (2002).
71. You, H., Dai, Y., Zhang, Z. & Ma, D. Improved performances of organic light-emitting diodes with metal oxide as anode buffer. *J. Appl. Phys.* **101,** 026105 (2007).
72. Gwinner, M. C. *et al.* Doping of Organic Semiconductors Using Molybdenum Trioxide: a Quantitative Time-Dependent Electrical and Spectroscopic Study. *Adv. Funct. Mater.* **21,** 1432–1441 (2011).
73. Kröger, M. *et al.* Role of the deep-lying electronic states of MoO3 in the enhancement of hole-injection in organic thin films. *Appl. Phys. Lett.* **95,** 123301 (2009).
74. Meyer, J., Shu, A., Kröger, M. & Kahn, A. Effect of contamination on the electronic structure and hole-injection properties of MoO3/organic semiconductor interfaces. *Appl. Phys. Lett.* **96,** 133308 (2010).
75. Kanai, K. *et al.* Electronic structure of anode interface with molybdenum oxide buffer layer. *Org. Electron.* **11,** 188–194 (2010).
76. Matsushima, T. *et al.* Interfacial charge transfer and charge generation in organic electronic devices. *Org. Electron.* **12,** 520–528 (2011).
77. Kanno, H., Giebink, N. C., Sun, Y. & Forrest, S. R. Stacked white organic light-emitting devices based on a combination of fluorescent and phosphorescent emitters. *Appl. Phys. Lett.* **89,** 023503 (2006).
78. Nicolai, H. T. *et al.* Space-charge-limited hole current in poly(9,9-dioctylfluorene) diodes. *Appl. Phys. Lett.* **96,** 172107 (2010).
79. Kim, J. S. *et al.* Kelvin probe and ultraviolet photoemission measurements of indium tin oxide work function : a comparison. *Synth. Met.* **111-112,** 311–314 (2000).
80. Wang, Z. B. *et al.* Highly simplified phosphorescent organic light emitting diode with >20% external quantum efficiency at >10,000 cd/m[sup 2]. *Appl. Phys. Lett.* **98,** 073310 (2011).
81. Jørgensen, M., Norrman, K. & Krebs, F. C. Stability/degradation of polymer solar cells. *Sol. Energy Mater. Sol. Cells* **92,** 686–714 (2008).
82. de Bruyn, P., Moet, D. J. D. & Blom, P. W. M. All-solution processed polymer light-emitting diodes with air stable metal-oxide electrodes. *Org. Electron.* **13,** 1023–1030 (2012).
83. Xie, F. *et al.* Low-Temperature Solution-Processed Hydrogen Molybdenum and Vanadium Bronzes for an Efficient Hole-Transport Layer in Organic Electronics. *Adv. Mater.* 2051–2055 (2013). doi:10.1002/adma.201204425
84. Lampande, R. *et al.* A highly efficient transition metal oxide layer for hole extraction and

transport in inverted polymer bulk heterojunction solar cells. *J. Mater. Chem. A* **1,** 6895 (2013).
85. Hammond, S. R. *et al.* Low-temperature, solution-processed molybdenum oxide hole-collection layer for organic photovoltaics. *J. Mater. Chem.* **22,** 3249 (2012).
86. Murase, S. & Yang, Y. Solution processed MoO3 interfacial layer for organic photovoltaics prepared by a facile synthesis method. *Adv. Mater.* **24,** 2459–62 (2012).
87. Girotto, C., Voroshazi, E., Cheyns, D., Heremans, P. & Rand, B. P. Solution-processed MoO_3 thin films as a hole-injection layer for organic solar cells. *ACS Appl. Mater. Interfaces* **3,** 3244–7 (2011).
88. Liu, F., Shao, S., Guo, X., Zhao, Y. & Xie, Z. Efficient polymer photovoltaic cells using solution-processed MoO3 as anode buffer layer. *Sol. Energy Mater. Sol. Cells* **94,** 842–845 (2010).
89. Meyer, J., Khalandovsky, R., Görrn, P. & Kahn, A. MoO3 films spin-coated from a nanoparticle suspension for efficient hole-injection in organic electronics. *Adv. Mater.* **23,** 70–3 (2011).
90. Tan, Z. *et al.* Efficient and stable polymer solar cells with solution-processed molybdenum oxide interfacial layer. *J. Mater. Chem. A* **1,** 657 (2013).
91. Xu, M.-F. *et al.* Aqueous solution-processed MoO3 as an effective interfacial layer in polymer/fullerene based organic solar cells. *Org. Electron.* **14,** 657–664 (2013).
92. Höfle, S. *et al.* Molybdenum oxide anode buffer layers for solution processed, blue phosphorescent small molecule organic light emitting diodes. *Org. Electron.* 1–5 (2013). doi:10.1016/j.orgel.2013.04.017
93. Stubhan, T. *et al.* High shunt resistance in polymer solar cells comprising a MoO[sub 3] hole extraction layer processed from nanoparticle suspension. *Appl. Phys. Lett.* **98,** 253308 (2011).
94. Jasieniak, J. J., Seifter, J., Jo, J., Mates, T. & Heeger, A. J. A Solution-Processed MoOx Anode Interlayer for Use within Organic Photovoltaic Devices. *Adv. Funct. Mater.* **22,** 2594–2605 (2012).
95. Mooney, J. & Radding, S. Spray Pyrolysis Processing. *Ann. Rev. Mater. Sci.* **12,** 81–101 (1982).
96. Coats, A. W. & Redfern, J. P. Thermogravimetric Analysis: A Review. *Analyst* **88,** 906–924 (1963).
97. Tauc, J. Optical properties and electronic structure of amorphous Ge and Si. *Mater. Res. Bull.* **3,** 37–46 (1968).
98. Urbach, F. The long-wavelength edge of photographic sensitivity and of the electronic absorption of solids. *Phys. Rev.* **92,** 1324 (1953).
99. Srikant, V. & Clarke, D. R. Optical absorption edge of ZnO thin films: The effect of substrate. *J. Appl. Phys.* **81,** 6357 (1997).
100. Lupan, O. *et al.* Effects of annealing on properties of ZnO thin films prepared by electrochemical deposition in chloride medium. *Appl. Surf. Sci.* **256,** 1895–1907 (2010).
101. Liu, Y. C., Hsieh, J. H. & Tung, S. K. Extraction of optical constants of zinc oxide thin films by ellipsometry with various models. *Thin Solid Films* **510,** 32–38 (2006).
102. Poon, C. Y. & Bhushan, B. Comparison of surface roughness measurements by stylus profiler, AFM and non-contact optical profiler. *Wear* **190,** 76–88 (1995).
103. Hansen, W. N. & Hansen, G. J. Standard reference surfaces for work function measurements in air. *Surf. Sci.* **481,** 172–184 (2001).
104. Helander, M. G., Greiner, M. T., Wang, Z. B. & Lu, Z. H. Pitfalls in measuring work function using photoelectron spectroscopy. *Appl. Surf. Sci.* **256,** 2602–2605 (2010).
105. Smits, F. M. Measurement of Sheet Resisitivities with the Four-Point Probe. *Bell Syst. Tech. J.* **37,** 711–718 (1958).
106. Patel, N. K., Cinà, S. & Burroughes, J. H. High-Efficiency Organic Light-Emitting Diodes. *IEEE J. Sel. Top. quantum Electron.* **8,** 346–361 (2002).
107. Zhao, X., Zheng, B., Li, C. & Gu, H. Acetate-derived ZnO ultrafine particles synthesized by spray

pyrolysis. *Powder Technol.* **100,** 20–23 (1998).
108. Martínez Casado, F. J. *et al.* Anhydrous lithium acetate polymorphs and its hydrates: Three-dimensional coordination polymers. *Cryst. Growth Des.* **11,** 1021–1032 (2011).
109. Le, X. S., Wang, M., Dang, Z. & Du, F. Y. Meaningful differences in spectral performance, thermal behavior, and heterogeneous catalysis between ammonium molybdate tetrahydrate and its adduct of b-cyclodextrin. *J. Phys. Chem. B* **114,** 3404–3410 (2010).
110. Huang, X. *et al.* A facile approach to fabricate solution-processable metal oxides for interfacial layer in polymer solar cells. *Org. Electron.* **15,** 1235–1243 (2014).
111. Jiebing, S. U. N. *et al.* Preparation and Characterization of Molybdenum Oxide Thin Films by Sol-Gel Process. *J. Sol-Gel Sci. Technol.* **27,** 315–319 (2003).
112. Jonda, C. H., Mayer, A. B. R., Stolz, U., Elschner, A. & Karbach, A. Surface roughness effects and their influence on the degradation of organic light emitting devices. *J. Mater. Sci.* **35,** 5645–5651 (2000).
113. Pereira, E. *et al.* Al-Doping Effect on the Surface Morphology of ZnO Films Grown by Reactive RF Magnetron Sputtering. **2013,** 761–767 (2013).
114. Suchea, M., Christoulakis, S., Katsarakis, N., Kitsopoulos, T. & Kiriakidis, G. Comparative study of zinc oxide and aluminum doped zinc oxide transparent thin films grown by direct current magnetron sputtering. *Thin Solid Films* **515,** 6562–6566 (2007).
115. Thomas, D. G. The exciton spectrum of zinc oxide. *J. Phys. Chem. Solids* **15,** 86–96 (1960).
116. Srikant, V. & Clarke, D. R. On the optical band gap of zinc oxide. *J. Appl. Phys.* **83,** 5447 (1998).
117. Lu, J. G. *et al.* Structural, optical, and electrical properties of (Zn,Al)O films over a wide range of compositions. *J. Appl. Phys.* **100,** 1–11 (2006).
118. Achour, Z. Ben *et al.* Effect of doping level and spray time on zinc oxide thin films produced by spray pyrolysis for transparent electrodes applications. *Sensors Actuators A Phys.* **134,** 447–451 (2007).
119. Lin, S.-S., Huang, J.-L. & Šajgalik, P. The properties of heavily Al-doped ZnO films before and after annealing in the different atmosphere. *Surf. Coatings Technol.* **185,** 254–263 (2004).
120. Cho, H. J. *et al.* The effect of annealing on Al-doped ZnO films deposited by RF magnetron sputtering method for transparent electrodes. *Thin Solid Films* **518,** 2941–2944 (2010).
121. Kim, H. *et al.* Electrical, optical, and structural properties of indium–tin–oxide thin films for organic light-emitting devices. *J. Appl. Phys.* **86,** 6451 (1999).
122. Bouzidi, A., Benramdane, N., Tabet-derraz, H., Mathieu, C. & Khelifa, B. Effect of substrate temperature on the structural and optical properties of MoO 3 thin films prepared by spray pyrolysis technique. *Mater. Sci. Eng. B* **97,** 6–9 (2003).
123. Ahire, D. V *et al.* Preparation of MoO3 Thin Films By Spray Pyrolysis And Its Gas Sensing Performance. *Int. J. Smart Sens. Intell. Syst.* **5,** 592–605 (2012).
124. Choi, H. *et al.* Production of molybdenum oxide particles with high yield by ultrasonic spray pyrolysis and their catalytic activity toward partial oxidation of n-dodecane. *J. Anal. Appl. Pyrolysis* **112,** 276–283 (2015).
125. Fiddes, A. *et al.* Preparation of ZnO films by spray pyrolysis. *J. Cryst. Growth* **159,** 210–213 (1996).
126. Puetz, J., Gasparro, G. & Aegerter, M. a. Liquid film spray deposition of transparent conducting oxide coatings. *Thin Solid Films* **442,** 40–43 (2003).
127. Novikov, S. V. Rough electrode surface: effect on charge carrier injection and transport in organic devices. *Macromol. Symp.* **212,** 191–200 (2004).
128. Soultati, A., Davazoglou, D., Vourdas, N., Giannakopoulos, K. P. & Kontos, A. G. Sol–gel

synthesized, low-temperature processed, reduced molybdenum peroxides for organic optoelectronics applications. *J. Mater. Chem. C.* 6290–6300 (2014). doi:10.1039/c4tc00301b

129. Irfan, I., James Turinske, A., Bao, Z. & Gao, Y. Work function recovery of air exposed molybdenum oxide thin films. *Appl. Phys. Lett.* **101,** 093305 (2012).
130. Wang, P.-S., Lo, Y.-Y., Tseng, W.-H., Chen, M.-H. & Wu, C.-I. Enhancing the incorporation compatibility of molybdenum oxides in organic light emitting diodes with gap state formations. *J. Appl. Phys.* **114,** 063710 (2013).
131. Zhang, Z. *et al.* Impact of Oxygen Vacancy on Energy-Level Alignment at MoOx/Organic Interfaces. *Appl. Phys. Express* **6,** 095701 (2013).
132. Kim, J. S. *et al.* Kelvin probe and ultraviolet photoemission measurements of indium tin oxide work function: a comparison. *Synth. Met.* **111,** 311–314 (2000).
133. Schlaf, R., Murata, H. & Kafafi, Z. . Work function measurements on indium tin oxide films. *J. Electron Spectros. Relat. Phenomena* **120,** 149–154 (2001).
134. Smith, G. C. Evaluation of a simple correction for the hydrocarbon contamination layer in quantitative surface analysis by XPS. *J. Electron Spectros. Relat. Phenomena* **148,** 21–28 (2005).
135. Wagner, C. D. *Handbook of x-ray photoelectron spectroscopy*. (Physical Electronics Division, Perkin-Elmer Corp, 1979).
136. *Handbook of Photoelectron Spectroscopy*. (Physical Electronics, 1993).
137. Vasilopoulou, M. *et al.* Vapor-deposited hydrogenated and oxygen-deficient molybdenum oxide thin films for application in organic optoelectronics. *Surf. Coatings Technol.* **230,** 202–207 (2013).
138. Redecker, B. M., Bradley, D. D. C., Inbasekaran, M., Wu, W. W. & Woo, E. P. High Mobility Hole Transport Fluorene- Triarylamine Copolymers. *Adv. Funct. Mater.* **11,** 241–246 (1999).
139. Harding, M. J., Maher, R. C., Cohen, L. F. & Campbell, a J. Tuning hole transport in a highly dispersed blend of chemically similar polyfluorene copolymers - art. no. 633314. *Proc. SPIE* **6333,** 633314 (2006).
140. Khan, R., Poplavskyy, D., Kreouzis, T. & Bradley, D. D. C. Hole mobility within arylamine-containing polyfluorene copolymers: A time-of-flight transient-photocurrent study. *Phys. Rev. B* **75,** 035215 (2007).
141. Wang, Z. B., Helander, M. G., Greiner, M. T., Qiu, J. & Lu, Z. H. Analysis of charge-injection characteristics at electrode-organic interfaces: Case study of transition-metal oxides. *Phys. Rev. B* **80,** 1–9 (2009).
142. Logan, S., Donaghey, J. E., Zhang, W., McCulloch, I. & Campbell, A. J. Compatibility of amorphous triarylamine copolymers with solution-processed hole injecting metal oxide bottom contacts. *J. Mater. Chem. C* **3,** 4530–4536 (2015).
143. Shen, Y., Hosseini, A. R., Wong, M. H. & Malliaras, G. G. How to make ohmic contacts to organic semiconductors. *Chemphyschem* **5,** 16–25 (2004).
144. Nicolai, H. T. *et al.* Unification of trap-limited electron transport in semiconducting polymers. *Nat. Mater.* **11,** 882–7 (2012).
145. de Jong, M. P., van IJzendoorn, L. J. & de Voigt, M. J. A. Stability of the interface between indium-tin-oxide and poly (3, 4-ethylenedioxythiophene)/poly (styrenesulfonate) in polymer light-emitting diodes. *Appl. Phys. Lett.* **77,** 2255–2257 (2000).
146. Murawski, C., Leo, K. & Gather, M. C. Efficiency Roll-Off in Organic Light-Emitting Diodes. *Adv. Mater.* **25,** 6801–6827 (2013).
147. Kozhukharov, S. & Tchaoushev, S. Spray pyrolysis equipment for various applications. *J. Chem. Technol. Metall.* **48,** 111–118 (2013).
148. Wang, S., Wang, W., Liu, Q., Zhang, M. & Qian, Y. Preparation and characterization of cerium (IV)

oxide thin films by spray pyrolysis method. *Solid State Ionics* **133,** 211–215 (2000).
149. Garniera, J., Achary, R. S. & Boutevillec, A. Influence of the Heating Mode and the Spray Introduction on Chemically Vapour Deposited Aluminium Doped Zinc Oxide Thin Films. *ECS Trans.* **25,** 1259–1265 (2009).
150. Yoshino, K. *et al.* Low-Temperature Growth of ZnO Films by Spray Pyrolysis. *Jpn. J. Appl. Phys.* **50,** 040207 (2011).
151. Yao, P., Hang, S. & Wu, M. Growth characteristics and properties of Al-doped ZnO thin films by DC magnetron sputtering from AZOY(R) target. *ICETI* **37,** (2012).
152. Liu, J. *et al.* High-efficiency inverted polymer solar cells with transparent and work-function tunable MoO(3)-Al composite film as cathode buffer layer. *Adv. Mater.* **24,** 2774–9 (2012).
153. Li, X., Xie, F., Zhang, S., Hou, J. & Choy, W. C. MoOx and V2Ox as hole and electron transport layers through functionalized intercalation in normal and inverted organic optoelectronic devices. *Light Sci. Appl.* **4,** e273 (2015).
154. Lee, B. R. *et al.* Highly efficient inverted polymer light-emitting diodes using surface modifications of ZnO layer. *Nat. Commun.* **5,** 4840 (2014).
155. Bolink, H. J., Coronado, E., Repetto, D. & Sessolo, M. Air stable hybrid organic-inorganic light emitting diodes using ZnO as the cathode. *Appl. Phys. Lett.* **91,** 223501 (2007).
156. Lee, H., Park, I., Kwak, J., Yoon, D. Y. & Lee, C. Improvement of electron injection in inverted bottom-emission blue phosphorescent organic light emitting diodes using zinc oxide nanoparticles. *Appl. Phys. Lett.* **96,** 44–47 (2010).
157. Terán-Escobar, G., Pampel, J., Caicedo, J. M. & Lira-Cantú, M. Low-temperature, solution-processed, layered V2O5 hydrate as the hole-transport layer for stable organic solar cells. *Energy Environ. Sci.* **6,** 3088 (2013).
158. Höfle, S. *et al.* Tungsten oxide buffer layers fabricated in an inert sol-gel process at room-temperature for blue organic light-emitting diodes. *Adv. Mater.* **25,** 4113–6 (2013).
159. Vasilopoulou, M. & Davazoglou, D. Hot-wire vapor deposited tungsten and molybdenum oxide films used for carrier injection/transport in organic optoelectronic devices. *Mater. Sci. Semicond. Process.* **16,** 1196–1216 (2013).